

AD 480 091

FINAL REPORT

RESEARCH ON THE STABILITY OF HIGH STRENGTH H₂O₂

CONTRACT NO. AF 04(611)-10216

By: Oliver W. Cass
Jean P. Paris
Albert M. Stock

E. I. du Pont de Nemours & Co.
Wilmington, Del.

March 15, 1966

REPRODUCED FROM
BEST AVAILABLE COPY

FOREWORD

The work herein reported was performed by Dr. Oliver W. Cass, Associate Laboratory Director, and Dr. Albert M. Stock, Research Chemist, Electrochemicals Department; and Dr. Jean P. Paris, Research Engineer, Radiation Physics Laboratory; all of E. I du Pont de Nemours & Co., Wilmington, Delaware; under Contract No. AF 34(611)-10216. This contract was sponsored by Advanced Research Projects Agency (ARPA Order No. 24), Washington, D.C. and monitored by Air Force Rocket Propulsion Laboratory, Research and Technology Division, Air Force Systems Command, Edwards Air Force Base, California, project monitor Lt. E. A. Irene/AFRL/RPCL.

This technical report has been reviewed, and is approved.

George F. Babits, Lt. Colonel, USAF
Chief, Propellant Division

ABSTRACT

This report covers work (a) on the low temperature (-60°C., -30°C., and 0°C.) stability in Pyrex glass of 90-100% hydrogen peroxide, (b) on the effect of container surfaces on the stability of such peroxide in the 50-70°C. temperature range, and (c) on the mechanism of hydrogen peroxide decomposition.

Carefully purified, or commercially stabilized, 90-100% hydrogen peroxide in Pyrex glass at -60°C. to 0°C. is stable and storable, with less than 1 ppm per day (0.04% per year) decomposition. At higher temperatures (50-70°C.), mildly irradiated "Teflon" FEP fluorocarbon as a container surface is exceedingly inert to high strength hydrogen peroxide, causing less than one-third the peroxide decomposition of a passivated aluminum surface, and less than one-half that of passivated Pyrex glass. Studies of the sites of attack of hydrogen peroxide on aluminum surfaces are described, together with methods of following the mechanism of decomposition of hydrogen peroxide catalyzed by metallic ions (both oxidizing and reducing) and radiation. This latter work may suggest superior stabilization systems for hydrogen peroxide.

TABLE OF CONTENTS

	<u>Page</u>
INTRODUCTION	1
SUMMARY - Section I.	2
Section II	6
MAJOR CONCLUSIONS.	9
SECTION I - Storage Stability of High Strength H ₂ O ₂ . . .	11
Discussion	11
Conclusions	18
Oxygen Solubility in Hydrogen Peroxide . . .	19
Experimental	20
References	32
Figures.	33
SECTION II- Surface Inert to High Strength H ₂ O ₂ and Decomposition Mechanisms of H ₂ O ₂ . . .	47
Introduction	47
Container Material-Hydrogen Peroxide Inter- actions	53
Reaction Mechanisms of Hydrogen Peroxide Decomposition	60
Tables	74
Figures.	92
References	113
APPENDIX I -Minimum Metal Container Surface.	116
APPENDIX II-Solid H ₂ O ₂ Container Surface	118
APPENDIX III - Concentration of 90% H ₂ O ₂ by Crystalliza- tion	124
APPENDIX IV- Effects of 90% Hydrogen Peroxide Upon Aluminum Surfaces.	128
Exhibit A-1; Electron Probe Microanalysis .	155

INTRODUCTION

This report summarizes the work performed by the Electrochemicals Department of E. I. du Pont de Nemours and Company under Contract No. AF 04(611)-10216, "Research on the Stability of High Strength H₂O₂".

The requirements of this contract are stated as follows:

1. The Contractor shall conduct a research program consisting of the following phases:

- a. Determine the inherent bulk stability of pure 90 to 100% hydrogen peroxide at temperatures ranging from -60°F. to +160°F. in the absence of catalyzing surfaces by using solid hydrogen peroxide as the wall.
- b. Determine the effect of wall surfaces on the bulk stability as secured above by electron spin resonance and infrared attenuated total reflected techniques employed on the interface.
- c. To subject the pure hydrogen peroxide in contact with a stable surface, if one is found, to radiation to induce instability and thus generate radicals whose interactions with the surface can be determined. The choice and use of the stable surface, if found, will be mutually agreed upon by the procuring activity and the contractor before this phase of study commences.

2. This program shall be directed toward the gathering of information affecting the storability of hydrogen peroxide. Emphasis will lie on the reliability and reproducibility of the data attained.

Section 1(a) experimentation was carried out primarily at the Research Laboratories of the Electrochemicals Department at Niagara Falls, New York, by Dr. A. M. Stock. Sections 1(b) and 1(c) work was carried out primarily at the Radiation Physics Laboratory of the Engineering Department at Wilmington, Delaware, by Dr. J. P. Paris.

As a result of the above separation of effort, this report is divided into two sections, Section I covering work at Niagara Falls, and Section II covering work at Wilmington.

SUMMARY

Section I

1. After considerable engineering study, followed by a few scouting experiments, it was concluded that determination of the high temperature stability of high strength H_2O_2 , surrounded by a container wall of frozen H_2O_2 , while feasible, could not be carried out within the limit of funds allocated to this contract. Suggested extension of the contract was not approved. Two engineering studies, one on a "minimum metal container surface" and one on "solid H_2O_2 container surface", are appended as Appendices I and II.

2. In view of (1) above, it was therefore decided to limit experiments on the storage stability of high strength H_2O_2 to temperatures at which H_2O_2 was solid, thus limiting the access of H_2O_2 molecules to the container surface. These temperatures were selected at $-30^\circ C.$ ($-22^\circ F.$) and $-60^\circ C.$ ($-76^\circ F.$). In addition, tests were included at $0^\circ C.$ ($32^\circ F.$) so that our results, taken in conjunction of those of Roth and Shanley (Ref. 4) would span the entire temperature range of $-60^\circ C.$ ($-76^\circ F.$) to $100^\circ C.$ ($212^\circ F.$). Equipment capable of detecting decomposition in the range of 1 ppm/day was assembled and tested.

3. Two-week stability tests were then set up at the three temperatures noted in (2) above, using as test samples 90% concentration stabilized commercial H_2O_2 from three manufacturers, 98% commercial concentration commercial H_2O_2 from one manufacturer, and highly purified, unstabilized H_2O_2 of both 90 and 99+% concentration, made from commercial Du Pont 90% concentration stabilized H_2O_2 . Procedures for securing these later two grades are outlined later in this report, while a discussion of concentration of 90% H_2O_2 to 99+% by crystallization (taken from unpublished Du Pont work) is appended as Appendix III.

Standard drop tests were carried out on solid high strength H_2O_2 to be certain that the solid state did not increase the sensitivity of the H_2O_2 to shock. These tests were carried out with a Gardner Variable Impact Tester (Catalog No. 1G-1120, Gardner Laboratory, Inc., Bethesda, Maryland). This instrument permits a known weight to fall from a known height onto a sample supported on an anvil. To carry out the impact tests, the anvil was removed and refrigerated to $-60^\circ C.$; the weight was raised to its maximum height and held at this point with a thin wire. The anvil was quickly replaced and solid H_2O_2 crystals placed on it; the weight was then released by cutting the wire. No evidence of detonation was observed under these conditions. In these tests, the manufacturer's impact calibrations were used without independent checking against calibration standards. To the limit of our equipment (50 inch-pounds impact), crystalline 99.5% concentration H_2O_2 was insensitive to impact.

4. Studies of the decomposition of commercial stabilized 90% H_2O_2 (triplicate samples) gave the following results:

a. At -60°C . all samples tested showed no decomposition (rates, if any, of less than 1 ppm per day). All samples were completely solid throughout the test.

b. At -30°C ., all samples contained a minor amount of liquid H_2O_2 . Four of the nine samples tested gave small, but measurable amounts of decomposition (0.9-2.1 ppm/day). The remaining samples showed no detectable decomposition.

c. At 0°C ., all samples were completely liquid. All three samples from one manufacturer showed decomposition rates of 3 to 5 ppm/day. The samples from the other two manufacturers showed very slow decomposition from just detectable to 1.5 ppm/day.

d. Repeat of these tests in a slightly modified, more sensitive, apparatus capable of detecting decompositions of 0.5 ppm/day confirmed the above rates:

- (1) At -60°C ., decomposition less than 0.5 ppm/day.
- (2) At -30°C ., decomposition barely detectable in some samples.
- (3) At 0°C ., a sample of the H_2O_2 that showed 3 to 5 ppm/day in test 4(c) above, gave about the same rate. One sample from a second manufacturer also indicated a 3 ppm/day rate. All three samples from a third manufacturer gave no measurable decomposition.

5. Study of the decomposition of commercial 98% H_2O_2 gave the following results:

- a. At -60°C ., no decomposition.
- b. At -30°C ., completely solid, no decomposition.
- c. At 0°C ., sample liquid, no decomposition (under 0.5 ppm/day).

6. Studies of the decomposition of highly purified, unstabilized 90% and 98%+ concentration H_2O_2 gave the following results (triplicate samples), in our more sensitive unit mentioned in 4(d) above:

- a. At -60°C ., no detectable decomposition.
- b. At -30°C ., no detectable decomposition.
- c. At 0°C ., 98%+ H_2O_2 : 0.9, 0.7, and "0.1" ppm/day decomposition
90% H_2O_2 : "0.3", "0.4", and 1.7 ppm/day decomposition

We are inclined to blame trace contamination for the two higher values for the 98%+, and the one higher value for the 90% material, and conclude that the decomposition rate of highly purified H_2O_2 is essentially undetectable at 0°C . in equipment capable of measuring decomposition rates in the under 0.5 ppm/day range.

7. On the basis of the above data, we conclude:

a. At -60°C . solid hydrogen peroxide shows no evidence of decomposition regardless of the presence or absence of stabilizers.

b. The onset of decomposition is associated with the appearance of a liquid phase at about -30°C . in the case of 90% H_2O_2 and at somewhat higher temperatures in the case of 98% H_2O_2 .

c. In the liquid phase (0°C .), decomposition rates of commercial high strength (90% and 98%) H_2O_2 range from a maximum of about 5 ppm/day to below the level of statistical significance.

d. In the liquid phase (0°C .), carefully purified unstabilized H_2O_2 is only slightly less stable than the most stable commercial H_2O_2 and considerably more stable than the least stable commercial H_2O_2 , indicating that stabilizers are not required for high stability provided high purity is maintained.

e. Only a rough correlation between low electrical conductivity and high stability was found, indicating that electrical conductivity per se is not a reliable indicator of stability.

Section II

1. Container Materials for Storage of High Strength H₂O₂

(a) Aluminum. High purity (99.6% or better) aluminum has been considered the best (most inert) material for construction of drums, storage tanks, and tank-cars used in high strength H₂O₂ storage and shipment. From our work it is apparent that the oxide sealing treatment of the aluminum surface before use is not perfect, and allows contact of the stored peroxide with the aluminum surface. Exact chemical nature of the oxide film could not be established. With contact of the aluminum surface by the H₂O₂, decomposition at the site of catalytically active heavy metal contaminate atoms appears certain. However, it was not possible to demonstrate the superior resistance of 99.999% aluminum over that of 99.93%. It also appears that scratches and mechanical damage to the aluminum surface before oxide sealing provide sites for preferential pitting attack on the surface. Suggestions for more definitive work are outlined in Appendix IV.

(b) Pyrex Glass. Literature values for the decomposition of high strength H₂O₂ stored in properly cleaned and passivated Pyrex glass were readily duplicated.

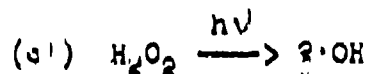
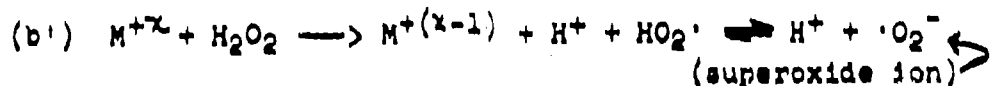
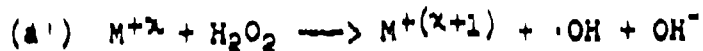
(c) Polyethylene. Examination of the surface of both linear and branched chain polyethylene indicated a temperature dependent attack by high strength H₂O₂. Development of the C-O, C=O, and O-H bands at 50° and 70°C. could be readily followed. Polyethylene is not a suitable material for containers for high strength H₂O₂.

(d) Fluorocarbon Polymers. "Teflon" TFE-fluorocarbon film showed no detectable surface attack by 90% concentration H₂O₂ after 500 hours at 70°C. However, a perfluorosulfonic acid ion-exchange membrane was rapidly attacked, giving noticeable C=O absorption after 2 hours. Our

most significant work was done with "Teflon" FEP-fluorocarbon resin as a container for high strength H_2O_2 . A sample bottle made from this resin initially caused about 50% more decomposition of high strength H_2O_2 stored in it at $70^\circ C$. for a 5-hour period than did a passivated Pyrex glass bottle. However, mild irradiation of the "Teflon" FEP bottle in air, while not adversely affecting the physical properties of the container, reduced its catalytic effect on contained 90% H_2O_2 to about half that of passivated Pyrex glass, and to about one-third that of passivated aluminum. Such an irradiated surface is the most inert that has been reported. We recommend consideration of such a container surface for long term H_2O_2 storage.

2. Reaction Mechanism of H_2O_2 Decomposition

Pure H_2O_2 is a very stable molecule. Decomposition studies therefore require an initiator to start the chain decomposition reactions. In our work we utilized (a) a reducing agent (titanous chloride), (b) an oxidizing agent (ceric salts), and an irradiation system (ultraviolet light). All three of these agents aided in the over-all understanding of the mechanism. The reactions involved are:



(a) Titanous Chloride as an Initiator. Rapid mixing flow cells were constructed to study the reaction of titanous chloride with H_2O_2 in an electron paramagnetic resonance (EPR) cavity. A rapid closing valve allowed "stop flow" studies, giving radical decay values, to be made in this same unit. In this unit the basic reaction was studied.

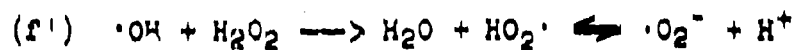
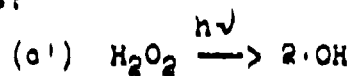
In addition, the effect of methanol or ethanol additions, change in pH, changes in H_2O_2 concentration, and the addition of ferrous ion to the system were examined. Methanol, for example, rapidly gave the hydroxy methyl radical.

(b) Ceric ion (nitrate-cerate ion) as an initiator. In the same system as used in 2(a) above, the reaction of H_2O_2 with $Ce(NO_3)_6^{-2}$ (nitrate-cerate ion) was examined. Good evidence was obtained that the reaction sequence was:



It was found that cupric ions added to this system drastically reduced the $\cdot O_2^-$ level. It is believed that this is the mechanism responsible for the catalytic decomposition of H_2O_2 by cupric ions. Methanol, on the other hand, did not react with $\cdot O_2^-$. This suggests that the stabilizing effect of methanol on H_2O_2 is possibly due to scavenging of $\cdot OH$ radicals.

(c) Photochemical dissociation of H_2O_2 . Equipment was constructed in which light from a low pressure mercury arc was appropriately filtered to isolate the 2537Å Hg line. This light was then used to decompose H_2O_2 as follows:



It was hoped to add a scavenging agent that would react completely with the superoxide ion ($\cdot O_2^-$), and by measuring the amount of reaction product, determine the quantum yield in the photolysis of H_2O_2 . We were able to do so, and confirmed literature data on the quantum yield determined by another method. The scavenging agent used,

tetranitromethane, appears to react quantitatively with the super-oxide ion.

MAJOR CONCLUSIONS

1. Either carefully purified, or suitably stabilized commercial, 90% and 98% H₂O₂ can be considered stable and storable at temperatures of 0°C. (32°F.) or below. Decomposition rates of less than 1.0 ppm/day should be readily attainable under these conditions in standard passivated aluminum storage vessels. This conclusion is borne out by unpublished Du Pont experience, in which solid 99%+ H₂O₂ has been stored in Pyrex glass at -30°C. for a three year period with no detectable decrease in concentration as measured by permanganate titration. It should be noted that H₂O₂ increases in density by about 15% upon freezing. Decomposition of 1 ppm/day of 90% H₂O₂ at 0°C. in an unvented container with 5% outage should not build up over 200 psig pressure in a 4 year period.

TYPICAL DECOMPOSITION RATES

Temperature, °C.	Decomposition Rates							
	Purified 98% H ₂ O ₂		Purified 90% H ₂ O ₂		Stabilized 98% H ₂ O ₂		Stabilized 90% H ₂ O ₂	
	ppm/day	%/yr.	ppm/day	%/yr.	ppm/day	%/yr.	ppm/day	%/yr.
-60	N.D.	N.D.	N.D.	N.D.	N.D.	N.D.	N.D.	N.D.
-30	N.D.	N.D.	N.D.	N.D.	N.D.	N.D.	0.5	0.018
0	0.7	0.025	0.3	0.010	N.D.	N.D.	0.6	0.022
30	39.5 ³	1.44 ³	-	-	29.9 ³	1.09 ³	408 ³	14.9 ³
66	{ 381 ³ 805 ³ }	{ 13.9 ³ 29.4 ³ }	-	-	27.47	17	14257	527

ND = no decomposition detected

In other unpublished Du Pont work, we have shown that, not only is solid H_2O_2 extremely stable, but also much less reactive than liquid H_2O_2 . At $-55^\circ C.$, we have maintained crystals of 99%+ H_2O_2 in contact with an active silver screen catalyst for 4 hours with no decomposition. We have also mixed solid 99%+ H_2O_2 with solid 99%+ hydrazine at $-70^\circ C.$ with no reaction. In the later case, warming the mixture to $-25^\circ C$ resulted in explosive decomposition of the mixture.

2. "Teflon" FEP fluorocarbon film, mildly irradiated in air, offers a surface for a storage container for 90% H_2O_2 that has only one-third the catalytic decomposition rate of a passivated aluminum surface.

3. It is possible, with modern physical tools, to follow concisely the growth and decay of short-lived intermediates in the catalytic decompositions of H_2O_2 . Further light has been shed on these complicated reactions. By selecting the proper scavenging agent for key intermediates in these chain reactions, superior H_2O_2 stabilizers might be developed.

SECTION I - STORAGE STABILITY OF HIGH STRENGTH H₂O₂

DISCUSSION

I. Preparation of Pure Hydrogen Peroxide

Essentially anhydrous hydrogen peroxide was prepared from commercial (Du Pont) 90% hydrogen peroxide by fractional crystallization followed by distillation under reduced pressure. By carrying out the crystallization at about -30°C. and accepting a moderate (40%) yield of crystals, it was possible to obtain 98-99% H₂O₂ by a single crystallization of the commercial 90% H₂O₂. Under these conditions large, well-formed crystals were obtained; in one case, the crystals attained a length of about 3 inches (See Figure S-1). The crystals were collected on a sintered glass filter, blanketed with dry nitrogen and allowed to melt slightly to remove the surface film of mother liquor. Distillation was carried out according to the procedure of Gross and Taylor(1), using a modified form of the apparatus described by these workers (See Figure S-2). As recommended in the literature(1,2), the distillation was conducted in the presence of a trace of NaOH. Distillation served primarily to remove ionic impurities and brought about only a slight increase in H₂O₂ concentration.

II. Electrical Conductivity of Pure H₂O₂

The electrical conductivity of pure H₂O₂ has been studied by several workers(3,5,6). Early investigators(5) have reported a specific conductance of 2 micromhos at 25°C. More recently, specific conductances of 0.82 micromho at 25°C.(5) and 0.39 micromho (temperature unspecified)(3) have been reported.

We studied the conductivity of pure H_2O_2 prepared by fractional crystallization and distillation as a means of determining its purity. The results of this study (see Table S-1 for data) can be summarized as follows:

- a. fractional crystallization reduced the conductivity of commercial 90% H_2O_2 to approximately half its initial value, (while increasing its concentration to 98+% H_2O_2).
- b. distillation of the crystallized H_2O_2 reduced its specific conductance to about 2 micromhos, the value reported in the early work of Outhertson and Mass(5).
- c. A second distillation of crystallized and once-distilled H_2O_2 reduced its specific conductance to 1.2 micromhos, a value greater than that reported in the more recent literature(3,6).
- d. the specific conductance of both 98+% H_2O_2 and "deionized" water increased on storage in contact with "Pyrex" glass.

We attribute our failure to achieve the lowest conductivity reported in the literature to handling and storage in "Pyrex" glass-ware and the presence of up to 2% water in the crystallized, distilled H_2O_2 . In the $H_2O-H_2O_2$ system specific conductance passes through a maximum(5); viz., the specific conductance of pure H_2O_2 is increased by the addition of water and the specific conductance of pure water is increased by the addition of H_2O_2 . We have limited our purification procedure to crystallization and a single distillation, since repeated distillation produced a relatively small decrease in conductivity. Since conductivity of the H_2O_2 samples is certain to increase during

the stability tests due to the prolonged contact with "Pyrex" glass, we question the significance of extremely low initial conductivity.

III. Rate of Decomposition of High Strength H₂O₂

Two series of decomposition rate experiments were carried out. In the first series, the decomposition rates of eight samples of commercial 90% H₂O₂ from three manufacturers and of three samples of commercial 98% H₂O₂ from a single manufacturer were determined. In these experiments the H₂O₂ samples were placed in specially designed decomposition flasks (see Figure S-5) in a modified Revco Model ULT-903 low temperature refrigerator. The flasks were connected to manometers constructed of 2 mm. "Pyrex" capillary tubing by means of 2 mm. "Pyrex" or 4 mm. "Teflon" capillary tubing. Both types of tubing proved satisfactory. "Teflon" offered the advantage of greater flexibility. The manometric fluid was colored kerosene (density = 0.800 g./ml. at 23°C.). (See Figure S-7 for a schematic drawing of the decomposition rate apparatus.) This type of decomposition rate apparatus was extremely sensitive. A barely detectable pressure change (2 mm. kerosene = 0.12 mm. Hg) was calculated to correspond to decomposition of from 0.10 to 0.14 ppm of the H₂O₂ samples. Theoretically, then, a decomposition of well under 1 ppm over the entire test period should have been detectable. Unfortunately, this small amount of decomposition fell well within the error imposed principally by temperature fluctuations within the refrigerator. For example, at -60°C., the indicated refrigerator temperature varied from -57.8 to -60.0°C. Since the decomposition flasks were immersed in a fluid of low heat capacity (air) with no provision for forced circulation, actual temperature inside the

*Registered Du Pont Trademark

decomposition flasks may have varied considerably from the indicated temperature. We indeed observed that fluctuations in pressure lagged considerably behind the corresponding changes in temperature. We estimate the possible error due to temperature fluctuation to be of the order of 10 ppm. Thus, over a two-week period of observation, decomposition at a rate of about 1 ppm/day should produce a pressure increase greater than the experimental error.

The results of the first series of decomposition rate studies can be summarized as follows.

A. At -60°C ., all samples were entirely in the solid state. Pressure variations within the decomposition flasks were random and gave no indication of accumulation of oxygen. (See Figure S-8 for plots of pressure vs. time for typical samples of 90% and 98% H_2O_2 .) Since a decomposition rate of 1 ppm/day should have caused a noticeable upward trend in pressure, we conclude that at -60°C . all the commercial H_2O_2 samples tested decompose at a rate of less than 1 ppm/day, if at all.

B. At -30°C ., the 98% H_2O_2 remained entirely in the solid phase, while the 90% H_2O_2 samples contained both a solid (major portion) and a liquid (minor portion) phase. At this temperature, four samples of 90% H_2O_2 showed evidence of decomposition (i.e., a decomposition rate of about 1 ppm/day or more). Calculated decomposition rates for these samples were 2.1, 1.1, 1.3 and 0.9 ppm/day, respectively. (See Table S-2, Samples #2, #7, #10 and #12.) Since none of the 98% H_2O_2 samples showed evidence of decomposition, we have concluded that the onset of decomposition is associated with the appearance of the liquid phase. (See Figure S-9 for typical plots of temperature vs. time for 90% H_2O_2 at -30°C . and Figure S-10 for a typical plot of pressure vs. time for 98% H_2O at -30°C .)

C. At 0°C., all eleven samples gave evidence of decomposition. Calculated decomposition rates varied from 0.5 to nearly 5 ppm/day (see Table S-2). In this case, we consider the rate of 0.5 ppm/day to be significant, since the H₂O₂ samples expand significantly on melting, thus decreasing the free volume of the decomposition flasks and increasing the sensitivity of the manometric systems to small amounts of evolved oxygen. Thus a calculated decomposition rate of 0.5 ppm/day at 0°C. may be statistically significant even though the calculated rate of 0.9 ppm/day at -30°C. may be of ^{marginal} statistical significance. Typical plots (Figure S-11) of pressure vs. time at 0°C. clearly show increasing trends even though calculated decomposition rates are as low as 0.5 ppm/day. The decomposition rates at 0°C. divided the samples into two sharply defined categories, namely, eight samples which decomposed at rates of 0.5 to 1.5 ppm/day, and three samples which decomposed at rates of 3 to 5 ppm/day. The three samples which decomposed at the higher rate represented 90% H₂O₂ from one of the three manufacturers. At the end of the decomposition rate experiment, the specific conductances of the samples were measured, in order to obtain an estimate of the relative amounts of ionic impurities present in the samples. The conductance data (see Table S-2) indicated that the amounts of ionic impurities were small and did not vary widely from sample to sample. However, the specific conductances of the three less stable samples were higher than those of most of the remaining more stable samples. If an ionic impurity was responsible for the lower stability of the three samples in question, it must have been a powerful catalyst for the decomposition.

In the second series of decomposition rate experiments, the following samples were used:

- a. three samples of unstabilized 98% H_2O_2 prepared from commercial (Du Pont) 90% H_2O_2 by fractional crystallization and distillation as described in the Experimental Section of this report.
- b. three samples of unstabilized 90% H_2O_2 prepared by dilution of the unstabilized 98% H_2O_2 with "deionized" (specific conductivity = 3×10^{-7} mho) water.
- c. five samples of commercial 90% H_2O_2 from three manufacturers.
- d. one sample of commercial 98% H_2O_2 .

The decomposition flasks used in the first series of experiments (see Figure S-5) were modified as shown in Figure S-6. The external lines connecting the decomposition flasks to the manometers were shortened by replacing the "Pyrex" glass capillary with heavy wall tubing of "Teflon" fluorocarbon resin. "Pyrex" lines within the refrigeration unit were not changed. We have estimated that these modifications increased the sensitivity of the apparatus to ca. 0.5 ppm/day at $-30^\circ C.$ and $-60^\circ C.$ and to ca. 0.2 ppm/day at $0^\circ C.$

The results of the second series of decomposition rate studies can be summarized as follows:

A. At $-60^\circ C.$, (all samples in the solid state), pressure changes over the samples (#1, #2 and #3) of unstabilized 98% H_2O_2 were small and random (see Figure S-12). Therefore we conclude that solid H_2O_2 requires no stabilizer against decomposition, provided high purity is maintained. Of the three samples (#4, #5 and #6) of unstabilized

90% H_2O_2 , two (#4 and #5) showed some signs of decomposition. In the case of sample #4, approximately half of the apparent gas evolution occurred during the first day of observation; thus the calculated decomposition rate for the final 13 days of observation was only half that for the entire 14-day period. The results obtained at higher temperatures ($-30^\circ C.$ and $0^\circ C.$) suggest that the apparent gas evolution from these samples was caused by failure to attain thermal equilibrium by the time observation was begun. (During the start-up phase of the run, the freezer temperature dropped considerably below the set-point due to mechanical misbehavior of the unit.) All samples (#7 through #12) of commercial H_2O_2 had apparent decomposition rates of doubtful statistical significance (i.e., 0.4 ppm/day or less).

B. At $-30^\circ C.$, the observed decomposition rates (Table S-3, Figure S-13) were below the level of statistical significance or of marginal statistical significance at most. The "negative" rates reported (Table S-3) for samples 9 through 12 can be attributed to failure of the samples to reach thermal equilibrium at the time of the initial observation. The rate plots in Figure S-3 show either little change or a slight increasing trend in the amount of H_2O_2 decomposed after the second observation.

C. At $0^\circ C.$, (see Table S-3, Figure S-14) five of the samples (#1, 2, 6, 10, and 11) decomposed at statistically significant rates. The calculated decomposition rates of samples #4, 5 and 12 were of marginal statistical significance; and those of the remaining samples were below the level of statistical significance. The low decomposition rates of the unstabilized samples confirm that a high degree of stability is possible without stabilizers, provided high purity is maintained.

In this group of samples (#1 through #6) there seemed to be at least a rough correlation between higher conductance and higher decomposition rate. The behavior of the various commercial samples (#7 through #12) was about the same as it had been in the first series of experiments, with one exception - the decomposition rate of the 90% H_2O_2 from Manufacturer C was higher than expected from the previous results. The conductance measurements do not indicate ionic contamination of the sample, although contamination by a nonionic material such as silicone grease cannot be entirely ruled out. In any case, the highest decomposition rates observed at $0^\circ C$. (ca. 3.5 ppm/day) are in agreement with those found in the first series of experiments (3 to 5 ppm/day).

On the basis of the two series of decomposition rate experiments, we have reached the following conclusions.

1. At $-60^\circ C$. solid hydrogen peroxide shows no evidence of decomposition regardless of the presence or absence of stabilizers.
2. The onset of decomposition is associated with the appearance of a liquid phase at about $-30^\circ C$. in the case of 90% H_2O_2 and at somewhat higher temperatures in the case of 98% H_2O_2 .
3. In the liquid phase ($0^\circ C$.), decomposition rates of commercial high strength (90% and 98%) H_2O_2 range from a maximum of about 5 ppm/day to below the level of statistical significance.
4. In the liquid phase ($0^\circ C$.), carefully purified unstabilized H_2O_2 is only slightly less stable than the most stable commercial H_2O_2 and considerably more stable than the least stable commercial H_2O_2 , indicating that stabilizers are not required for high stability provided high purity is maintained.

5. Only a rough correlation between low electrical conductivity and high stability was found, indicating that electrical conductivity per se is not a reliable indicator of stability.

IV. Oxygen Solubility in Hydrogen Peroxide

In their careful study of the rate of decomposition of pure hydrogen peroxide at somewhat higher temperatures, Roth and Shanley(3) corrected the volume of oxygen evolved for dissolved oxygen. Since no data on the solubility of oxygen in hydrogen peroxide were available, they used the water solubility of oxygen as an approximation. We consider this correction unnecessary in the case of liquid hydrogen peroxide. Our results indicate that liquid hydrogen peroxide decomposes at a finite rate, even at temperatures approaching its melting point. Therefore, under normal circumstances, we would expect liquid hydrogen peroxide to be saturated with dissolved oxygen. It might be argued that samples which were cooled and then held at low temperatures (as in our experiments) might not become saturated with oxygen at the lower temperature for a considerable time. We discount this possibility on the following grounds: first, our samples were normally stored for considerable periods at about -50°C. prior to the start of the decomposition experiments; second, prompt oxygen evolution from decomposing liquid samples was observed (see Fig. S-11 and S-14). Finally, extrapolation of the data of Roth and Shanley predicts a decomposition rate of 1-2 ppm/day for pure hydrogen peroxide at 0°C. We consider that our measured decomposition rates of 1.7 ppm/day are in good agreement with the data of Roth and Shanley.

It is somewhat more difficult to justify neglecting the oxygen solubility (or entrapment) in solid hydrogen peroxide. Our experiments clearly demonstrate that no measurable amount of oxygen was evolved over a two-week period by solid hydrogen peroxide. This observation does not rule out the possibility that some actual decomposition occurred with the oxygen remaining dissolved or entrapped in the solid peroxide. Our experiments at -30°C . were run immediately following the experiments at -60°C . It has already been pointed out that a liquid phase existed in the 90% H_2O_2 samples. With the solid and liquid phases existing in equilibrium, the solid should be purged of entrapped oxygen. Thus during the early stages of the stages of the experiment at -30°C . oxygen should be evolved both by purging from the solid H_2O_2 and by decomposition of the liquid. Thus, as the solid is purged of oxygen, the rate of oxygen evolution should decrease; this phenomenon has not been observed (see Figures S-10 and S-13). We cannot rule out the possibility that solid hydrogen peroxide decomposes at an infinitesimal rate. However, the lack of measurable gas evolution over an extended period is sound evidence that solid H_2O_2 is, in the practical sense, "stable" and storable.

EXPERIMENTAL

I. Cleaning of Glassware

All glassware used in contact with H_2O_2 was cleaned by the procedure of Shanley and Roth(3) which consists of soaking the glassware for 24 hours in 10% NaOH, rinsing with distilled water, soaking for 24 hours in 10% HNO_3 , then for 48-72 hours in concentrated HNO_3 , rinsing thoroughly with distilled water, then with "deionized" water and finally drying in a forced draft oven at 125°C .

II. Crystallization of H₂O₂

The sample to be crystallized was placed in a beaker of appropriate size and cooled in a freezer kept at about -30°C. If crystallization had not set in by the time the sample reached thermal equilibrium, the liquid was seeded with a few H₂O₂ crystals. After the onset of crystallization, the sample was left in the freezer overnight. The crystals were collected on a sintered glass filter under a stream of dry nitrogen and allowed to melt slightly. The melted H₂O₂ was drawn off and the crystals transferred to a clean glass bottle with a vented aluminum screw cap. The bottle was covered loosely with a polyethylene bag to exclude moisture and stored in a freezer maintained at ca. -30°C.

III. Distillation of H₂O₂

The apparatus was assembled as in Figure S-2 and ca. 800 g. of approximately 98% H₂O₂ and 1-4 drops 50% NaOH charged to the still pot (A). A small quantity of ice was placed in the first trap (D) to dilute any H₂O₂ reaching this point. The still pot (A) and first receiver (B) were immersed in water baths; the second receiver (C) and traps (D and E) were immersed in solid CO₂-trichloroethylene baths. Distillation was carried out at a pressure of ca. 1 mm Hg. The still pot water bath was maintained at 35-43°C. so that the H₂O₂ distilled without ebullition. The temperature at the still head was 26-28°C. A forerun of ca. 250 g. was collected in the second receiver (C). The first receiver (B) was then cooled to -5° to -10°C. with an ice-NaCl bath and the main fraction collected in it. In a typical distillation, the various fractions gave the following assays: forerun, 97.9% H₂O₂; main fraction, 99.3% H₂O₂; residue 99.5% H₂O₂.

IV. Assay of H₂O₂ Samples

Hydrogen peroxide samples were assayed by titration with standard KMnO₄ in the presence of excess H₂SO₄ (4).

V. Preparation of Unstabilized H₂O₂

Unstabilized 98% H₂O₂ was prepared by crystallization and distillation of Du Pont 90% H₂O₂ as described above. Unstabilized 90% H₂O₂ was prepared by dilution of unstabilized 98% H₂O₂ with "deionized" water.

VI. Conductivity Measurements

Two special conductivity cells (shown in Figure S-3) were constructed. The electrodes were cast from pure tin (Fisher Scientific Co., assay 99.95% Sn) and polished to yield parallel flat surfaces. The circular electrode faces were 20-25 mm in diameter and were positioned about 4 mm apart. The electrodes were set in tapered ground glass joints by means of tight-fitting plugs of "Teflon" fluorocarbon resin, and were connected into the bridge circuit by means of "Teflon"-insulated silvered copper wires fused into the upper parts of the electrodes. The entire conductivity apparatus is shown in Figure S-4. The constant temperature bath was maintained at $25.00 \pm 0.05^\circ\text{C}$. by means of a "Pyrex" glass cooling coil through which tap water was passed at a constant slow rate and an intermittent quartz heating element controlled by a mercury-to-wire thermoregulator with an electronic relay. Resistance of the test liquid was measured with a five-decade alternating current bridge with a "magic eye" null point indicator (Model RC 1B, Industrial Instruments, Inc.).

Prior to use, the glass parts of the conductivity cells were cleaned by the standard procedure (see "Cleaning of Glassware", above). The electrodes were cleaned by soaking overnight in 90% H₂O₂, then overnight in distilled water. The cells were assembled and calibrated against 10⁻³ N KCl. After calibration, the cells were rinsed at least 10 times with "deionized" water. The conductivity of "deionized" water was then determined in the cells before any H₂O₂ samples were introduced. The cells were dried by drawing air through them with a water aspirator. The H₂O₂ sample was placed in a specially cleaned glass stoppered flask, which was placed in the constant temperature bath for 1-2 hours to bring the sample to thermal equilibrium with the bath. The required amount of H₂O₂ (35 ml. for cell "A", 65 ml. for cell "B") was introduced into the cell with a specially cleaned pipette. The resistance of the sample was determined as quickly as possible and the specific conductance calculated therefrom. The H₂O₂ sample was cautiously poured from the cell into a large excess of water and discarded. The cell was then rinsed and dried as above.

Since the electrodes were movable, care was taken not to change their position once the cells were calibrated. The cells were periodically taken apart for cleaning and repolishing (if necessary) of electrode faces, re-assembled and re-calibrated.

VI. Decomposition Rates

The total volume of each decomposition flask and head assembly (Figures S-5 and S-6) was determined by weighing the contained water, taking into account the overlap of the ground glass joint. (Density of water was taken to be 1.00 g./ml.) The volume of the connecting tubing was calculated from the weight of water contained in a known length of the tubing. The total volume of each assembly (V_t) was

obtained by summation of the volumes of its components. Approximately 500 ml. of H_2O_2 was placed in each flask and weighed by difference. The flasks were placed in the refrigerator, fitted with their head assemblies, connected to the differential manometers, and (after considerable difficulty) sealed.

Note: A leakage problem was encountered during the early stages of the first series of experiments. At $-60^{\circ}C.$, silicone lubricant failed to seal the ground glass joints, even though they were spring-loaded. Satisfactory seals were obtained by "doping" the outside of the joints with sodium silicate solution. When the sodium silicate had thoroughly dried, the joints were tested under both internal and external pressure. All systems except one (which therefore was not used) withstood 59 mm. Hg internal pressure (1000 mm. kerosene, full scale on manometer) and 30 mm. Hg external pressure. During the course of the experiment, the differential between internal and external pressure remained within these limits. No such leakage problems were encountered with the redesigned decomposition flasks (Figure S-6) used in the second series of experiments.

The refrigerator was set to the desired temperature and started; the manometer stopcocks were left open until it was felt that the entire system had reached thermal equilibrium. Normally several days were allowed for thermal equilibration. A pressure reading was taken shortly after the stopcocks were closed and at approximately daily intervals thereafter for the duration of the experiment. Data recorded were: (1) date and time of reading, (2) room temperature in $^{\circ}K$,

(3) refrigerator temperature (T) in °K., (4) barometric pressure (P_0) in mm. Hg, (5) height of kerosene in left arm of manometer (h_1) in mm. (6) height of kerosene in right arm of manometer (h_r) in mm. (The left arm of each manometer was open to the atmosphere and the right arm connected to the appropriate decomposition flask.) From these data were calculated the total pressure (P_1) in each decomposition assembly (equation 2), the apparent partial pressure of oxygen evolved by decomposition of H_2O_2 (equation 4) and the apparent fraction of H_2O_2 decomposed (equation 9 or 10).

VIII. Methods of Calculation

A. Fraction of H_2O_2 Decomposed

Let P_2 = barometric pressure in mm. Hg

" h_1 = height of kerosene in left (atmosphere) arm of manometer

h_r = height of kerosene in right (assembly) arm of manometer

ΔP = difference in pressure (mm. Hg) between exterior and interior of assembly

P_1 = pressure (mm. Hg) inside assembly

(Equation 1)
$$P_1 = P_2 + \Delta P$$

(If $P_1 > P_2$, ΔP is positive; if $P_1 < P_2$, ΔP is negative.)

Taking density of kerosene = 0.800 and density of Hg = 13.546,

$$\Delta P = \frac{0.800}{13.546}(h_1 - h_r) = 0.059(h_1 - h_r)$$

Therefore,

(Equation 2)
$$P_1 = P_2 + 0.059(h_1 - h_r)$$

Let P_0 = partial pressure (mm. Hg) of evolved oxygen at standard temperature (273.2°K.)

P_t^* = pressure (mm. Hg) inside assembly at time t, corrected to standard temperature

P_0^* = pressure (mm. Hg) inside assembly at time 0 (arbitrarily chosen) corrected to standard temperature

T_t = refrigerator temperature at time t .

T_o = " " " " o.

(Equation 3) $P_o = P_t^* = P_o^*$

where $P_o^* = P_1(t) \frac{273.2}{T_t}$

and $P_o^* = P_1(o) \frac{273.2}{T_o}$

Therefore,

(Equation 4) $P_o = P_1(t) \frac{273.2}{T_t} = P_1(o) \frac{273.2}{T_o}$

Let V_f = free volume of assembly in ml.

V_t = total " " " " "

V_s = volume of H_2O_2 sample (ml.) under experimental conditions

(Equation 5) $V_f = V_t - V_s$

$V_s = W_s/d_s$ where W_s is the sample weight (g.) and d_s is the density (g./ml.) of the sample

Therefore,

(Equation 6) $V_f = V_t - W_s/d_s$

Assuming $d_s = n_h d_h + n_w d_w = 1.71 n_h + 0.915 n_w$

where n_h and n_w are the weight fractions of H_2O_2 and water, respectively

d_h and d_w are the densities (g./ml.) of solid H_2O_2 and ice, respectively

Then

(Equation 7) $V_f = V_t - W_s / (1.71 n_h + 0.915 n_w)$

let F = fraction (in ppm) of H_2O_2 sample decomposed

" M_o = moles O_2 evolved

M_h = moles H_2O_2 in original sample

V_{stp} = volume of O_2 evolved at standard temperature
(273.2°K) and pressure (760 mm. Hg)



$$\text{(Equation 8)} \quad F = \frac{2M_o}{M_h} \times 10^6$$

Since $M_h = n_h W_h / 34.02$ (34.02 = gram molecular weight of H_2O_2)

and $M_o = V_{stp} / 22,400$ (22,400 = gram molar volume of O_2 in ml.)

where $V_{stp} = V_f (P_o / 760.0) = V_f P_o / 760.0$

$$M_o = V_f P_o / (760.0)(22,400) = V_f P_o / 1.702 \times 10^7$$

By substitution

$$\text{(Equation 9)} \quad F = \frac{2(34.02)(10^6)V_f P_o}{(1.802)(10^7)n_h W_h} = \frac{68.04 V_f P_o}{17.02 n_h W_h} = \frac{2.997 V_f P_o}{n_h W_h}$$

By collecting constants

$$\text{(Equation 10)} \quad F = K P_o$$

$$\text{where} \quad K = \frac{3.997 V_f}{n_h W_h}$$

- NOTES: 1. Equation 8 assumes that the decomposition rate is so small that the H_2O_2 concentration remains constant, i.e., the decomposition reaction is pseudo zero order in H_2O_2 .
2. The entire volume of gas was assumed to be at refrigerator temperature, although the gas in the capillary tubing (ca. 3% of the total) was at room temperature (293.7-297.7°K) during the experiment. We would expect only a relatively small error in oxygen partial pressure from this assumption.
3. No correction was made for oxygen solubility in solid H_2O_2 .

B. Rates of Decomposition

Rates of decomposition were calculated from the integrated zero-order rate equation $-\Delta[\text{H}_2\text{O}_2] = k \Delta t$ by the method of least squares as follows. The above equation is of the type $y = ax$ (straight line passing through the origin).

Letting $x = \Delta t$ and

$$y = -\Delta[\text{H}_2\text{O}_2]$$

the rate constant (k) is given by

$$\text{(Equation 11) } a = k = \frac{-\Delta[\text{H}_2\text{O}_2]}{\Delta t}$$

Applying the least squares method a (-k) is given by

$$\text{(Equation 12) } a = \frac{\sum xy}{\sum x^2}$$

C. Calculation of Standard Deviation

The standard deviation (σ) is calculated as follows:

(equation 13) $y \text{ calc.} = ax$ where $y \text{ calc.}$ is the calculated value of $-\Delta[\text{H}_2\text{O}_2]$ for each value of Δt .

(Equation 14) $\Delta y = y \text{ obs.} - y \text{ calc.}$ where $y \text{ obs.}$ is the observed value of $-\Delta[\text{H}_2\text{O}_2]$ for each value of Δt .

The standard deviation (σ) is given by

(Equation 15) $\sigma = \sqrt{\frac{\sum (\Delta y)^2}{(N-1)}}$ where N is the number of observations of $-\Delta[\text{H}_2\text{O}_2]$

TABLE S-1

SPECIFIC CONDUCTANCE OF H₂O₂ AND DEMINERALIZED H₂O

<u>Substance</u>	<u>Description</u>	<u>Specific Conductance^a Micromhos</u>
H ₂ O ₂	Commercial 90%, as received	11.5
H ₂ O ₂	Commercial 90%, after concentration by crystallization	5.0
H ₂ O ₂	Purified by crystallization and single distillation ^b	2.1
H ₂ O ₂	Purified by crystallization and single distillation ^b , stored two weeks	2.7
H ₂ O ₂	Purified by crystallization and single distillation ^c	1.8
H ₂ O ₂	Purified by crystallization and double distillation ^c	1.2
H ₂ O	Freshly deionized	0.3
H ₂ O	Deionized, stored 2 hr. in Pyrex glass	0.4
H ₂ O	" " 2 wk. " " "	1.7

(a) Reported conductivity of purified H₂O₂

0.82 micromho at 25°C. - Schumb, Ind. Eng. Chem. 41, 992 (1949)

<2 micromhos at 25°C. - Cathbertson and Mason, J. Am. Chem. Soc. 52, 484 (1930)

0.39 micromho - Roth and Shanley, Ind. Eng. Chem. 45, 2343 (1953)

(b) 1 millimole NaOH added to 22-mole H₂O₂ charge.

(c) 4 millimoles NaOH added to 22-mole H₂O₂ charge.

TABLE S-2
 DECOMPOSITION RATES OF COMMERCIAL H₂O₂
 (FIRST SERIES)

Sample Number	% H ₂ O ₂	Manufac-turer ^a	Temp. ^b °C.	Specific Conductance, Micromhos	Aqueous KCl Equivalent ^c PPM	k ^d PPM/Day	σ ^e	Observations Discarded ^f
1	90	A	-30 0	16.8	8.5	0.5 3.3	6.4 6.3	None
2	90	A	-30	15.7	8.0	2.1 4.8	6.8 4.4	"
3	90	A	-30 0	17.4	8.8	0.6 3.7	6.7 1.6	" Δt=10
4	98		-30 0	15.1	7.7	0.4 1.5	5.7 1.5	None Δt=10
5	98		-30 0	16.9	8.6	0.2 0.6	3.5 1.2	Δt=6 Δt=10
6	98		-30 0	18.6	9.4	0.2 0.6	4.4 1.4	Δt=6 Δt=4, Δt=10
7	90	B	-30 0	12.5	6.3	1.1 0.6	5.9 1.6	Δt=6 Δt=10
8	90	B	-30 0	11.5	5.8	-0.3 0.6	8.5 1.8	None Δt=10
10	90	C	-30 0	15.5	7.9	1.3 0.6	4.3 4.2	Δt=3, Δt=6 None
11	90	C	-30 0	11.2	5.7	0.6 1.5	6.6 2.6	" "
12	90	C	-30 0	13.8	7.0	0.3 0.5	7.1 3.7	" "

^aThe 98% H₂O₂ was obtained from a single manufacturer. The 90% H₂O₂ was obtained from three manufacturers, designated A, B and C.

^bActual temperature ranges were -33.3°C. to -27.8°C. at nominal -30°C. and -5.6°C. to +2.2°C. at nominal 0°C.

^cConcentration in parts per million of an aqueous KCl solution with the same specific conductance as the H₂O₂ sample.

^dCalculated from the integrated zero-order rate equation, $-\Delta[\text{H}_2\text{O}_2] = k\Delta t$ by the method of least squares. At -30°C., rates of 0.9 ppm/day or less are of doubtful significance; at 0°C., rates of 0.4 ppm/day or less are of doubtful significance.

^eStandard deviation of observed $-\Delta[\text{H}_2\text{O}_2]$ from $-\Delta[\text{H}_2\text{O}_2]$ calculated from rate equation.

^fIf the observed $-\Delta[\text{H}_2\text{O}_2]$ differed from the calculated $-\Delta[\text{H}_2\text{O}_2]$ by more than 2σ, the observation was rejected and k and σ recalculated using the remaining observations. The process was repeated until no calculated value of $-\Delta[\text{H}_2\text{O}_2]$ differed from the observed value by more than 2σ.

H₂O₂ DECOMPOSITION RATESSECOND SERIES

Sample Number	H ₂ O ₂	Manufacturer ^b	Temp., °C.	k ^o ppm/day	δ ^d	Observations Discarded ^e	Specific Conductance ^g Micromhos
1	98	-	-60	-0.1	1.8	None	4.0
			-30	0.3	2.0	"	
			0	0.9	2.2	"	
2	98	-	-60	0.0	1.9	"	3.9
			-30	0.3	2.6	"	
			0	0.7	1.7	"	
3	98	-	-60	0.1	2.3	"	3.7
			-30	0.3	3.7	"	
			0	0.1	0.3	"	
4	90	-	-60	1.0	4.6	see note f. None	3.9
			-30	0.5	3.8		
			0	0.5	1.2		
5	90	-	-60	0.6	2.5	"	3.5
			-30	0.4	3.3	"	
			0	0.4	1.3	"	
6	90	-	-60	0.2	2.3	"	4.0
			-30	0.5	3.6	"	
			0	1.7	3.6	"	
7	90	B	-60	0.2	1.7	"	12.2
			-30	0.4	3.5	"	
			0	0.1	1.1	"	
8	90	B	-60	0.4	2.0	"	12.1
			-30	0.5	3.1	"	
			0	0.1	1.0	"	
9	90	A	-60	0.3	2.2	"	12.5
			-30	-0.1	3.5	"	
			0	0.2	1.1	"	
10	90	C	-60	0.3	1.5	At=7	12.8
			-30	-0.1	3.9	None	
			0	3.6	7.3	"	
11	90	A	-60	0.2	1.4	At=7	16.8
			-30	-0.5	3.5	None	
			0	3.5	7.3	"	
12	98	-	-60	0.4	2.0	"	15.5
			-30	-0.6	0.6	"	
			0	0.3	1.1	"	

^aActual temperature ranges were -98.4 to -62.2°C. at nominal -60°C.; -26.3 to -33.3°C. at nominal -30°C.; -5.0 to +1.1°C. at nominal 0°C.

^bSamples 1, 2 and 3 were prepared by fractional crystallization and distillation of Du Pont 90% H₂O₂; samples 3, 4 and 5 were prepared by dilution of fractionally crystallized and distilled H₂O₂ with "deionized" water. The remaining samples were commercial H₂O₂. Commercial 9% H₂O₂ was supplied by three manufacturers, designated A, B and C.

^cCalculated from integrated zero-order rate equation $-\Delta[\text{H}_2\text{O}_2] = k\Delta t$ by the method of least squares. At -30° and -30°C., rates of 0.5 ppm/day or less are of doubtful significance; at 0°C., rates of 0.2 ppm/day or less are of doubtful significance.

^dStandard deviation of experimentally observed values of $-\Delta[\text{H}_2\text{O}_2]$ from the calculated values.

^eObservations were discarded if they differed from the calculated $-\Delta[\text{H}_2\text{O}_2]$ by more than 2 δ .

^fSecond value of rate constant was determined by taking the second rather than the initial manometer reading as zero time ($\Delta t=0$).

^gDetermined at end of experiment.

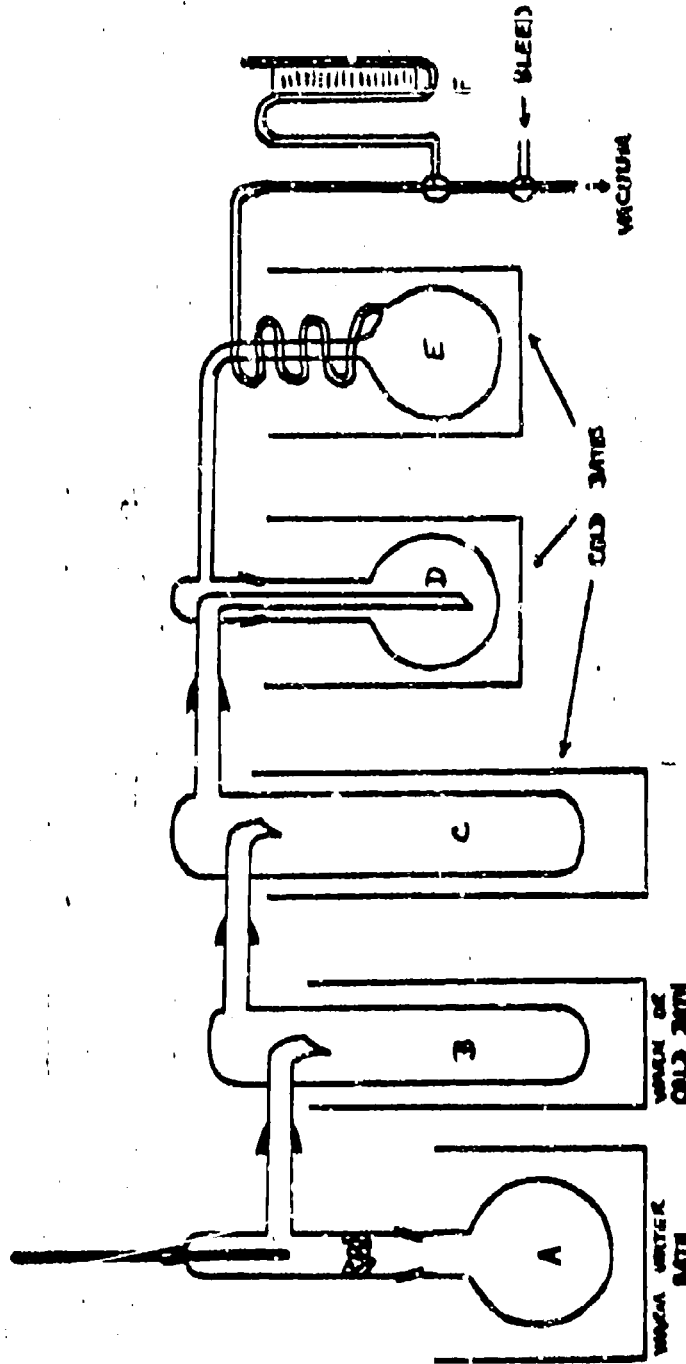
REFERENCES

1. P. M. Gross, Jr. and R. C. Taylor, J. Am. Chem. Soc., 72, 2075 (1950).
2. R. C. Young, "Specific Conductivity of Hydrogen Peroxide Solutions", Report No. 4, Navy Bureau of Ordnance, Contract No. NOrd-9107, Task C, Massachusetts Institute of Technology, Division of Industrial Cooperation, Feb. 28, 1946.
3. E. M. Roth, Jr. and E. S. Shanley, Ind. Eng. Chem. 45, 2343 (1953).
4. F. J. Welcher (ed.), Standard Methods of Chemical Analysis, Sixth Edition, Vol. II, D. Van Nostrand Co., Inc., Princeton, N. J., 1962, p. 1318.
5. A. C. Cuthbertson and O. Maas, J. Am. Chem. Soc., 52, 484 (1930).
6. W. C. Schumb, Ind. Eng. Chem., 41, 992 (1949).
7. E.S. Shanley and F. P. Greenspan, Ind. Eng. Chem. 39, 1536 (1947)

FIGURE S-1
HYDROGEN PEROXIDE CRYSTALS



FIGURE S-2
LARGE SCALE DISTILLATION APPARATUS



- A - POT
- B - MAIN PRODUCT RECEIVER
- C - FORE-RUN RECEIVER
- D - TRAP
- E - TRAP
- F - MANDREL

FIGURE S-3
CONDUCTIVITY CELLS

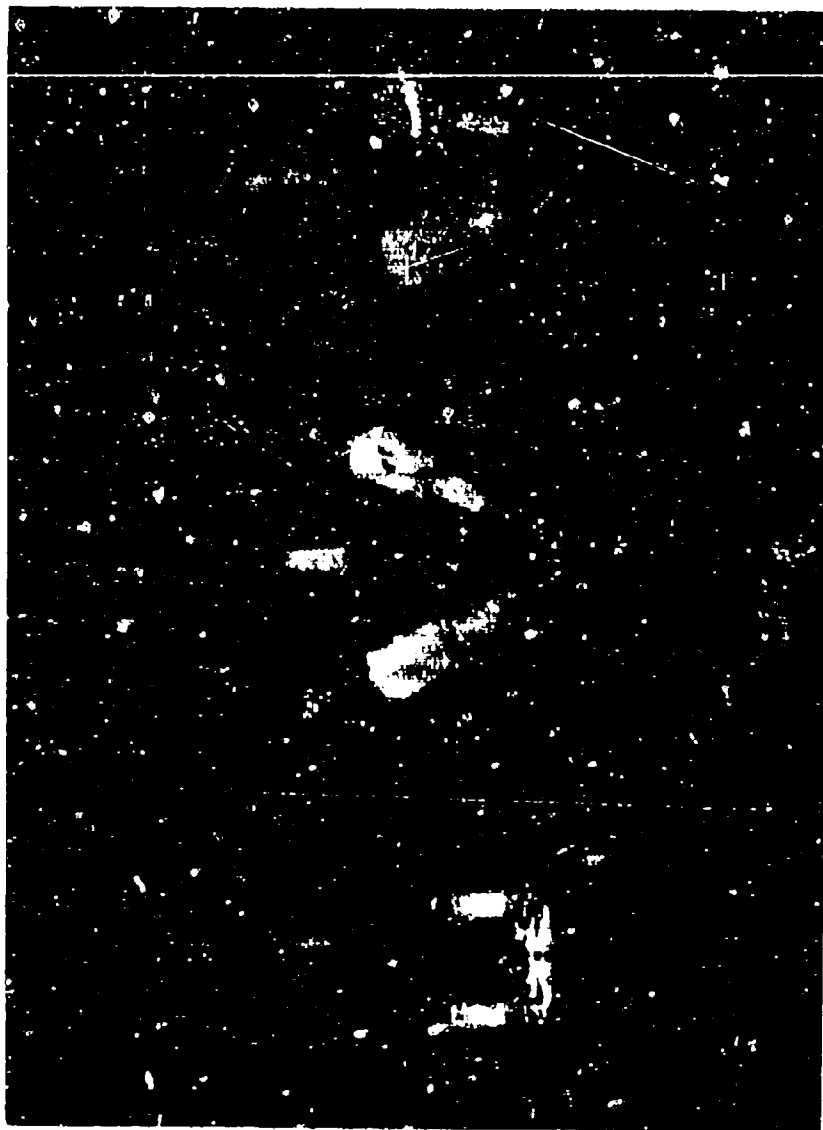


FIGURE S-4
CONDUCTIVITY APPARATUS



FIGURE S-5

DECOMPOSITION FLASK (SERIES 1)

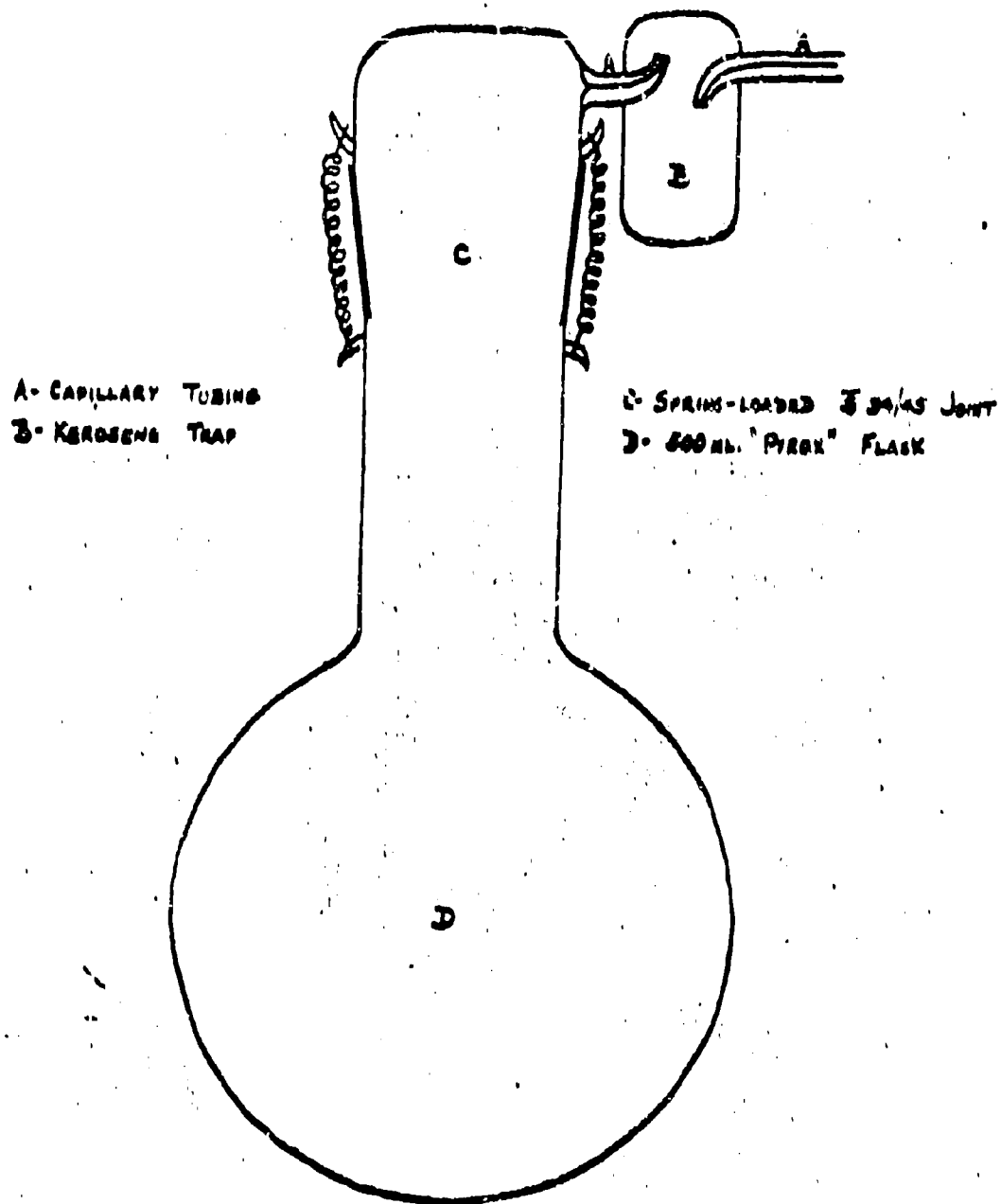
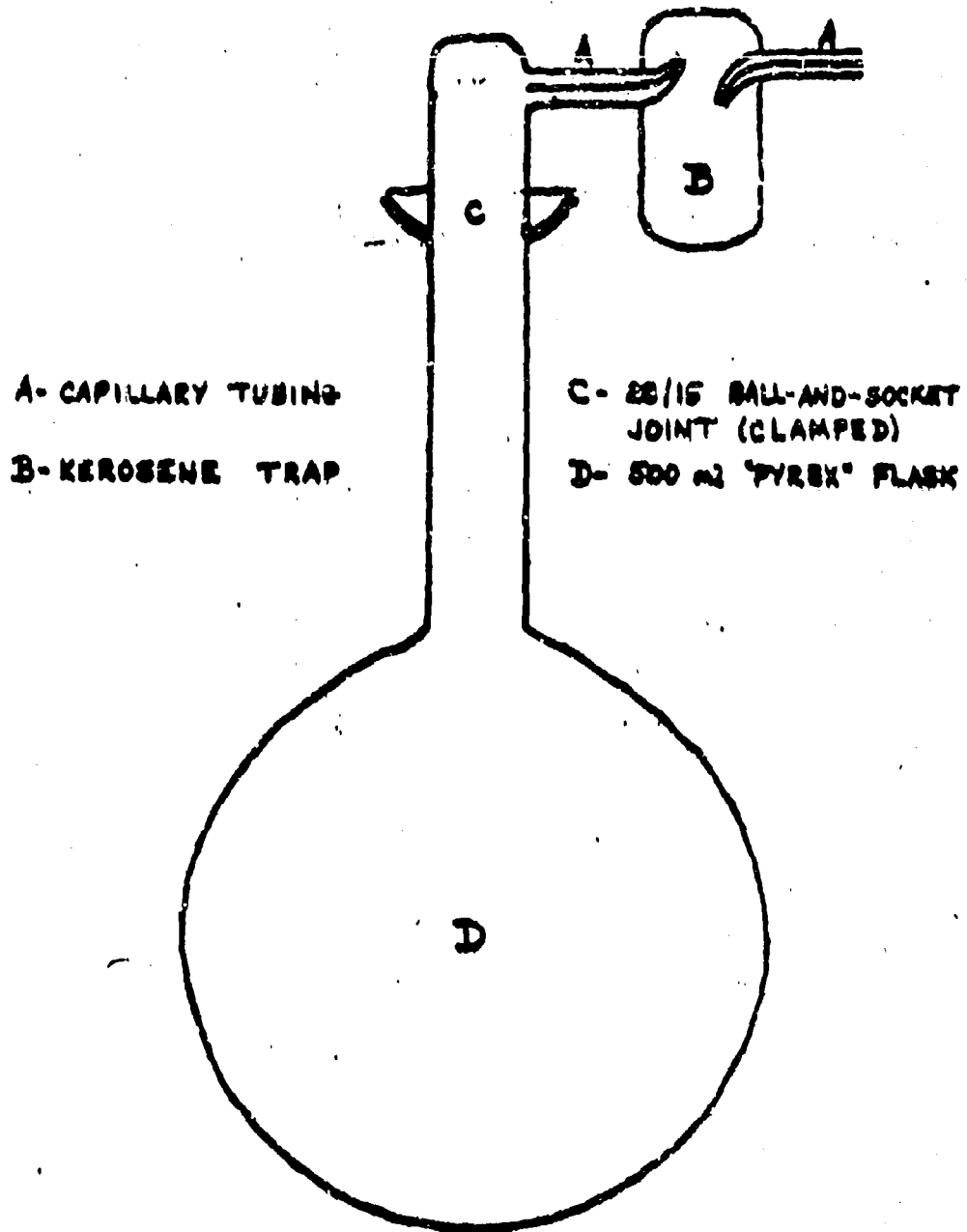
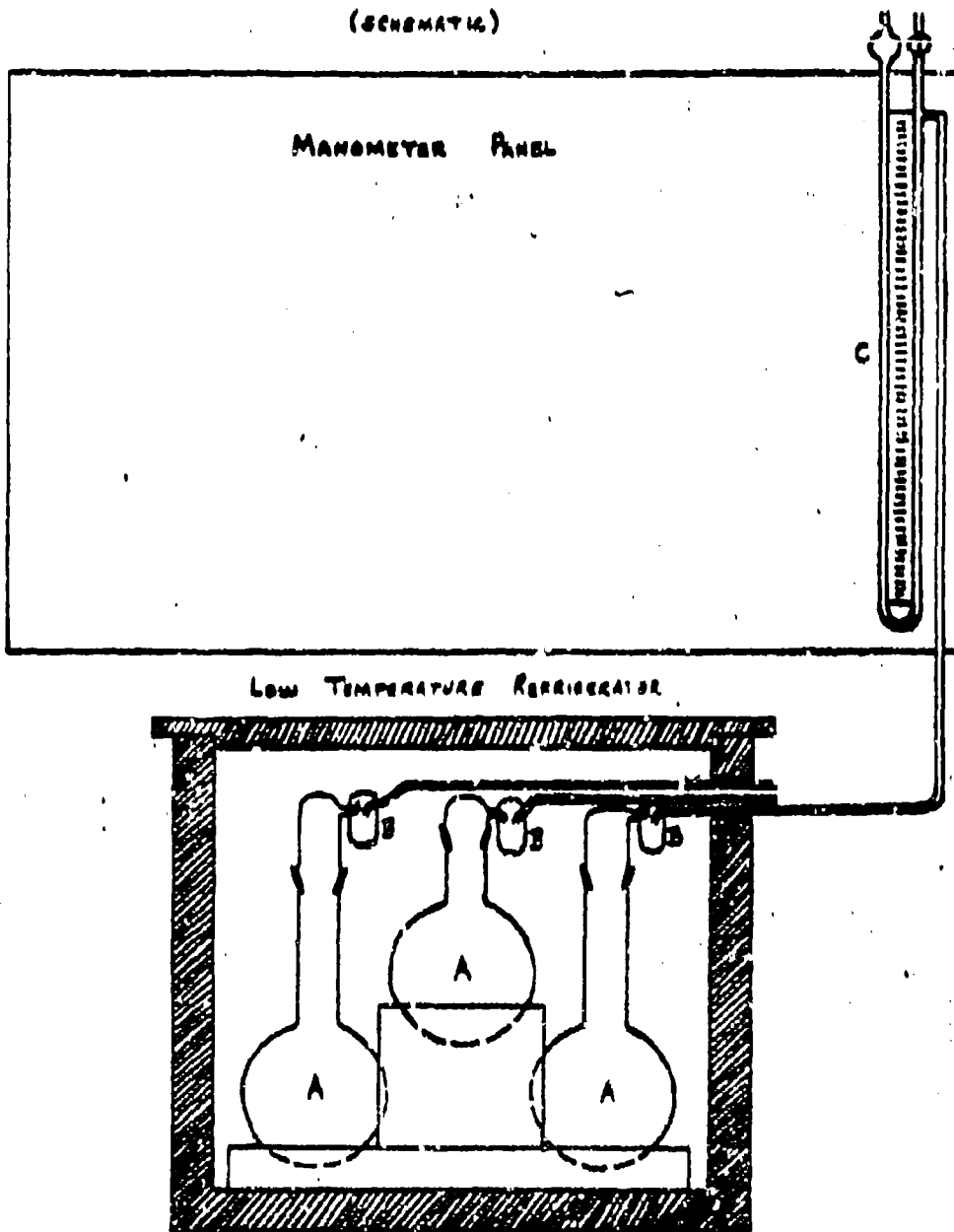


FIGURE 5-6
DECOMPOSITION FLASK (SERIES 2)



39

FIGURE S-7
 DECOMPOSITION RATE APPARATUS
 (SCHEMATIC)



A- DECOMPOSITION FLASKS (3 or 12 shown) B- KEROSENE TRAPS (3 or 12 shown)
 C- KEROSENE DIFFERENTIAL MANOMETER (1 or 12 shown)

FIGURE 5-8
 OXYGEN EVOLUTION - COMMERCIAL H_2O_2
 SERIES 1, $-60^\circ C$

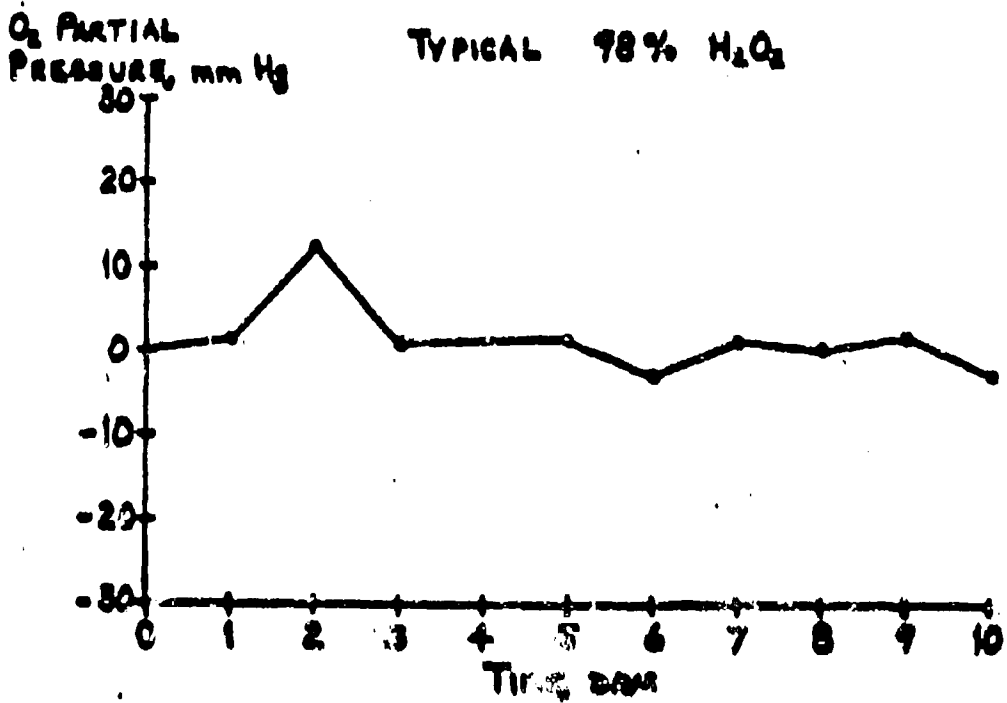
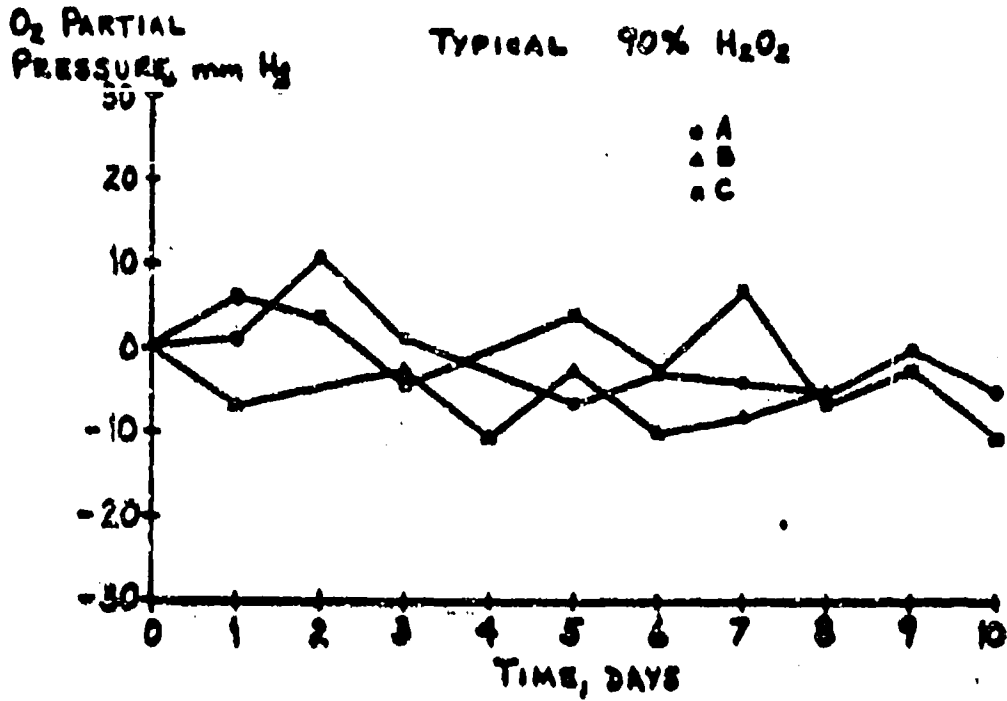


FIGURE 5-7
 TYPICAL DECOMPOSITION RATES - 90% H₂O₂
 SERIES 1, -30°C.

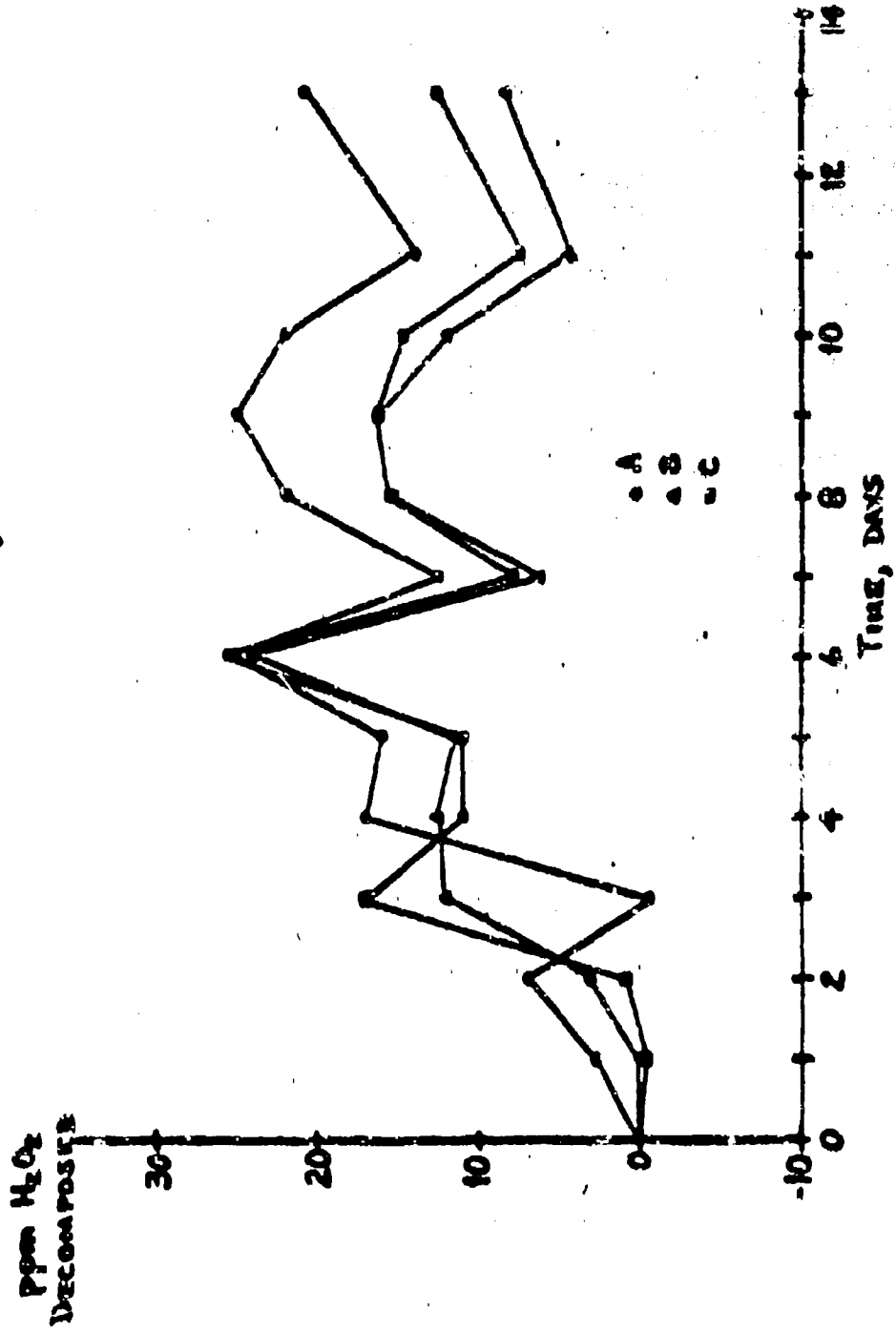


FIGURE S-10
TYPICAL OXYGEN EVOLUTION - 93% N₂O₂
SERIES 1, -30°C.

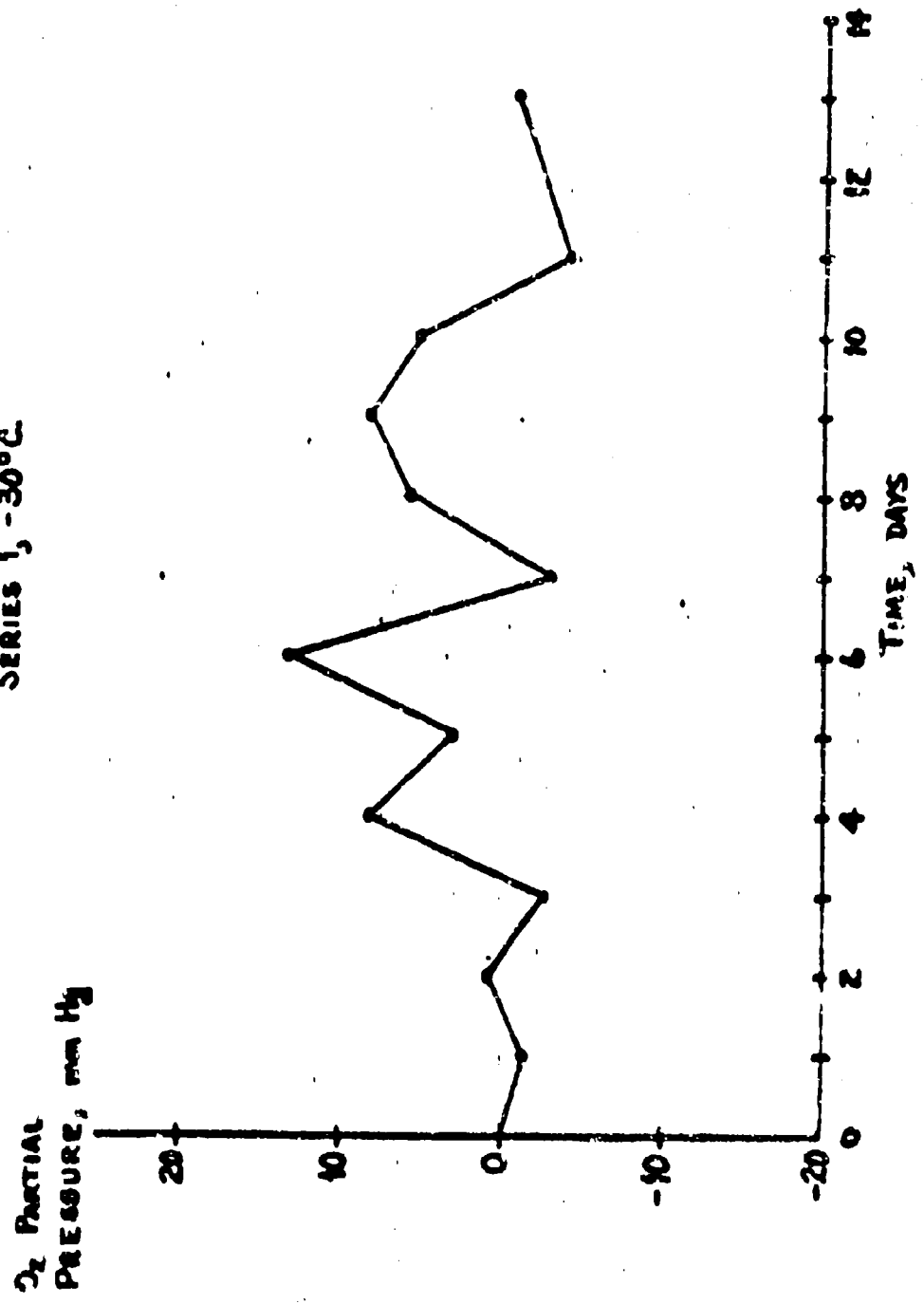


FIGURE 5-11
TYPICAL DECOMPOSITION RATES
SERIES I, 0°C.

13

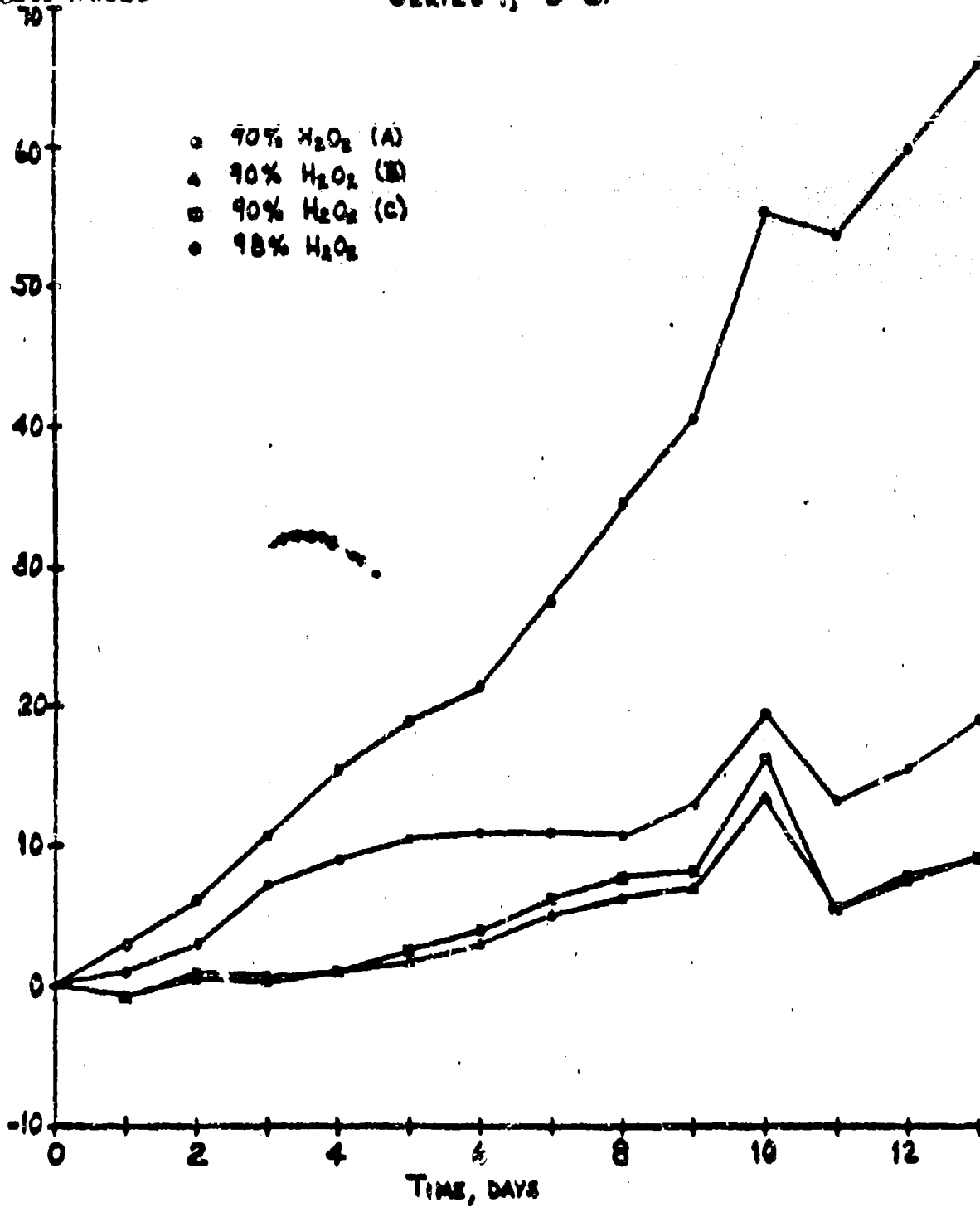
ppm H_2O_2
DECOMPOSED

FIGURE S-12
TYPICAL OXYGEN EVOLUTION
SERIES 2, -60°C.

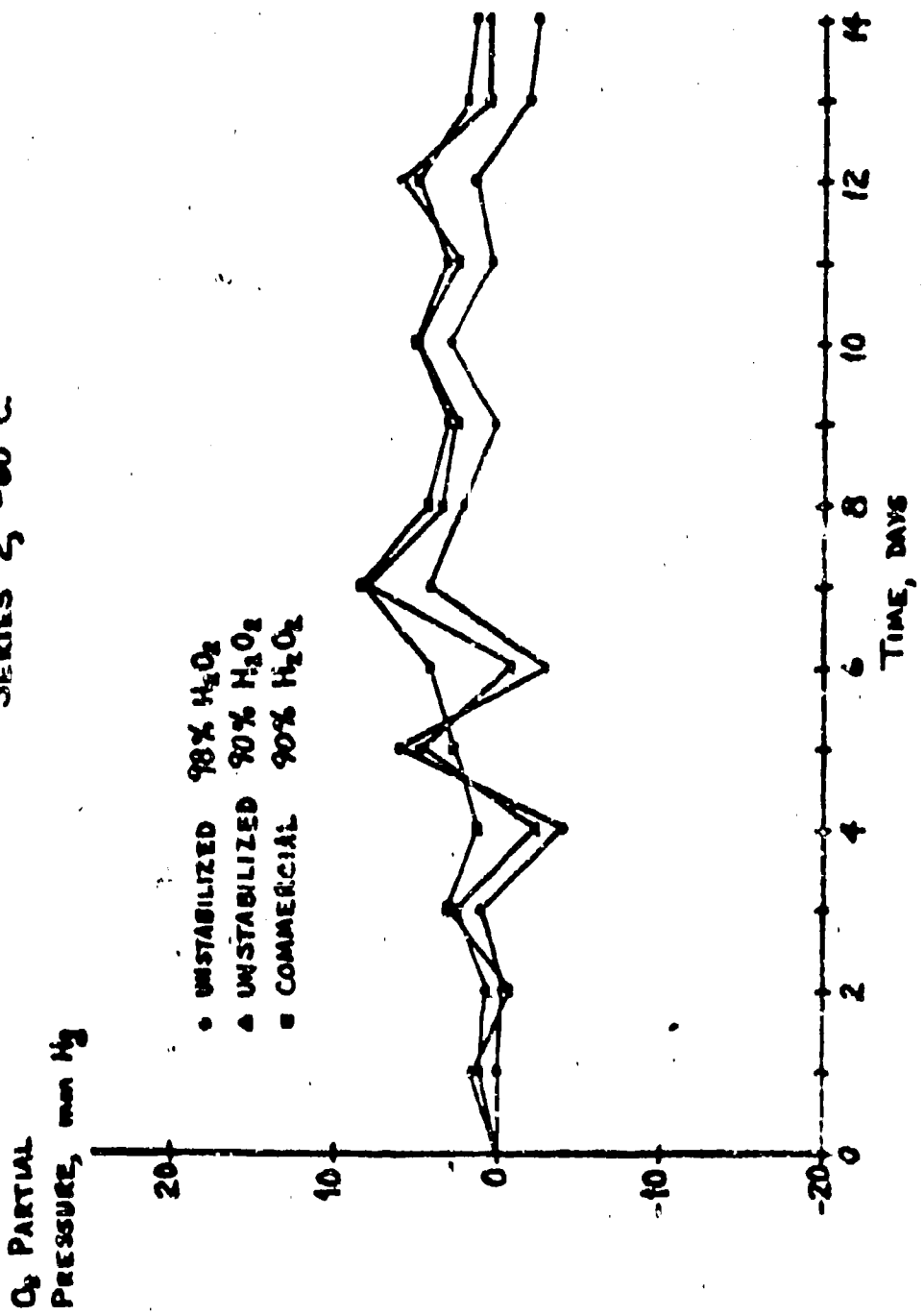


FIGURE S-13
TYPICAL OXYGEN EVOLUTION
SERIES 2, -30°C.

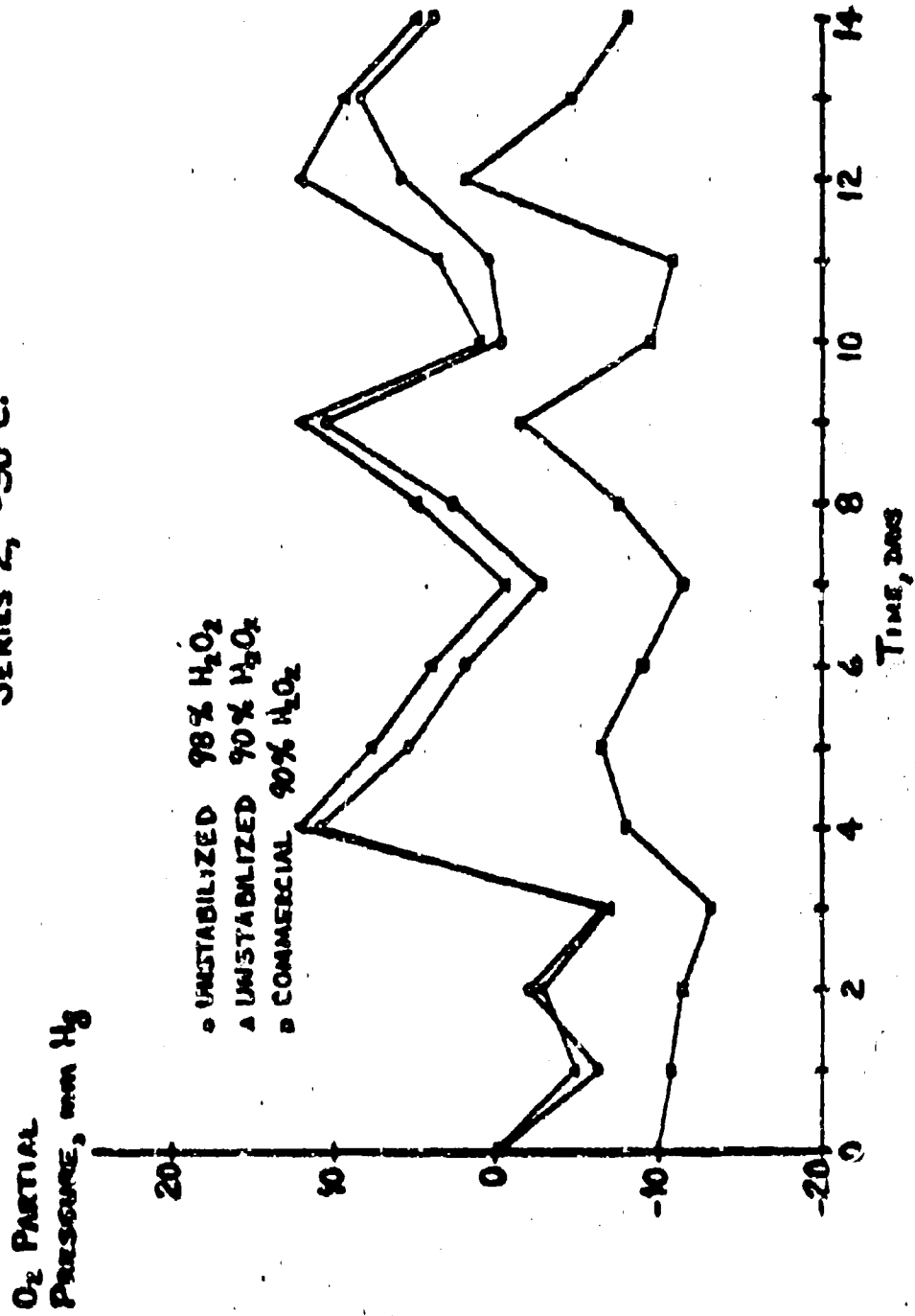
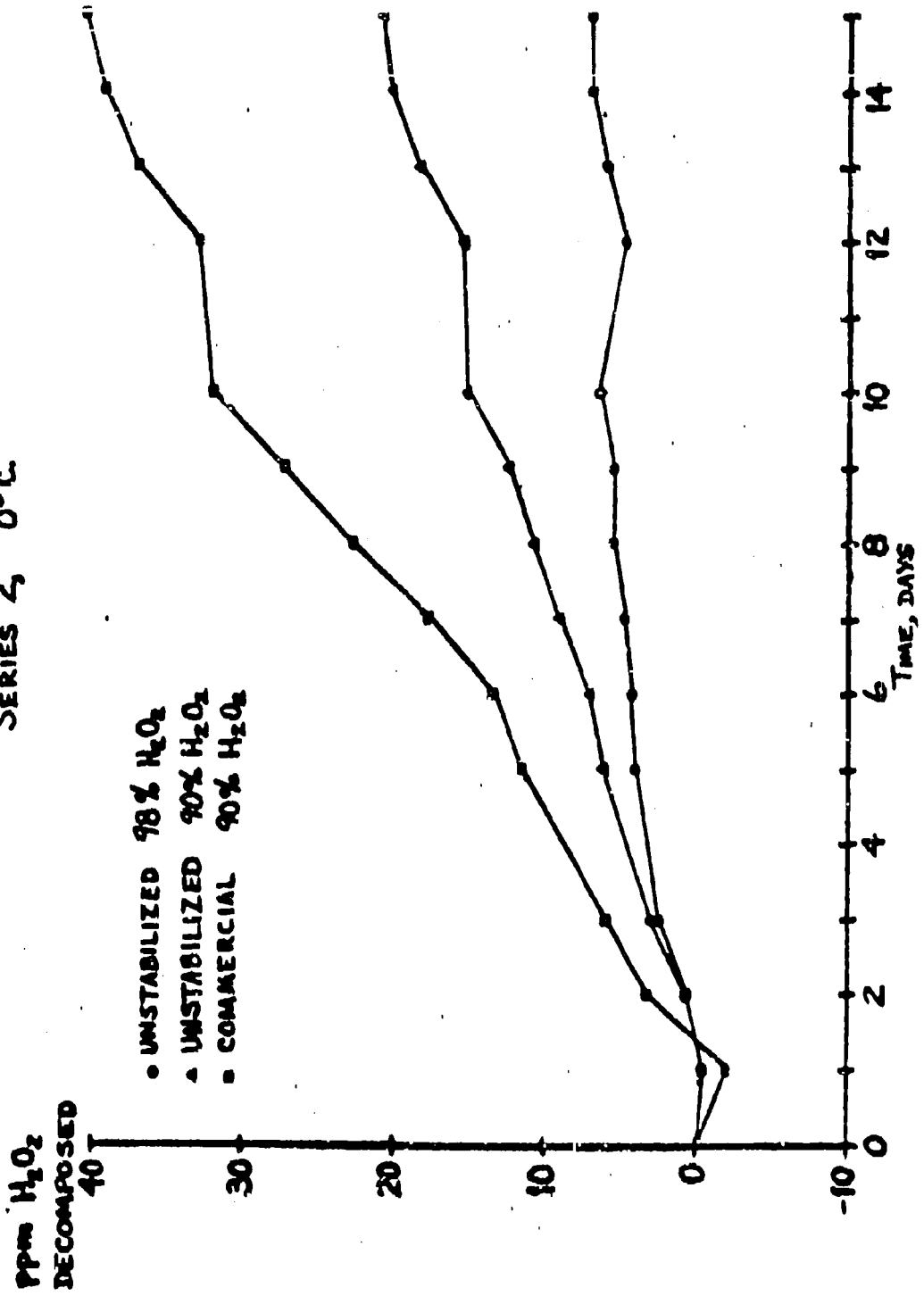


FIGURE S-14
TYPICAL DECOMPOSITION RATES
SERIES 2, 0°C.



SECTION II - SURFACE INERT TO HIGH STRENGTH H_2O_2
AND DECOMPOSITION MECHANISMS OF H_2O_2

Introduction

The stability of high strength hydrogen peroxide depends largely on the nature of the container in which it is stored and the concentration of adventitious impurities present in solution or in suspension. Empirical studies on container materials and additives during the past 50 years have produced a variety of techniques for passivating container surfaces and decreasing the activity of catalytic ions present in solution. It is the purpose of this study to examine the reaction mechanisms of hydrogen peroxide in order to understand the basic chemistry involved in hydrogen peroxide-container interactions and hydrogen peroxide-catalytic ion interactions.

The experimental program developed to analyze these reactions included:

- (a) Electron spin resonance studies on flowing solutions of hydrogen peroxide rapidly mixed with a catalyst,
- (b) Optical absorption studies on flowing solutions of hydrogen peroxide rapidly mixed with a catalyst,
- (c) Attenuated total reflectance studies on surfaces exposed to high strength hydrogen peroxide,

- (d) Gasometric analysis of high strength hydrogen peroxide solutions at elevated temperatures.
- (e) Photochemical initiation studies on hydrogen peroxide solutions with additives, and
- (f) Electron irradiation of container materials.

A brief review of the current literature regarding hydrogen peroxide and the intermediates formed during the decomposition reactions is presented to form the basis for understanding the reaction mechanisms. The transient free radicals generated during the decomposition process are hydroxyl ($\cdot\text{OH}$) and perhydroxyl ($\cdot\text{O}_2\text{H}$) together with their ionized forms ($\cdot\text{O}^-$ and $\cdot\text{O}_2^-$).

The bond dissociation energies of the principal species present in solution are shown in Table I. In H_2O , H_2O_2 and $\cdot\text{OH}$, the H-O dissociation energy is 100 kcal. or greater which indicates high stability toward rupture or chemical reaction involving that bond. The weaker bonds as indicated in Table I are the O-O bond in H_2O_2 (56 kcal.) and the H-O bond in $\text{HO}_2\cdot$ (36 kcal.).

The electron affinities of $\cdot\text{OH}$, $\text{HO}_2\cdot$ and O_2 are tabulated in Table II. These values indicate that both $\cdot\text{OH}$ and $\text{HO}_2\cdot$ are powerful oxidizing agents and that $\cdot\text{O}_2^-$ can act as a reducing agent by supplying 79 kcal. It is the

reducing power of $\cdot O_2^-$ which leads to the chain reaction of hydrogen peroxide.

The most thoroughly studied metal ion catalyzed decomposition reaction of hydrogen peroxide has been carried out using the ferrous-ferric system. The energetics of the individual steps involved have been compiled by Uri¹ and are presented in Table III along with the known rate constants. The ratio of k_6/k_7 was found to be 1.0 at pH 2.6 and decreased at lower pH values² (probably due to protonation of $\cdot O_2^-$). Since most of the rate constants for this partial series of reactions are as yet unknown, a more thorough discussion of the kinetics is not warranted. One of the main problems in a discussion of transition metal ions is that the free ion is rarely present in solution. Instead, there is some form of complex with the solvent or anions in solution. In the ferric-ferrous system, for example, the coordination number is 6 for each ion and may include water, hydroxyl ions and other anions in solution. If each form is the hexahydrate, then the system would be well characterized by a single redox potential, but this is unlikely.

The acid-base equilibrium involved in hydrogen peroxide reactions, excluding metal ions, are reasonably well established. These values, shown in Table IV), indicate

that (a) in strong acid solutions ($\text{pH} < 2$) only the protonated forms of $\cdot\text{O}^-$, HO_2^- , $\cdot\text{O}_2^-$ and HO_3^- need to be considered, (b) in neutral solution $\text{HO}_2\cdot$ is largely ionized, and (c) in strongly basic solutions $\cdot\text{OH}$, H_2O_2 , $\text{HO}_2\cdot$ and H_2O_3 are at least partially ionized. It is obvious that these equilibria lead to a multiplicity of reactions, few of which can be neglected.

One example will serve to illustrate the proliferation of competing reactions upon ionization. In basic solutions, the hydroxyl radical ionizes to $\cdot\text{O}^-$ and H^+ , followed by the reaction of $\cdot\text{O}^-$ with O_2 to give the ozonide ion, O_3^- . The series of eight reactions shown in Table V explain why there have been reports in the literature of smelling ozone in peroxide solutions.

To study the reaction mechanisms of hydrogen peroxide, it is necessary to generate sufficiently high concentrations of the intermediates for observation by some analytical technique. Pulse radiolysis, flash photolysis and rapid flow systems are currently producing valuable data on these systems. A summary of the transients observed is presented in Table VI, some of their most important rate constants in Table VII, and optical absorption data in Table VIII.

The hydroxyl radical is one of the most reactive chemical species known. It can abstract hydrogen atoms or electrons from virtually any organic or inorganic compound to form a bond whose energy is over 120 kcal./mole. In high strength hydrogen peroxide solutions, practically all hydroxyl radicals formed by any means would react with hydrogen peroxide ($k = 4.5 \times 10^7 \text{ M}^{-1} \text{ sec}^{-1}$) to generate the somewhat less reactive perhydroxyl radical.



When, in addition to hydrogen peroxide, there are inorganic and/or organic additives in solution, the chemistry can become much more complex. Table IX presents the rate constants for the reaction of hydroxyl radicals with the halide ions Cl^- , Br^- and I^- . No reaction with the fluoride ion is

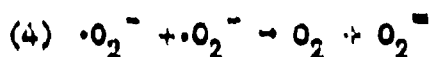
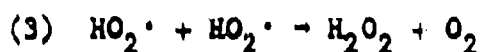


(where X = Cl, Br or I)

predicted or has been found. The reaction of hydroxyl radicals with chloride ions is very sensitive to pH, being almost diffusion controlled in acid solution and several orders of magnitude slower in neutral solution.

Only a few studies have been reported so far on the oxidation rates of metal ions by hydroxyl radicals. These are shown in Table X and indicate very rapid reactions with such ions as Fe^{+2} , $\text{Fe}(\text{CN})_6^{+4}$, Sn^{+2} , Tl^{+1} and Ce^{+3} . Inorganic anions such as CO_3^- , CNS^- , NO_2^- , SO_3^- , HSO_3^- , and HSO_4^- are also oxidized by hydroxyl radicals with rate constants ranging from 10^7 to $10^9 \text{ M}^{-1} \text{ sec}^{-1}$ as shown in Table XI.

Whereas the reactivity of the hydroxyl radical is now reasonably well characterized, such is not the case for the longer lived perhydroxyl radical. The main facts known about perhydroxyl are that its $\text{pK} = 4.5 \pm 0.2$ and that the termination reactions, 3 and 4, have rate constants of



5×10^6 and $3 \times 10^7 \text{ M}^{-1} \text{ sec}^{-1}$, respectively. Therefore, in acid solution having $\text{pH} \sim 2$ and concentrations of $\text{HO}_2 \cdot$ at 10^{-8} M , the lifetime of $\text{HO}_2 \cdot$ would be about 3 seconds. At the same pH, the lifetime of $\text{HO}_2 \cdot$ would be about 3 msec in $10^{-5} \text{ M HO}_2 \cdot$ solutions. All reactions of $\text{HO}_2 \cdot$ studied in pH ranges of 3-7 must also include considerations of the

$\cdot O_2^-$ form since the reactivity of $HO_2\cdot$ and $\cdot O_2^-$ would be expected to differ markedly.

Experimental

The experimental studies on the stability of high strength hydrogen peroxide are divided into two major sections. The first describes work done on container material-hydrogen peroxide interactions and the second on reaction mechanisms of hydrogen peroxide decomposition.

A. Container Material-Hydrogen Peroxide Interactions

The ideal container material for high strength hydrogen peroxide should have a surface which in no way contributes to the decomposition of the hydrogen peroxide container therein. The best candidates having inert surfaces are metals which form a continuous insoluble oxide coating, glass in which catalytic sites have been passivated, and plastics having no reactive functional groups. From these groups, aluminum, pyrex glass, polyethylene and "Teflon"[®] were chosen for detailed study with respect to stability toward 90% hydrogen peroxide.

1. Aluminum - High purity aluminum (99.6% or greater) is considered to be one of the best container materials for high strength hydrogen peroxide. The normal treatment prior to use includes washing, oxidizing with nitric acid, steaming to seal the oxide pores and rinsing with high strength

hydrogen peroxide. In order to maintain long term stability, the oxide coating formed in this manner should not be weakened on standing in contact with the peroxide.

A typical aluminum composition used is Type 1060 which has impurity limits of 0.25% Si, 0.35% Fe, 0.05% Cu, 0.03% Mn, 0.03% Mg, 0.05% Zn, and 0.03% Ti. Although the impurity levels appear to be very low, only a trace of iron or copper contamination in the peroxide could cause considerable catalytic decomposition.

The resistance of a passivated aluminum 1060 surface was tested in the following manner. Small strips of aluminum (1/2" x 2" x 1/32" thick) were exposed to nitric acid, then dyed by immersing in a hot aqueous solution of "Pontamine" Fast Turquoise 8GLA, then sealed by exposure to steam for 1/2 hour. The blue dye was added as a tracer to follow the condition of the oxide film. After a final wash, the test strips were exposed to 90% hydrogen peroxide at 66°C. Ten minutes exposure of the passivated aluminum to the hot peroxide solution caused complete bleaching of the blue surface.

It is apparent that a surface treated in the usual manner is not completely sealed. The additive may be free to migrate out, the peroxide may diffuse in and destroy the dye, or both effects may be operative. In either event, an

extensive study on the nature of the oxide coating on aluminum containers would be required to determine the rate of peroxide attack.

A series of high purity aluminum foils (99.45 - 99.999% Al) were exposed to 90% hydrogen peroxide at 66°C for times up to 300 hours. The degree of surface attack on these samples was studied by Mr. N. A. Nielsen of the Du Pont Engineering Department using optical and electron microscopy. Results of these studies are reported in Appendix A.

Two routes are available for increasing the acceptability of aluminum containers. One method is to use higher purity aluminum, and the other is to increase the quality of the oxidizing treatment.

2. Pyrex Glass - Pyrex and quartz are regarded as excellent container materials, although in some cases the possibility of breakage may present a problem. Surfaces of these materials must be scrupulously cleaned as in the case of aluminum. Washing with hot nitric acid and distilled water followed by a rinse with high strength hydrogen peroxide usually provides a passivated surface.

Data taken on the decomposition of 90% hydrogen peroxide in a passivated and unpassivated pyrex bottle are presented in Figure 1 for comparison with "Teflon" FEP containers.

The value of 1.06% decomposition per week at 66°C for a passivated container compares favorably with the rate of 1.0% reported in the literature.³⁷

3. Polyethylene - At room temperature, polyethylene has a very high rating for compatibility with 90% hydrogen peroxide. However, at its melting point, a detonation reaction occurs.³⁸

Analyses of the surface of polyethylene samples were carried out using a Wilks Model 12 double-beam internal reflection attachment for the Perkin-Elmer 221 infrared spectrophotometer. Use of this instrument, shown in Figure 1, allows film samples to be alternately exposed to high strength hydrogen peroxide solutions and then analyzed without altering the surface. Figure 2 shows the equipment used for exposing the film samples to 90% hydrogen peroxide at various temperatures. The holders are constructed entirely of "Teflon."

The relative rate of attack of polyethylene by 90% hydrogen peroxide at 50°C and 70°C is shown in Table XII. The results indicate a very strong temperature dependence for the growth of the C-O band at 1050 cm^{-1} and the C=O band at 1710 cm^{-1} , and a somewhat slower rate for the C-O band at 1640 cm^{-1} and the O-H band at 3400 cm^{-1} .

A comparison of the rate of oxidation of linear and branched polyethylene by 90% hydrogen peroxide at 70°C was also carried out by attenuated total reflectance (ATR) analysis. Data presented in Tables XIII and XIV show that the free carbonyl at 1710 cm^{-1} which forms readily in branched polyethylene is completely absent in oxidized linear polyethylene.

Infrared absorption spectra taken on the film samples showed no C-O, C=O or O-H absorption indicating that the attack was, in fact, only at the surface of the film sample. In view of the mechanism of hydrogen peroxide decomposition, it is expected that attack by hydroxyl radicals would start the oxidation of polyethylene. Continued oxidation can then occur at the functional group leading to a rapid chain reaction. Therefore, polyethylene containers should be considered unsuitable for high strength hydrogen peroxide at elevated temperatures.

4. Fluorocarbon Polymers - "Teflon" films were studied using the same ATR equipment and exposure technique described for polyethylene films. Exposure of "Teflon" film to 90% hydrogen peroxide for 500 hours at 70°C generated no change in the surface composition observable by ATR analysis.

Similar studies were carried out on an experimental perfluorosulfonic acid ion exchange membrane. As shown in

Figure 3, there is a growth of a carbonyl band at 1630 cm^{-1} and a hydroxyl band at 3400 cm^{-1} after 2 hours exposure to 90% hydrogen peroxide at 70°C . The hydroxyl band is due principally to the absorbed water in the membrane, but the carbonyl absorption indicates definite oxidation of the polymer.

Although perfluorocarbons having functional groups, such as sulfonic acids, may be unacceptable in contact with high strength hydrogen peroxide at elevated temperatures, the unsubstituted materials appear to be exceptionally stable. Quantitative studies on containers fabricated from "Teflon" FEP do not appear to have been published in the literature. For this reason, "Teflon" FEP bottles were obtained for comparison tests with pyrex and aluminum containers.

Figure 4 shows the rate of oxygen evolution from a 383-ml sample of 90% hydrogen peroxide in a "Teflon" FEP bottle at 66°C . The rate observed was linear for the period studied (5 hours). The constant temperature water bath together with the apparatus for measuring the oxygen evolved is shown in Figure 5. Also shown in Figure 4 are the rates of decomposition of 90% hydrogen peroxide in an unpassivated pyrex bottle, a passivated pyrex bottle and an irradiated "Teflon" FEP bottle (dose = $1.3 \times 10^{-2}\text{ kcal./cm}^2$). The experimental setup for

irradiating the "Teflon" FEP bottle with 2 Mev electrons from a resonant transformer is shown in Figure 6.

The decomposition rate data is summarized in Table XV for a number of aluminum alloys, pyrex and "Teflon" FEP. Hydrogen peroxide in the irradiated "Teflon" FEP container has approximately one-third the decomposition rate as that in a passivated aluminum container.

Additional irradiation experiments were run on "Teflon" FEP to determine the optimum conditions for improving the stability for the hydrogen peroxide contained therein. Figure 7 indicates that the initial irradiation (1-2 minutes at 0.5 ma) gives most of the improvement in stability observed. At low doses of irradiation, the physical properties of "Teflon" FEP are not changed significantly but at high doses (6.6×10^{-2} kcal./cm²) the plastic changes to a very brittle structure (see Figure 8).

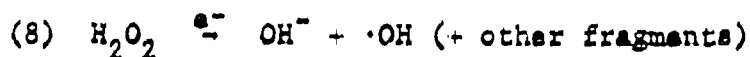
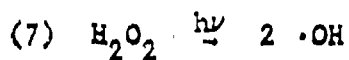
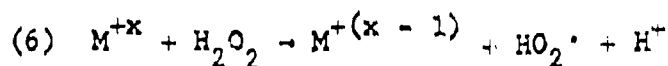
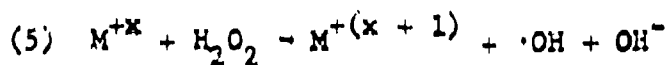
To determine the feasibility of retaining the stability and the physical strength in the low dose irradiation experiments, a series of "Teflon" FEP films were studied. As shown in Table XVI, dose rates of up to 2.0×10^{-2} kcal./cm² in air at 40°C result in films which are still very pliable (> 300% elongation) and tough (13 lbs. break strength for a 1" wide film .005" thick).

The effect of oxygen and water vapor on the irradiation vs. stability was characterized by irradiating a number of 100-ml "Teflon" FEP bottles under controlled conditions. The elimination of both oxygen and water vapor was accomplished using a dry argon purge during irradiation at both room temperature and 230°C. Decomposition tests after irradiation, shown in Table XVII, indicate very small changes with doses of 6.6×10^{-3} and 1.3×10^{-2} kcal./cm². The effect of oxygen in the absence of water vapor was carried out using a dry oxygen purge during irradiation. A dose of 1.3×10^{-2} kcal./cm² gave an enhancement of stability from 1.5% decomposition/week to 0.48%. The effect of water in the absence of oxygen was determined by filling a bottle with degassed water. A dose of 1.3×10^{-2} kcal./cm² gave an enhancement of stability from 1.8% decomposition/week to 1.1%. An air purge gave results essentially the same in an oxygen purge during irradiation. These results, which are summarized in Table XVII, indicate that a low dose of electron irradiation in an oxygen atmosphere at room temperature produces the maximum degree of stability for 90% hydrogen peroxide solutions.

B. Reaction Mechanisms of Hydrogen Peroxide Decomposition

It has been well established that pure hydrogen peroxide is a very stable material. Therefore, the decomposition

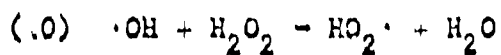
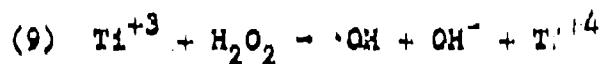
studies require an initiator to start the chain reaction. This initiation step may involve (a) a reducing agent, (b) an oxidizing agent, (c) ultraviolet radiation, or (d) electron irradiation. These initiators lead to the following series of reactions:



Experimental studies were carried out on a model reducing system using titanous chloride, a model oxidizing system using ceric salts, and a photochemical system using 2537 Å irradiation. Each of these reactions aids in the understanding of the over-all reaction mechanism.

1. Titanous Chloride-Hydrogen Peroxide - Rapid mixing flow cells were constructed to study the reaction of titanous chloride with hydrogen peroxide in an electron paramagnetic resonance (EPR) cavity. An early design was made of "Teflon" as shown in Figure 9 but was later substituted for quartz of the type described by Borg.³⁹ The first observation of a free radical intermediate in this reaction was by Dixon and Norman⁴⁰

who noted a single line spectrum which they assigned to the hydroxyl radical. Using the same reactants, Piette, et al.⁴¹ observed two lines which they assigned to $\text{NO}_2\cdot$ (low field) and $\cdot\text{OH}$ (high field). These radicals are thought to arise simply from reactions 5 and 6.



However, these early workers did not consider the following features of this reaction scheme:

- (a) Since the rate of reaction of $\cdot\text{OH}$ with H_2O_2 is $4.5 \times 10^7 \text{ M}^{-1}\text{sec}^{-1}$, the lifetime of free $\cdot\text{OH}$ in $10^{-2} \text{ M H}_2\text{O}_2$ would be extremely short. It is probable that a complex of the $\cdot\text{OH}$ is formed initially with the titanium ion to increase its lifetime in solution.
- (b) The interfering reaction of chloride ions with hydroxyl radicals in acid solution could lead to a series of radicals based on $\text{Cl}\cdot$ reactions.
- (c) Since the pK of $\text{HO}_2\cdot = 4.5 \pm 0.2$, the ionization of $\text{HO}_2\cdot$ can not be neglected.

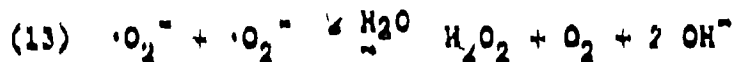
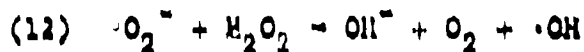
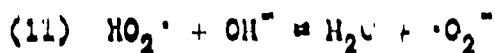
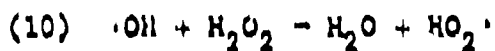
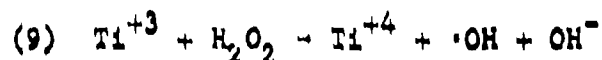
- (d) The assignment of the HO_2^{\cdot} to the low field EPR absorption and the $\cdot\text{OH}$ to the high field absorption was based on rates of reactivity. These rates may be markedly altered if complexed forms of the radicals are present.

To clarify the details of the titanous chloride-hydrogen peroxide reaction, a number of rapid flow experiments (> 100) were run in which the concentration of TiCl_3 , H_2O_2 and H^+ concentrations were varied while the EPR absorption was monitored.

In each experiment, two liters of the titanous solution and two liters of the hydrogen peroxide solution were prepared in the pressurized reservoirs shown in Figure 9. Pressures of up to 15 p.s.i.g. of nitrogen over the solutions allowed mixing of the solutions in the 10 milliliter mixing chamber in about 1 millisecond using flow rates of 600 cc./minute.

The EPR spectrum observed for a typical mixture of 10^{-3} M TiCl_3 with 10^{-3} M H_2O_2 is shown in Figure 10. The two lines are easily resolved and each have a line width at half maximum intensity of about 1 gauss. Addition of 0.1 M methanol to the reacting solution replaces the observed two line spectrum with the three line spectrum of hydroxymethyl. Similarly, by adding ethanol, the one line hydroxyethyl spectrum is observed.

The effect of hydrogen ion concentration on the high field absorption is shown in Figure 11. At high $[H^+]$, the high field absorption nearly disappears, giving only the single low field line observed by Dixon and Norman.⁴⁰ Figure 12 shows the effect of hydrogen peroxide concentration on the high field absorption, in which there is a linear increase of intensity with respect to the square root of the hydrogen peroxide concentration. This dependence would be expected from the following series of reactions involving the superoxide ion.



Assuming a steady state concentration of $\cdot O_2^-$ is attained, then

$$[\cdot O_2^-] = \sqrt{k [\cdot OH] [H_2O_2]}$$

Spectra run on neutral solutions, where the reaction of hydroxyl with chloride ion would not be expected to interfere,

also gave the two line pattern shown in Figure 10. These data, combined with the pH and hydrogen peroxide concentration studies, suggest that the high field line observed is $\cdot O_2^-$ and the low field line is $\cdot OH$ (or a complexed form of $\cdot OH$).

Stopped flow studies on the titanous chloride-hydrogen peroxide system were studied by incorporating a fast closing (100 μ sec) valve at the exit of the flow system. Figure 13 shows the growth and decay observed in the reaction of 1.3×10^{-2} M $TiCl_3$ with 1.3 M H_2O_2 . At point A, the flow was started by opening the valve. Solutions of equal proportions were mixed at a combined flow rate of 300 cc./minute. The maximum signal for a steady flow was observed at point B, approximately 50 msec after the valve was opened. Closing the valve (point C) caused a further increase in signal level to point D. The transient radical concentration then decayed to one-half of its maximum value in about 200 msec.

The observed kinetics of the reaction are governed almost entirely by the initiation step 9, whose rate constant is $1.5 M^{-1} sec^{-1}$.⁴¹ Both the propagation and termination reactions have rate constants from 10^7 to $10^9 M^{-1} sec^{-1}$ as shown in Table VII.

A large number of flow experiments were run with the analogous ferrous ion reduction of hydrogen peroxide described in Table III. This reaction, called Fenton's reagent, is the classic technique for generating hydroxyl radicals in solution for reaction with organic materials. However, even under optimum conditions of high H_2O_2 concentration ($> 1 M$) and low ferrous concentrations ($< 10^{-3} M$), no transient radicals could be observed.

The effect of added ferrous ion on the hydroxyl radical signal in the $Ti^{+3}-H_2O_2$ system was studied by adding ferrous sulfate to the titanous solution. Concentration of 6×10^{-4} to $6 \times 10^{-3} M Fe^{+2}$ in a solution of $10^{-3} M TiCl_3$ reacted with $10^{-2} M H_2O_2$ solution markedly decrease the steady state concentration of hydroxyl radicals, as shown in Figure 14. This decrease is expected due to the rapid reaction of hydroxyl radicals with ferrous ions ($k = 2.6 \times 10^8 M^{-1} sec^{-1}$).

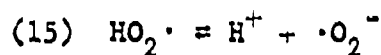
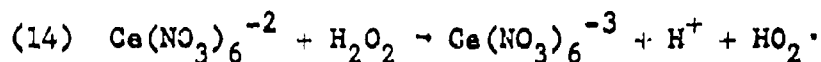
3. Ceric Oxidation of Hydrogen Peroxide - The ceric ion oxidation of hydrogen peroxide has long been used as an analytical method for the determination of hydrogen peroxide in various solutions, particularly those containing organic materials such as alcohols and ethers.⁴² Using a flow system similar to that described in the previous section, Saito and Bielski^{9,10}

observed a single line EPR signal with $g = 2.016$ and a line width of 27 gauss for the ceric sulfate-hydrogen peroxide reaction. Using ceric ammonium nitrate and hydrogen peroxide in acid solution, Pietta, et al.⁴¹ observed a single line at $g = 2.0185$ having a line width of 1 gauss. Our studies confirmed these results and showed very erratic effects dependent on acid strength.

The chemistry of the ceric ion is dependent on its particular complex in solution. Ceric sulfate in dilute solutions of sulfuric acid forms the sulfato-cerate complex, $\text{Ce}(\text{SO}_4)_4^{-4}$, whereas ceric ammonium nitrate is originally in the nitrate-cerate form $\text{Ce}(\text{NO}_3)_6^{-2}$. The only form of Ce^{+4} never observed (contrary to the reactions normally written) is that indicated as the free ion. Since the reactions of the cerate ions with hydrogen peroxide involve electron transfer, one of the most important properties of the system is the effect of complexing on the electrode potential. Standard electrode potentials for ceric complexes vary from 1.28 to 1.70 volts depending on the acid present (HCl , 1.28 V; H_2SO_4 , 1.44 V; HNO_3 , 1.61 V; HClO_4 , 1.70 V).⁴³

To avoid the complex equilibrium of anions in the ceric coordination sphere, the reaction of the nitrate-cerate ion with hydrogen peroxide was carried out in neutral solutions.

A very strong single line spectrum having a line width of about 1 gauss was found which is assigned to the superoxide ion. The reaction sequence postulated is:



Absorption spectra were taken on the nitrate- and sulfato-ceric complexes for their analysis in the optical flow cell (Figure 15). Figure 16 shows the effect of sulfuric acid on the nitrate complex. The broad absorption of the nitrate-cerate complex from 250 to 300 m μ is converted to that of the sulfato-cerate complex in 1 N sulfuric acid having ϵ_{max} at 320 m μ . The sulfato-cerate absorption generated from the nitrate-cerate (Figure 17) compares favorably with that produced from ceric sulfate in 1 N sulfuric acid. The short wavelength absorption at 240 m μ is primarily due to the displaced nitrate ion.

Figures 18 and 19 show the spectra obtained on (I) unreacted, (II) flowing, and (III) final (after complete reaction) solutions of nitrate-cerate and sulfato-cerate with hydrogen peroxide. In each case, there were no new transient absorption bands observed, and the final spectra were identical to those of the flowing systems (200 cc./minute).

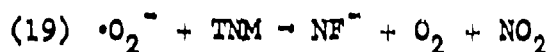
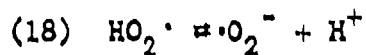
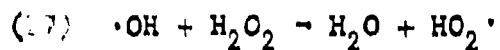
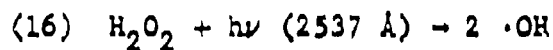
Of particular importance is the reactivity of the superoxide ion with various additives such as cupric ions, ferric ions, and methanol. Table XVIII correlates the data taken on these materials added to the nitrate-cerate-hydrogen peroxide reaction. Methanol, in concentrations up to 3.0 M, had no effect on the superoxide signal and generated no new absorption lines, such as those previously observed for hydroxymethyl ($\cdot\text{CH}_2\text{OH}$) when hydroxyl radicals are present in the generating system. Ferric ions showed no effect up to 10^{-3} M, but cupric ions dramatically decreased the $\cdot\text{O}_2^-$ concentration even at the 1.25×10^{-5} M additive level. Since the concentration of $\cdot\text{O}_2^-$ in solution is about 10^{-5} M, then the rate constant for the superoxide reduction of cupric ions must be comparable to the disproportionation reaction ($3 \times 10^7 \text{ M}^{-1}\text{sec}^{-1}$).

These studies provide an insight into both the catalytic decomposition of hydrogen peroxide by copper ions and the inhibition of the decomposition noted by adding methanol to peroxide solutions.^{44,45,46} The rapid reaction of cupric ions with $\cdot\text{O}_2^-$ gives confirmation of the reducing power of the superoxide intermediate. The lack of reaction of methanol with $\cdot\text{O}_2^-$ suggests that the stabilizing effect by the alcohol functions through hydroxyl scavenging.

No evidence for hydroxyl radicals was observed in any of the reactions so that it is concluded that the reaction of superoxide with hydrogen peroxide is at least 10^5 times slower than the disproportionation step for superoxide. This comes about through the ratio of $\cdot O_2^-/H_2O_2$ ($\sim 10^{-5} M/2 \times 10^{-1} M$) present in the solution.

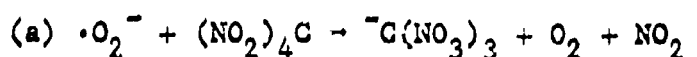
4. Photochemical Dissociation of Hydrogen Peroxide -

Numerous studies have been reported in the literature on the photochemical dissociation of hydrogen peroxide to hydroxyl radicals and subsequent reactions thereafter. The objective of further studies on this system was to convert the hydroxyl radicals to perhydroxyl using the reaction with excess hydrogen peroxide and then trap the perhydroxyl (or superoxide) with a scavenger. This was accomplished using tetranitromethane (TNM) through the following series of reactions. [NF⁻ represents the nitroform ion ${}^-C(NO_2)_3$.]



71
- 25 -

The reaction of tetranitromethane with the superoxide ion was first studied by Henglein and Jaspert.⁴⁷ They noted that the γ -radiolysis of water produced a species (O_2^-) which reacted with TNM to produce the nitroform ion.



Further studies by Czapski and Bielski⁴⁸ on electron-irradiated aqueous solutions indicated that neither TNM nor NF^- reacts with hydrogen peroxide above pH 2. This lack of reactivity eliminates a large number of secondary reactions which would be initiated by the cyclic reactions with hydrogen peroxide. Using pulse radiolysis studies on aqueous TNM solutions, Rabani, Mulac and Matheson⁴⁹ determined the rate constants for the reaction of $\cdot\text{O}_2^- + \text{TNM}$ ($k = 1.9 \times 10^9 \text{ M}^{-1}\text{sec}^{-1}$) and $\text{HO}_2\cdot + \text{TNM}$ ($k < 2 \times 10^5$).

The photolysis experiments were carried out using a low-pressure mercury arc with the filter system shown in Figure 20 to isolate the 2537 Å line. A 1-cm path length through 1 atm. chlorine gas plus a 1-cm path length through a saturated solution of $\text{NiSO}_4\text{-CoSO}_4$ aqueous solution gave an absorbance greater than 2 from 320 to 550 m μ . In addition to isolating the 2537 Å Hg line, the filters also prevented

absorption and possible photolysis of NF^- by radiation in the 350 $\text{m}\mu$ region. Calibration of the radiation intensity was determined by ferrioxalate actinometry using the method of Hatchard and Parker.⁵⁰ Ultraviolet analyses of the nitroform ion generated were obtained using a Cary 14 spectrophotometer at 350 $\text{m}\mu$ ($\epsilon = 1.5 \times 10^4$).

The quantum yield for production of nitroform from TNM in 10^{-2} M H_2O_2 solutions was found to be 1.13 ± 0.10 . Assuming complete conversion of hydroxyl to perhydroxyl and trapping by TNM, the primary quantum yield for photolysis of H_2O_2 is one-half that for nitroform formation or 0.56 ± 0.05 . Figure 21 shows both the growth of NF^- in the early stages of photolysis and the ultimate destruction of NF^- on continued irradiation.

Studies by Volman and Chen,⁵¹ using allyl alcohol to trap the hydroxyl radicals formed during photolysis indicated a primary quantum yield of 0.54 ± 0.05 . The excellent agreement of yields based on both hydroxyl and perhydroxyl trapping techniques indicates that:

- (a) There is quantitative conversion of hydroxyl to perhydroxyl and
- (b) There is quantitative trapping of superoxide and perhydroxyl by tetranitromethane.

Acknowledgments

The author is indebted to Dr. V. Reilly of the Electrochemicals Department for technical discussions regarding high-strength hydrogen peroxide, Mr. N. A. Nielsen of the Engineering Department for both discussions and experimental work on the surface structure of oxidized aluminum, and Dr. N. Weston of the Engineering Department for electron microprobe analyses of aluminum samples. The enthusiastic assistance of Mr. J. White of the Radiation Physics Laboratory in carrying out the bulk of the experimental work described in this report is gratefully acknowledged.

J. P. Paris/gad
10/20/65

TABLE IBond Dissociation Energies¹

<u>Reaction</u>	<u>D, kcal.</u>
$\text{HOH} \rightarrow \text{H}\cdot + \cdot\text{OH}$	121
$\text{H}_2\text{O}_2 \rightarrow 2 \cdot\text{OH}$	56
$\text{H}_2\text{O}_2 \rightarrow \text{H}\cdot + \text{HO}_2\cdot$	102
$\cdot\text{OH} \rightarrow \text{H}\cdot + \text{O}$	100
$\text{HO}_2\cdot \rightarrow \text{H}\cdot + \text{O}_2$	36

TABLE II

Elemental Analysis of the Polymer

<u>Analysis</u>	<u>Found, %</u>
$C_{10}H_{12}O_2$ (g) = 0.10 (mg)	130
$H_{10}O_2$ (g) = 0.10 (mg)	101
O_2 (g) = 0.10 (mg)	99

TABLE III

Kinetics and Reaction Rates for Ferric-Ferrous
Catalyzed Hydrogen Peroxide Decomposition

	Reaction Step	Heat, kcal	Rate $M^{-1}sec^{-1}$	Ref.
(1)	$Fe^{+2} + H_2O_2 \rightarrow (Fe^{+3}OH^-) + OH$	- 6	12.6 ± 0.3 at $0^\circ C$ 03.0 ± 0.7 at $25^\circ C$	1 2
(2)	$OH + H_2O_2 \rightarrow H_2O + HO_2^{\cdot}$	+ 19	4.3×10^7	3
(3)	$Fe^{+2} + H_2O_2 \rightarrow O_2 + OH^- + (Fe)$	+ 14		
(4)	$Fe^{+2} + OH \rightarrow Fe^{+3} + OH^-$	+ 42	2.0×10^{11}	4
(5)	$Fe^{+2} + HO_2^{\cdot} \rightarrow Fe^{+3} + HO_2^-$	- 19		
(6)	$Fe^{+2} + O_2^{\cdot -} \rightarrow Fe^{+3} + O_2$	+ 10	*	5
(7)	$Fe^{+2} + HO_2^- \rightarrow Fe^{+3} + HO_2^{\cdot}$	- 19	*	6
(8)	$(Fe^{+3}OH^-) + OH \rightarrow Fe^{+2} + H_2O_2$	- 6		

* $k_2/k_1 = 1.0$ at $pH = 4.0$

TABLE IVAcid-Base Equilibria

	<u>Reaction</u>	<u>pK</u>	<u>Ref.</u>
(1)	$\cdot\text{OH} + \text{OH}^- \rightleftharpoons \cdot\text{O}^- + \text{H}_2\text{O}$	11.9 ± 0.2	15
(2)	$\text{H}_2\text{O}_2 + \text{OH}^- \rightleftharpoons \text{HO}_2^- + \text{H}_2\text{O}$	11.6	6
(3)	$\text{HO}_2\cdot + \text{OH}^- \rightleftharpoons \cdot\text{O}_2^- + \text{H}_2\text{O}$	4.5 ± 0.2	7
(4)	$\text{H}_2\text{O} + \text{H}_2\text{O} \rightleftharpoons \text{H}_3\text{O}^+ + \text{OH}^-$	14	
(5)	$\text{H}_2\text{O}_3 + \text{OH}^- \rightleftharpoons \text{HO}_3^- + \text{H}_2\text{O}$	9-10	8

TABLE VReactions Promoted By $\cdot\text{O}^-$

- (1) $\cdot\text{O}^- + \text{O}_2 = \text{O}_3^-$
- (2) $\text{O}_3^- + \text{H}_2\text{O} = \text{HO}_3^- + \text{OH}^-$
- (3) $\text{O}_3^- + \text{H}_2\text{O}_2 = \text{O}_3 + \text{OH}^- + \cdot\text{OH}$
- (4) $\text{O}_3^- + \cdot\text{OH} = \text{O}_3 + \text{OH}^-$
- (5) $\text{O}_3^- + \cdot\text{O}_2\text{H} = \text{O}_3 + \text{O}_2\text{H}^-$
- (6) $\text{O}_3^- + \text{HO}_2^- = \text{O}_3 + \text{OH}^- + \cdot\text{O}^-$
- (7) $\text{O}_3^- + \cdot\text{O}^- + \text{H}_2\text{O} = \text{O}_3 + 2 \text{OH}^-$
- (8) $\text{O}_3 = \text{O}_2 + \text{O}\cdot$

79
TABLE VI

Generation and Observation of Peroxide Fragments and Products

<u>Species Postulated</u>	<u>Method of Observation</u>	<u>Method of Observation*</u>	<u>Ref.</u>
HO_2^\cdot	a) $\text{Ce}^{+4} + \text{H}_2\text{O}_2$	D - EPR	9, 10
	b) Pulse radiolysis of aqueous solutions	D - Optical absorption spectrum	3
	c) Radiolysis of water	I - Optical absorption spectra of products	8
$\cdot\text{O}_2^-$	a) Pulse radiolysis of aqueous solutions	D - Optical absorption spectrum	11
$\cdot\text{OH}$	a) Pulse radiolysis of aqueous solutions	D - Optical absorption spectrum	12
	b) $\text{Ti}^{+3} + \text{H}_2\text{O}_2$	D - EPR	13
$\cdot\text{O}^-$	a) Pulse radiolysis of aqueous solutions	I - Rate of ferrocyanide oxidation	5
O_3^-	a) Photolysis of hydrogen peroxide	D - Optical absorption spectrum	14
H_2O_4	a) $\text{O}_3 + \text{H}^\cdot$	I - Analysis of decomposition product	15
	b) Glow discharge in water vapor	I - Analysis of decomposition product	15
H_2O_3	a) Radiolysis of water	I - Reaction with ferrous sulfate	8

*Code: D = direct observation of the species
 I = indirect observation of the species

TABLE VII

Rate Constants for Peroxide Fragments

<u>Reaction</u>	<u>k (M⁻¹sec⁻¹)</u>	<u>Ref.</u>
$\cdot\text{OH} + \cdot\text{OH} \rightarrow \text{H}_2\text{O}_2$	1.2×10^{10}	5
$\cdot\text{O}^- + \cdot\text{O}^- \rightarrow \text{O}_2^{\cdot-}$	2×10^9	5
$\text{H}_3\text{O}_2 + \text{H}^+ \rightarrow \text{H}_3\text{O}^+ + \text{O}_2$	6	8
$\cdot\text{OH} + \text{H}_2\text{O}_2 \rightarrow \text{HO}_2\cdot + \text{H}_2\text{O}$	4.5×10^7	3
$\text{HO}_2\cdot + \text{HO}_2\cdot \rightarrow \text{H}_2\text{O}_2 + \text{O}_2$		
at pH 0.5-1.5	4.8×10^6	9
pH 1.7-3.0	5.4×10^6	11
pH 2.0-3.0	4.4×10^6	8
pH 2.7	2.5×10^6	16
$\cdot\text{O}_2^- + \cdot\text{O}_2^- \rightarrow \text{O}_2 + \text{O}_2^{\cdot-}$		
at pH 5.0-7.0	3.4×10^7	11
pH 5.0-8.0	3.0×10^7	8
pH 5.5	2.9×10^7	17

TABLE VIIIOptical Absorption Data on H₂O₂ Fragments

<u>Species</u>	<u>λ (Å)</u>	<u>ϵ</u>	<u>Ref.</u>
HO ₂ [·]	2537 2300 (max.)	830 ± 125 1150	11
·O ₂ ⁻	2537 2400 (max.)	980 ± 140 1060	11
·OH	~ 2600 (shoulder)	~ 10 ³	12

TABLE IXRate Constants of Hydroxyl Radicals with Halogen Ions

<u>Reactant</u>	<u>pH</u>	<u>k (M⁻¹-sec⁻¹)</u>	<u>Ref.</u>
Cl ⁻	0	4 x 10 ⁹	18
	0	4 x 10 ⁹	19
	3	2 x 10 ⁷	19
Br ⁻	0	1.6 x 10 ¹⁰	18
	0-2	3.6 x 10 ¹⁰	20
	7	1.3 x 10 ⁸	21
	7	1.3 x 10 ⁹	22
	7	1.3 x 10 ⁸	23
I ⁻	7	1.6 x 10 ⁹	24
		~ 1.2 x 10 ⁹	25

TABLE X

Rate Constants of Hydroxyl Radicals with Metal Ions

<u>Reactant</u>	<u>pH</u>	<u>k (M⁻¹sec⁻¹)</u>	<u>Ref.</u>
Fe ⁺²	1	3.0 x 10 ⁸	26
	0	> 10 ⁸	27
	1.57	3.2 x 10 ⁸	28
	2.0	2.6 x 10 ⁸	29
	2.1	2.5 x 10 ⁸	28
	1.0	3.2 x 10 ⁸	30
Fe(CN) ₆ ⁺⁴	2.5-10.5	2.1 x 10 ⁹	31
Sn ⁺²	0.1	2 x 10 ⁹	32
Tl ⁺¹	0.1	8.5 x 10 ⁹	33
Ce ⁺³	0.1	2.2 x 10 ⁸	33,34

TABLE XIRate Constants of Hydroxyl Radicals with Various Anions

<u>Reactant</u>	<u>pH</u>	<u>k (M⁻¹sec⁻¹)</u>	<u>Ref.</u>
CO ₃ ⁻	7	8 x 10 ⁷	23
CNS ⁻	7	1.3 x 10 ⁹	23
OH ⁻		3.6 x 10 ⁸	24, 35
NO ₂ ⁻	7	2.5 x 10 ⁹	36
SC ₃ ⁻	7	1.2 x 10 ⁹	23
HSO ₃ ⁻	7	2.1 x 10 ⁹	23
HSO ₄ ⁻	0.1	3.3 x 10 ⁷	32

TABLE XII

Temperature Effect on Oxidation of Polyethylene Film by 90% H₂O₂

ATR (ν) cm^{-1}	Relative Absorbance Values					
	$\frac{2 \text{ hours}}{50^\circ\text{C}}$	$\frac{4 \text{ hours}}{50^\circ\text{C}}$	$\frac{70^\circ\text{C}}{70^\circ\text{C}}$	$\frac{23 \text{ hours}}{50^\circ\text{C}}$	$\frac{70^\circ\text{C}}{70^\circ\text{C}}$	$\frac{143 \text{ hours}}{50^\circ\text{C}}$
1050	.01	.02	.02	.03	.05	.16
1640	.01	.02	.02	.03	.05	.08
1710	.00	.00	.01	.01	.04	.07
3400	.01	.02	.03	.05	.08	.16

251

TABLE XIIIOxidation of Branched Polyethylene Film by 90% H₂O₂

<u>Hours Exposure to 90% H₂O₂ at 70°C</u>	<u>ATR Absorption Peaks (cm⁻¹) (Relative Absorbance Values)</u>				
	<u>1050</u>	<u>1100</u>	<u>1640</u>	<u>1710</u>	<u>1400</u>
0	0	0	0	0	0
2	0	0	0	0	.01
6	.02	.02	0	0	.03
29	.03	.03	.01	.01	.03
150	.04	.04	.02	.02	.04
518	.13	.13	.14	.14	.13

17

TABLE 22

Validation of Linear Polarization Vials in RSH MIRA

Solute Concentration in 100 mg/l at 10°C	Air Absorption Factor (m ²) (Relative Absorption Value)				
	1000	1000	1000	1000	1000
0	.01	.01	.01	0	0
1	.02	.02	.02	0	.02
2	.03	.03	.03	0	.03
3	.04	.04	.04	0	.04
4	.05	.05	.05	0	.05

TABLE IV

Stability of RFA (Hydrogen Peroxide) in Various Containers

<u>Sample Container</u>	<u>Rate of Decomposition per Week at 80°C (176°F)</u>
Aluminum alloys*	
Alcoa 1086	1.5
Alcoa 1100	3.0
Alcoa 1180	1.5
Alcoa 1810	1.5
Inactivated Pyrex**	1.0 (approx.)
Uninactivated Pyrex***	4.7
Passivated Pyrex***	1.80
Uninactivated "Inillon" Pyrex	1.84
Inactivated "Inillon" Pyrex (1.5 x 10 ⁵ negative)	0.44

*Data taken from Bulletin No. 104, House Chemical Division of Food Machinery and Electrical Association, 1941
 **Data taken from Bulletin No. 10-23, Supplement B, Food Manufacturing Chemicals Association, Inc., Chemical News Sheet on Hydrogen Peroxide, 1961.
 ***Data taken from this report, see Figure 4.

TABLE XVI

Physical Test Data on Irradiated "Mylar" FEP Films.

(Film samples were all 1" wide x 5" long x 0.005" thick.
Duplicate samples were run for each test.)

	Dose (kcal./cm ²) <u>2 Max. Electron</u>	<u>% Elongation</u>	<u>Lbs. Applied at Break</u>
	None	460	19.0
		420	16.7
Samples Irradiated in Air at 40°C	6.0 x 10 ⁻³	390	13.5
		360	14.3
	2.0 x 10 ⁻²	370	12.9
		390	13.8
	3.3 x 10 ⁻²	?	11.0
		3	10.7
	6.0 x 10 ⁻²	5	8.8
		2	8.5
Samples Irradiated in Argon at 250°C	4.4 x 10 ⁻³	110	10.7
		270	11.4
	2.0 x 10 ⁻²	17	11.3
		17	11.7
	3.3 x 10 ⁻²	27	12.4
		23	
	6.0 x 10 ⁻²	20	
		17	

TABLE XVII

Effect of Electron Irradiation of "Teflon"[®] FEP Container
on Stability of 90% Hydrogen Peroxide

Sample Bottles: 130-ml capacity

Volume of 90% Hydrogen Peroxide: 100-ml

Temperature for Measurement of Decomposition: $66 \pm 1^\circ\text{C}$

<u>Treatment of "Teflon" FEP Bottle</u>	<u>Rate of Decomposition per Week at 66°C (% of total)</u>
(1) Argon purge at room temperature	
a) no irradiation	1.3
b) 6.6×10^{-3} kcal./cm ²	1.1
c) 1.3×10^{-2} kcal./cm ²	0.88
(2) Argon purge at 230°C	
a) no irradiation	1.06
b) 6.6×10^{-3} kcal./cm ²	1.09
c) 2.6×10^{-2} kcal./cm ²	0.97
(3) Air purge at room temperature	
a) no irradiation	1.27
b) 1.3×10^{-2} kcal./cm ²	0.45
(4) Oxygen purge at room temperature	
a) no irradiation	1.54
b) 6.6×10^{-3} kcal./cm ²	0.56
c) 1.3×10^{-2} kcal./cm ²	0.48
(5) Bottle filled with degassed water	
a) no irradiation	1.8
b) 6.6×10^{-3} kcal./cm ²	1.0
c) 1.3×10^{-2} kcal./cm ²	

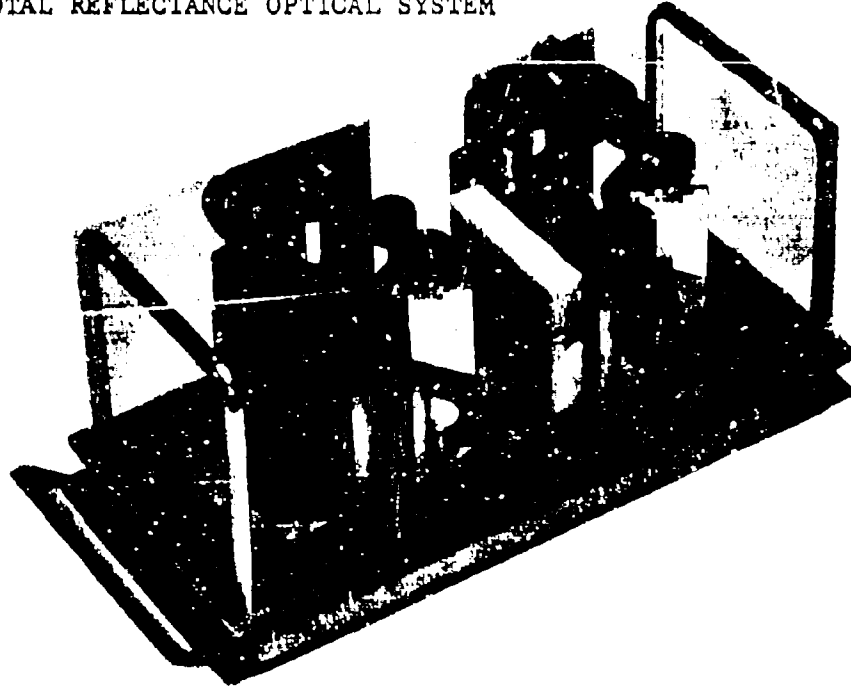
TABLE XVIII

Effect of Additives on Superoxide EPR Absorption

	Mixture		Flow Rate (ml/min.)	Relative Conc. of $\cdot O_2^-$
	Solution A	Solution B		
(1)	10^{-3} M $(NH_4)_2Ce(NO_3)_6$	0.2 M H_2O_2	300	63
(2)	10^{-3} M $(NH_4)_2Ce(NO_3)_6$ 1.25×10^{-5} M $CuSO_4$	0.2 M H_2O_2	300	35
(3)	10^{-3} M $(NH_4)_2Ce(NO_3)_6$ 1.0×10^{-3} M $FeCl_3$	0.2 M H_2O_2	300	62
(4)	10^{-3} M $(NH_4)_2Ce(NO_3)_6$	0.2 M H_2O_2 1.5 M Methanol	300	63
(5)	10^{-3} M $(NH_4)_2Ce(NO_3)_6$	0.2 M H_2O_2 3.0 M Methanol	300	63

FIGURE 1

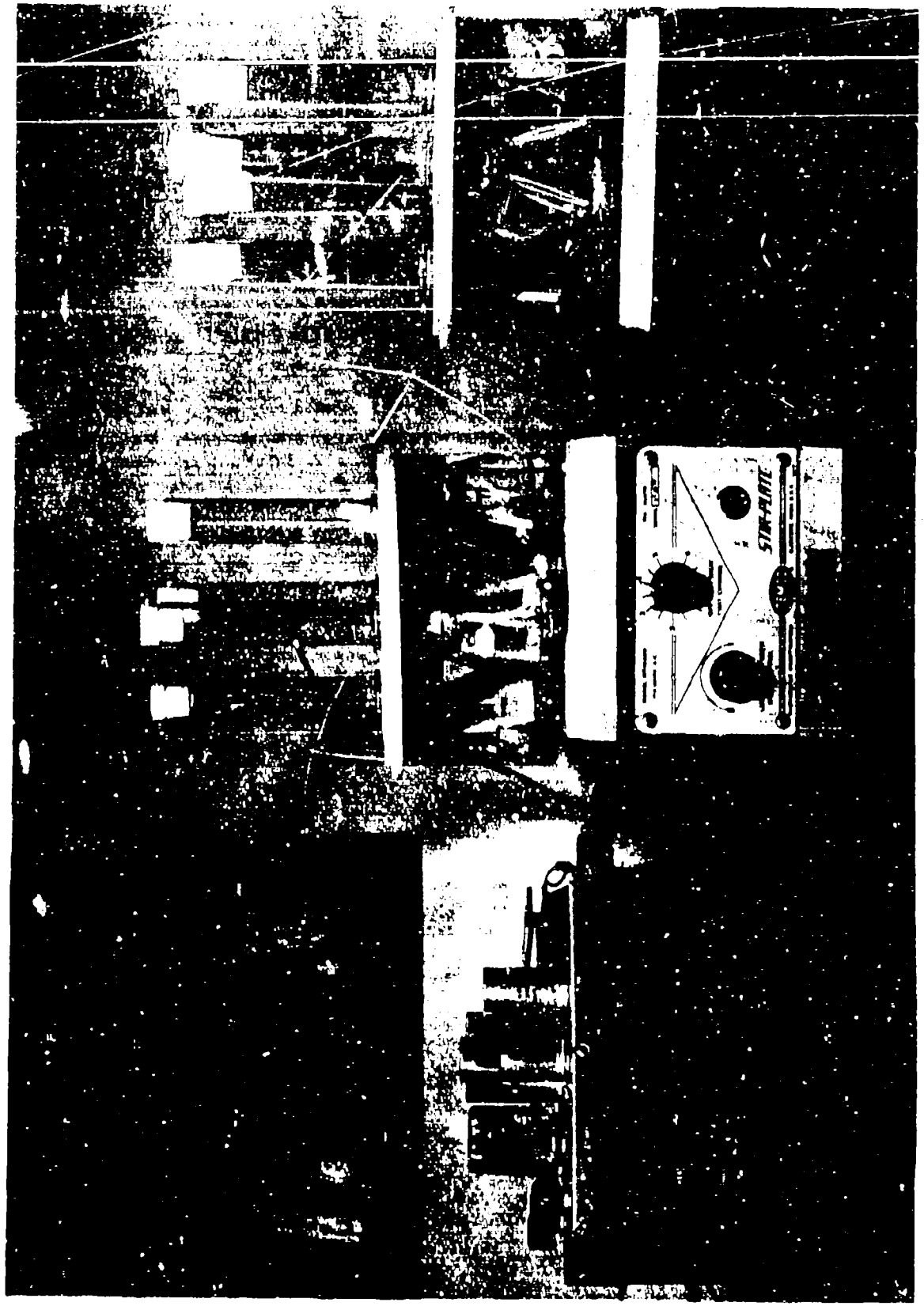
ATTENUATED TOTAL REFLECTANCE OPTICAL SYSTEM



EXPLODED VIEW OF SAMPLE HOLDER FOR ATR



CONSTANT TEMPERATURE BATHS FOR HYDROGEN PEROXIDE ATTACK OF POLYMER FILMS



EFFECT OF 90% HYDROGEN PEROXIDE ON A PERFLUORO
ION EXCHANGE MEMBRANE - ATR SPECTRUM

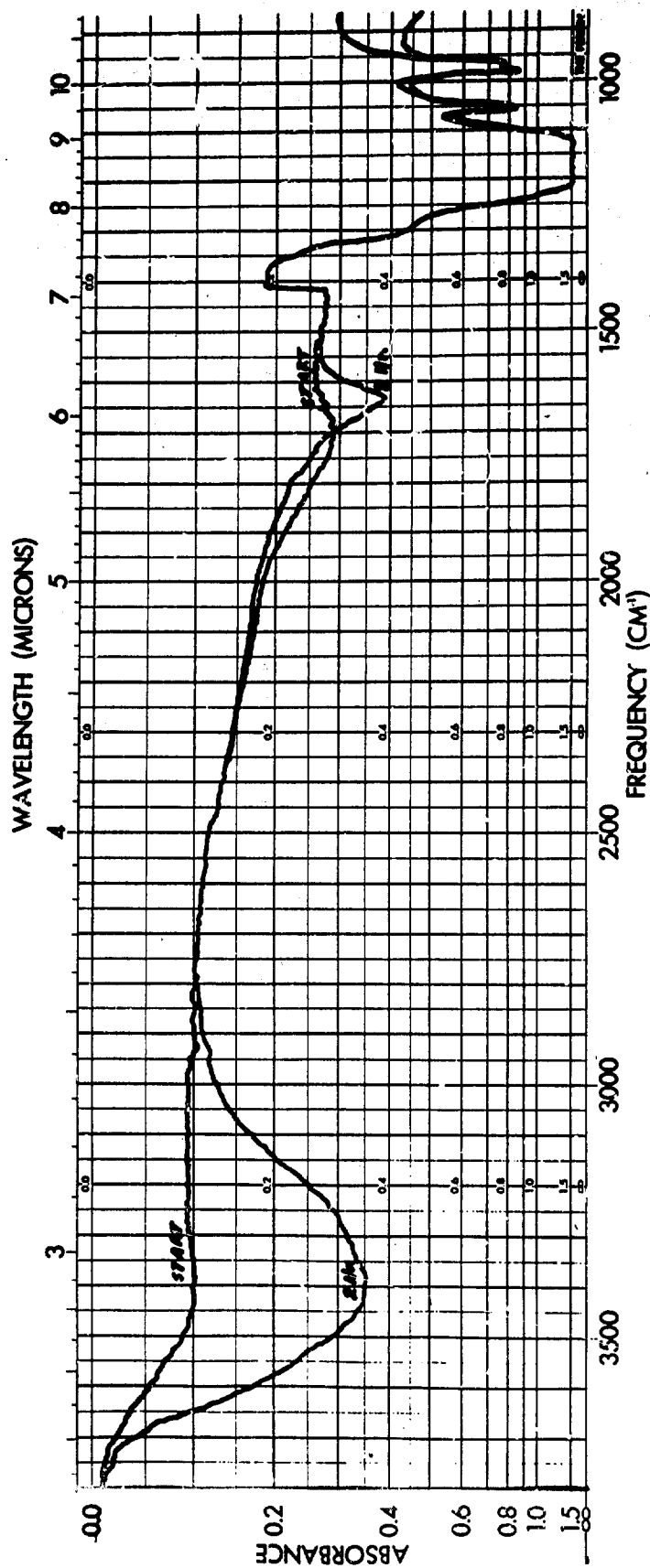


FIGURE 3

FIGURE 4

95

DECOMPOSITION RATE OF 90% HYDROGEN PEROXIDE IN PYREX AND "TEFLON" FEP CONTAINERS

- A-1 - 383 ml. 90% H₂O₂ in FEP bottle at 66°C (no irradiation)
- A-2 - Same as A-1 after irradiation FEP bottle (2 Mev. electron irradiation at 0.5 ma for 3 minutes)
- B-1 - 383 ml. 90% H₂O₂ in 16 oz. glass sample bottle (no passifying)
- B-2 - Same as B-1 after passifying glass bottle

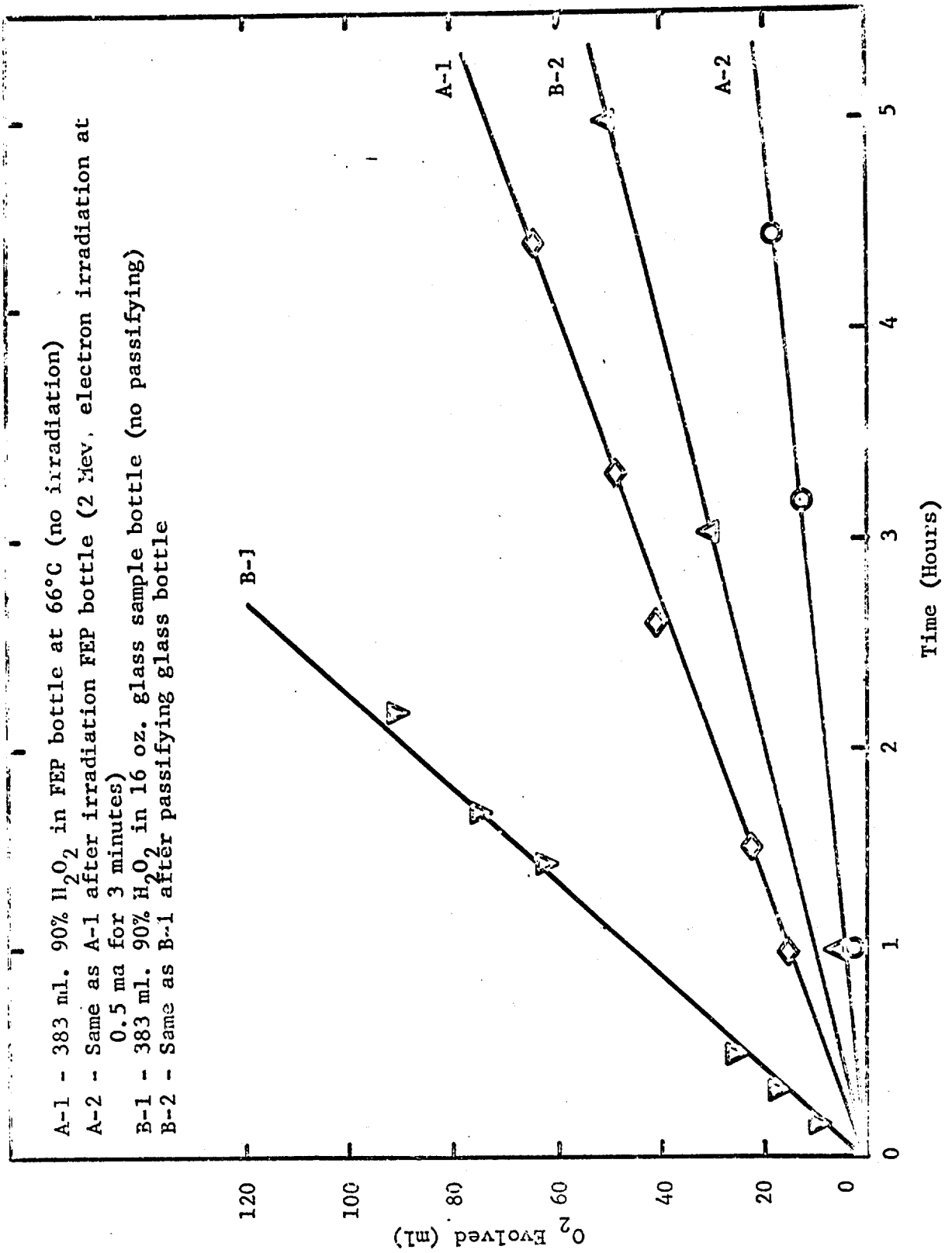


FIGURE 5

CONSTANT TEMPERATURE BATH FOR
90% HYDROGEN PEROXIDE DECOMPOSITION STUDIES

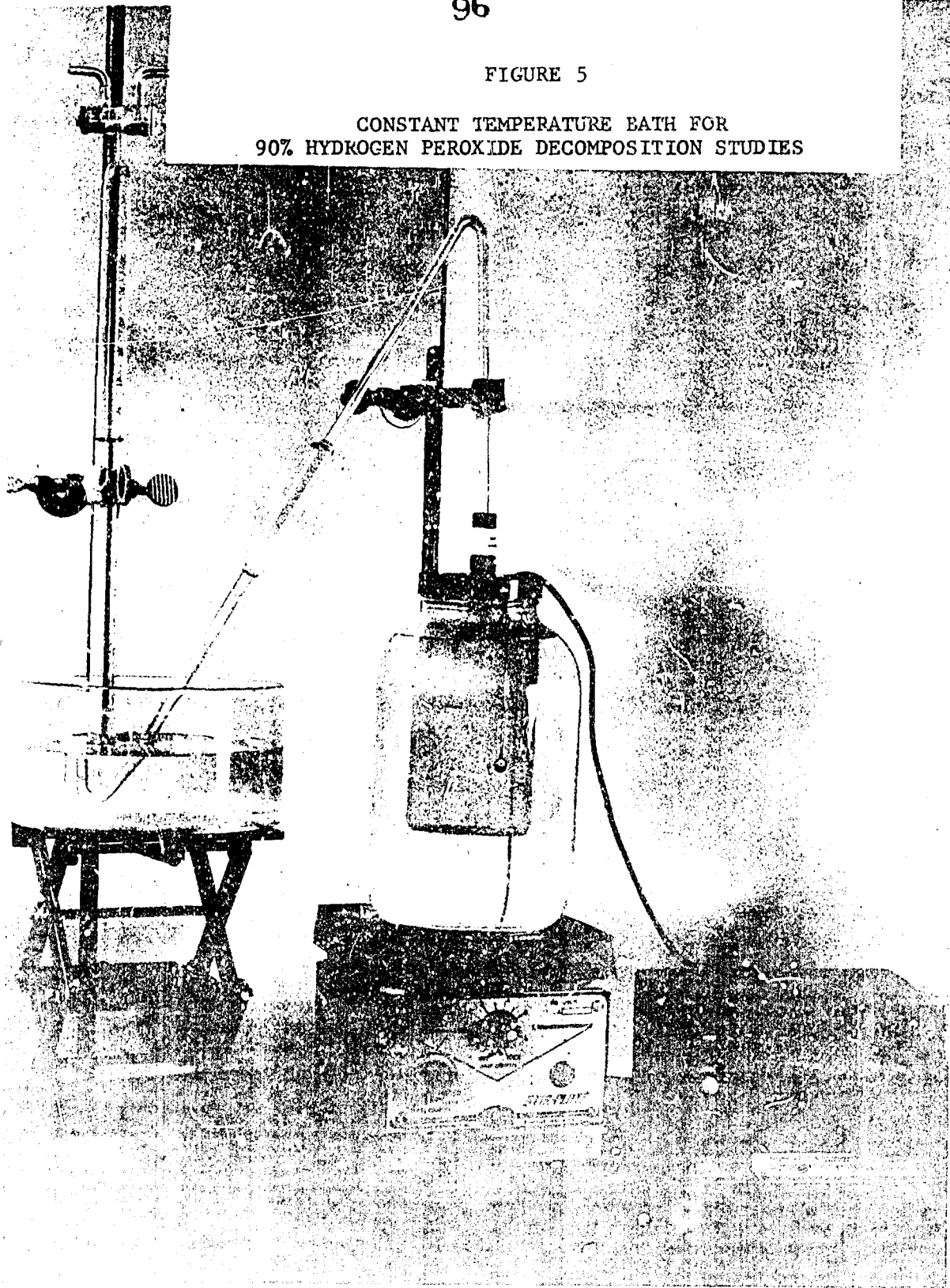


FIGURE 6
ELECTRON IRRADIATION OF ROTATING "TEFLON" FEP BOTTLE

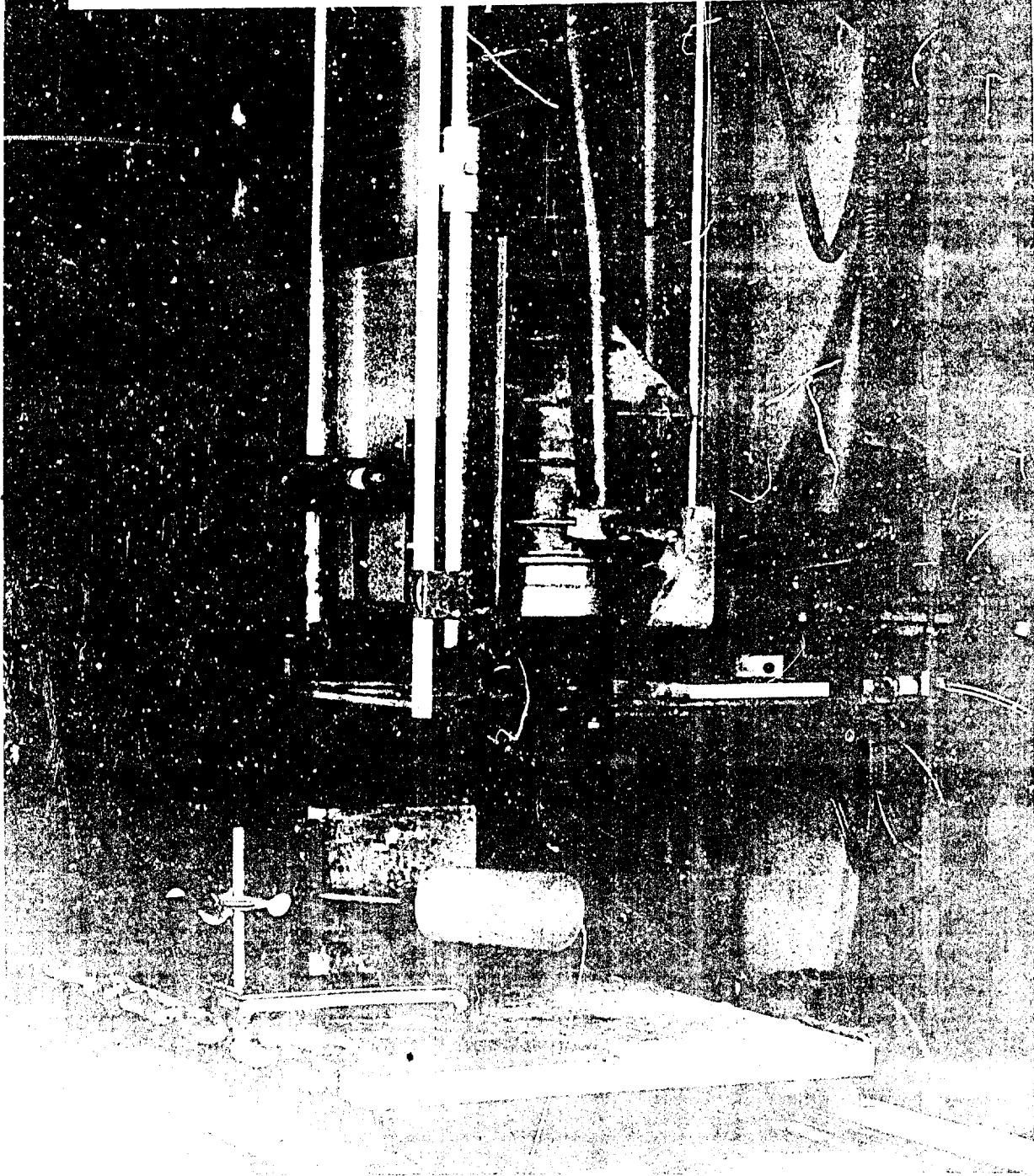


FIGURE 7

98

EFFECT OF ELECTRON IRRADIATION OF "TEFLON" FEP CONTAINER ON THE DECOMPOSITION
RATE OF HYDROGEN PEROXIDE.

Sample - 383 ml of 90% H_2O_2 in a "Teflon" FEP bottle at $66^\circ C$

Dose Rate - 6.6×10^{-3} kcal/cm²/min.

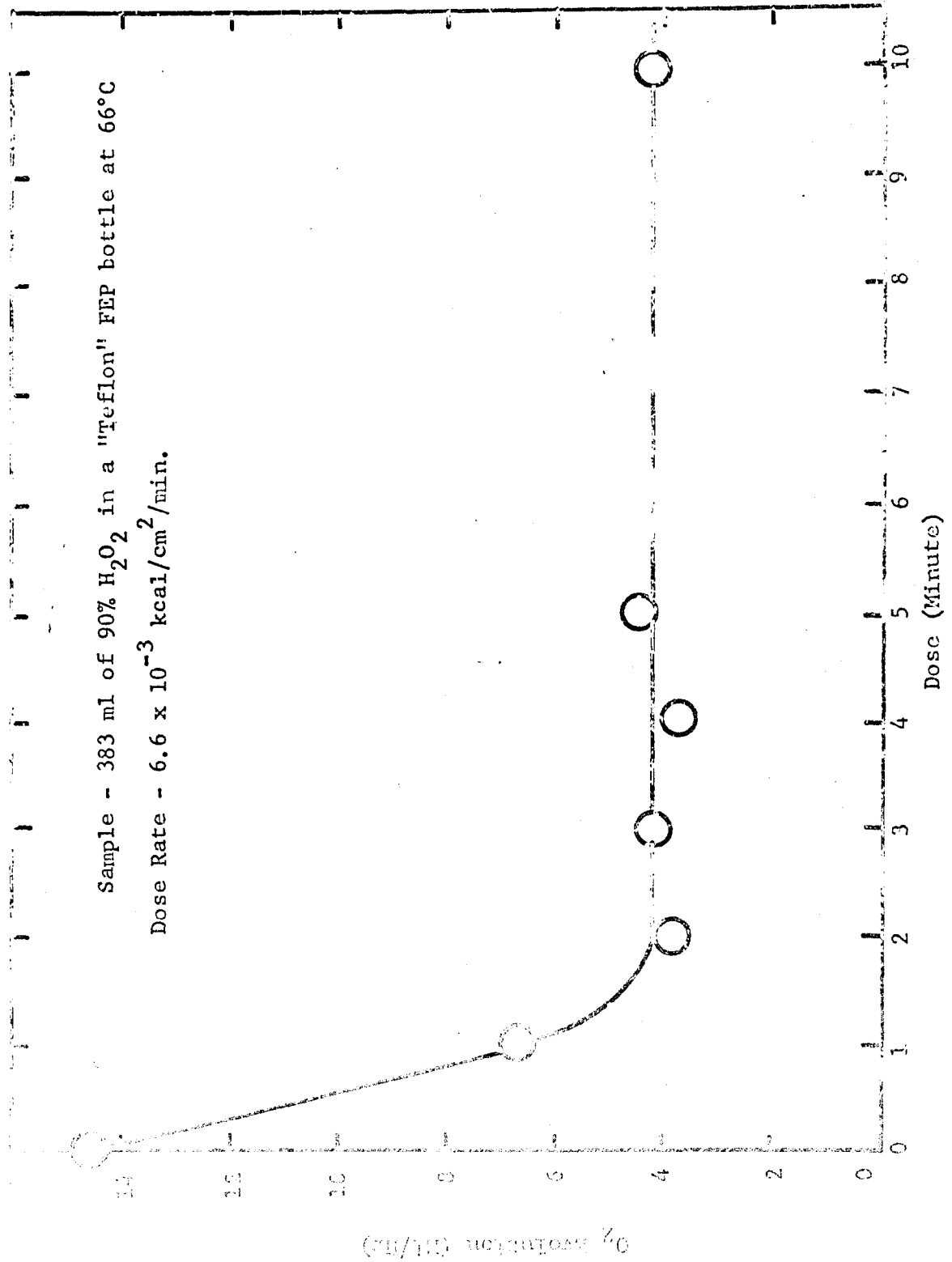
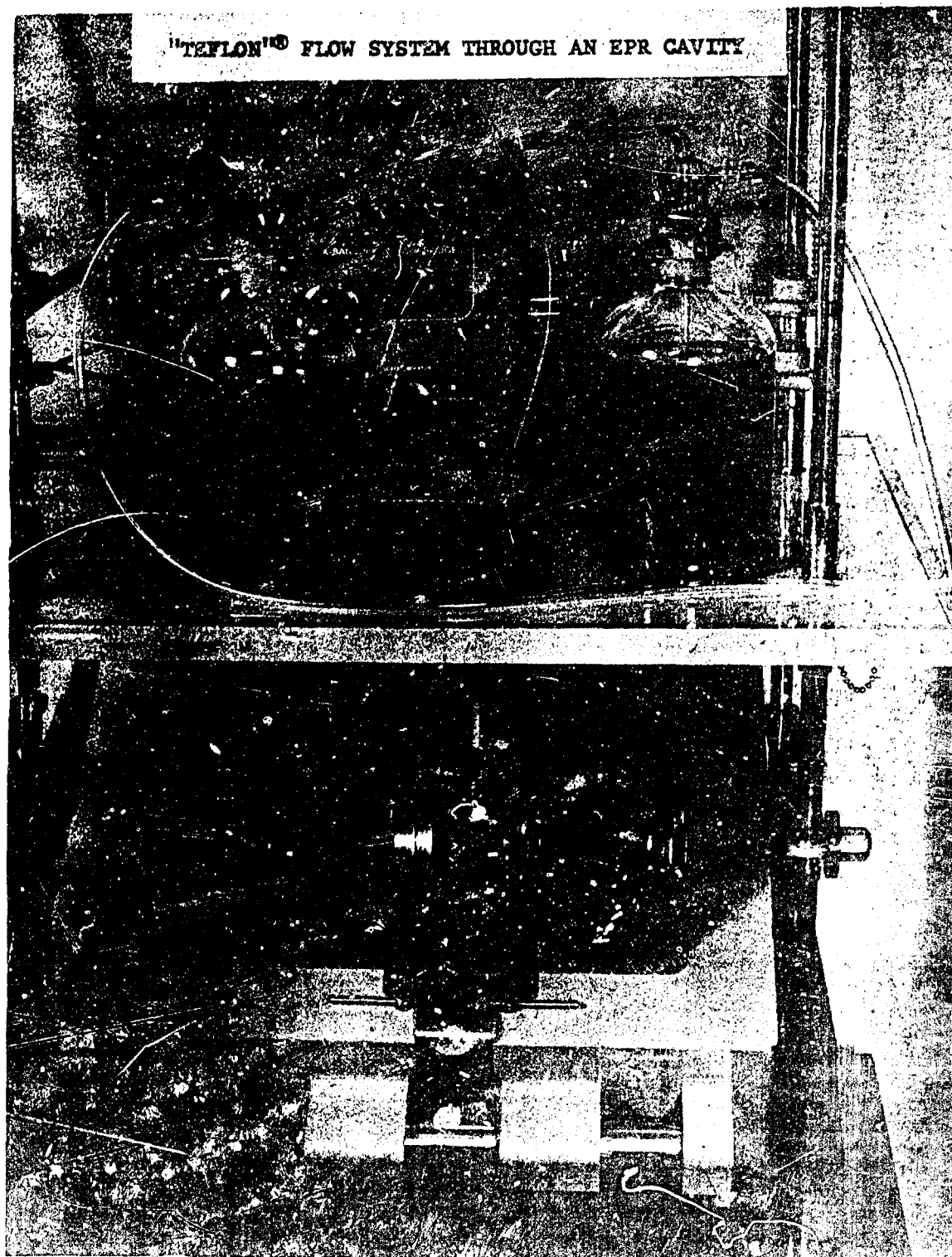


FIGURE 8

RADIATION DAMAGE TO "TEFLON" FEP BOTTLE
(DOSE: 6.6×10^{-2} kcal./cm.²)





101

FIGURE 10

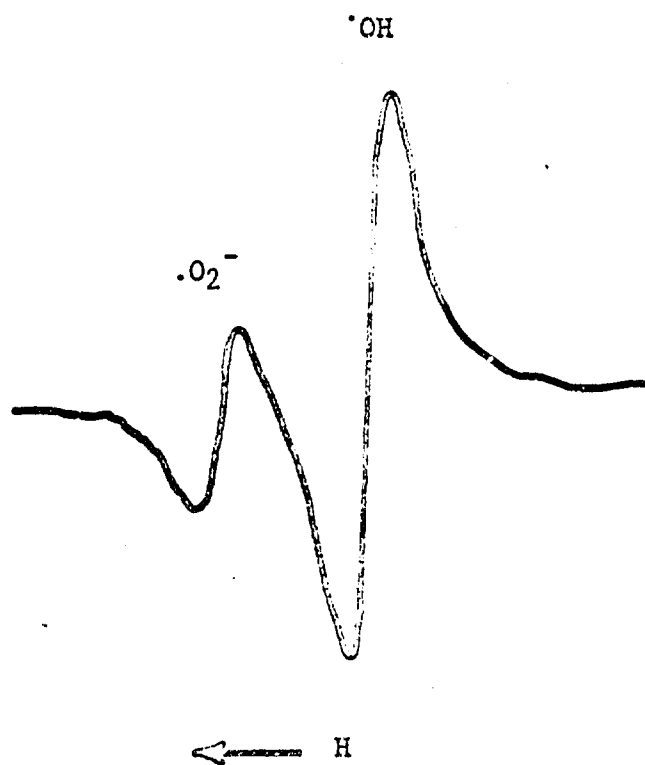
EPR SPECTRUM OF THE HYDROXYL RADICAL
AND SUPEROXIDE ION

FIGURE 11

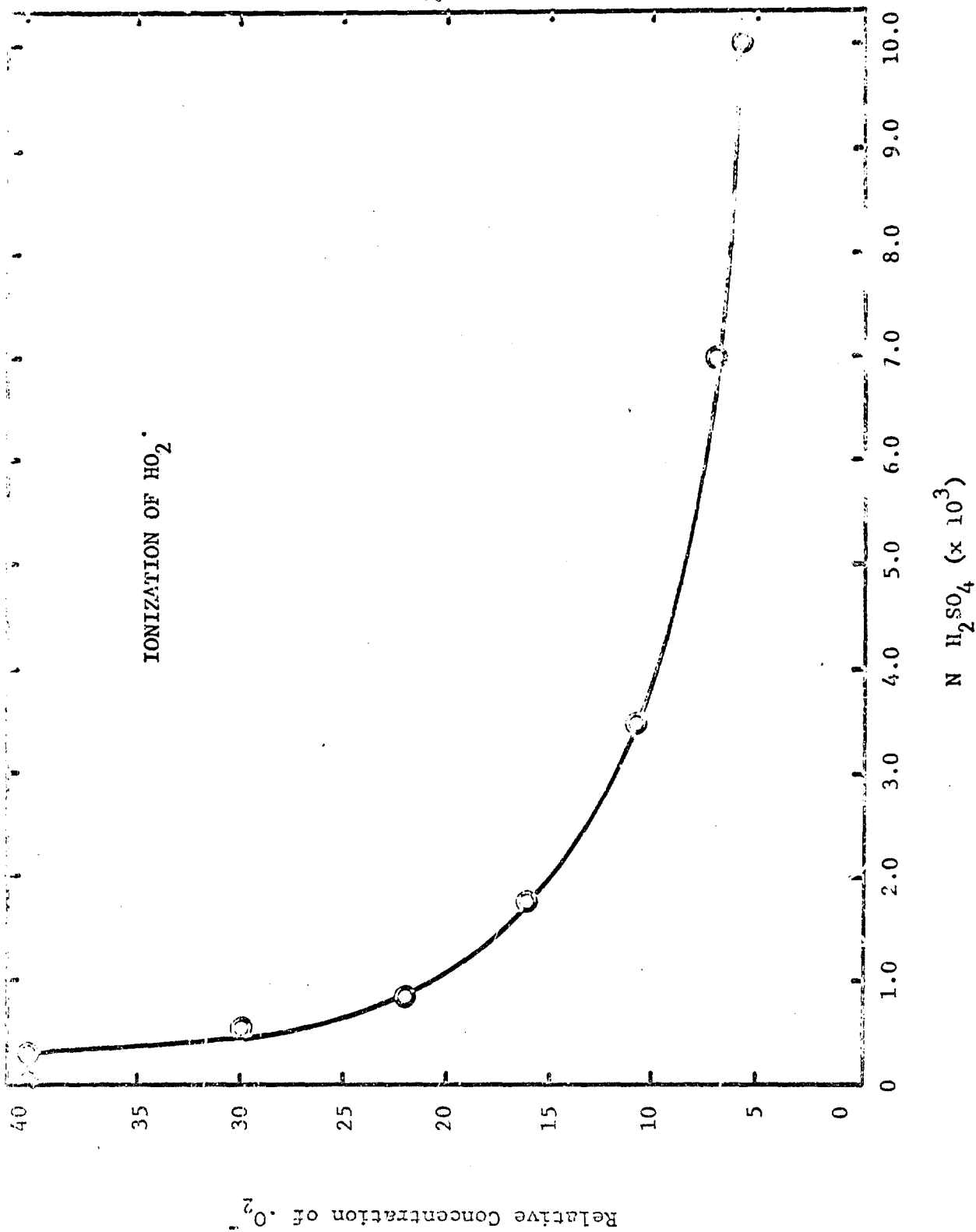


FIGURE 12

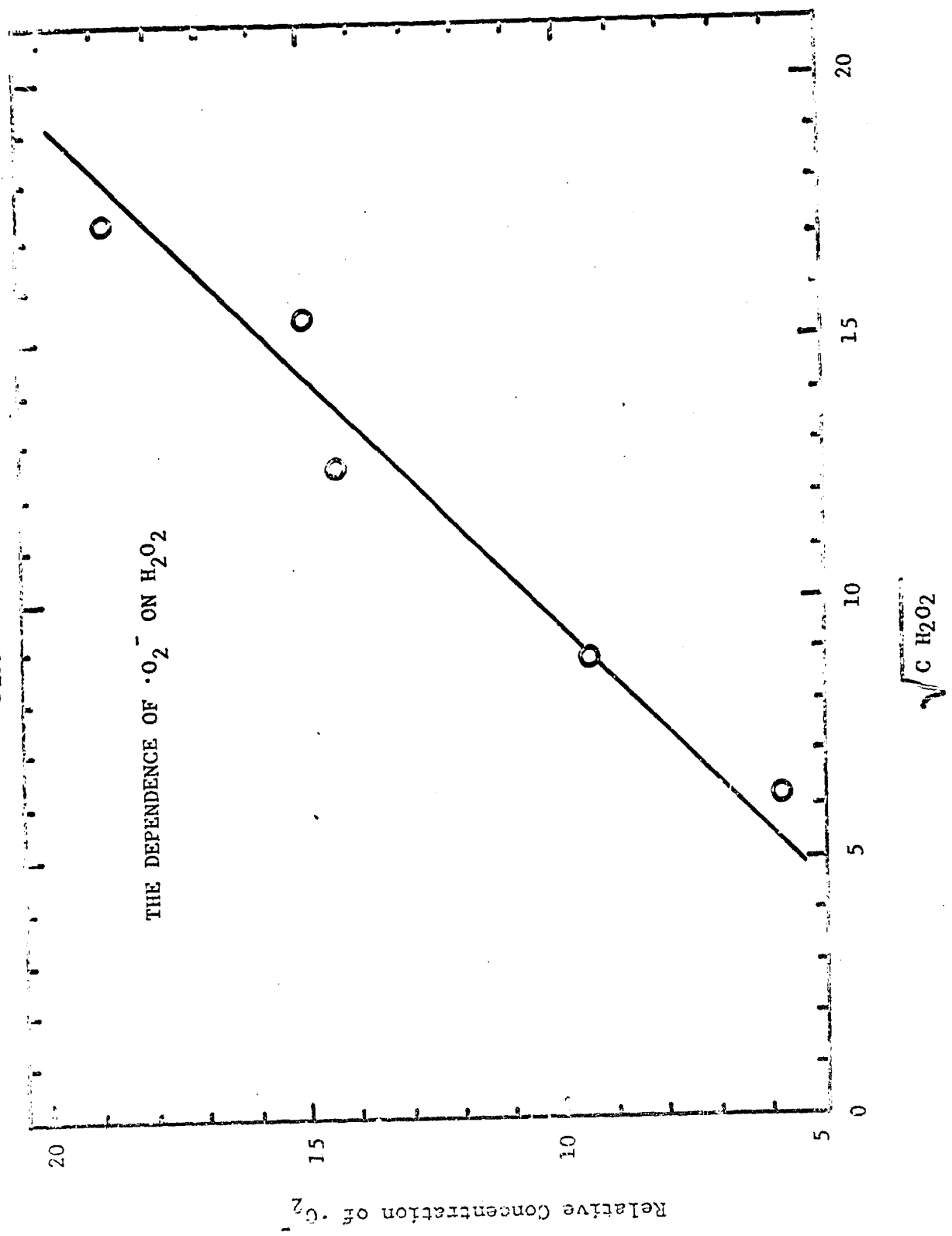


FIGURE 13
 STOPPED FLOW STUDIES ON Ti^{4+} - H_2O_2 REACTION

- A - Valve opened. 300 cc/min.
- B - Maximum signal for flow rate, 300 cc/min.
- C - Valve closed
- D - Maximum signal developed after flow stopped.

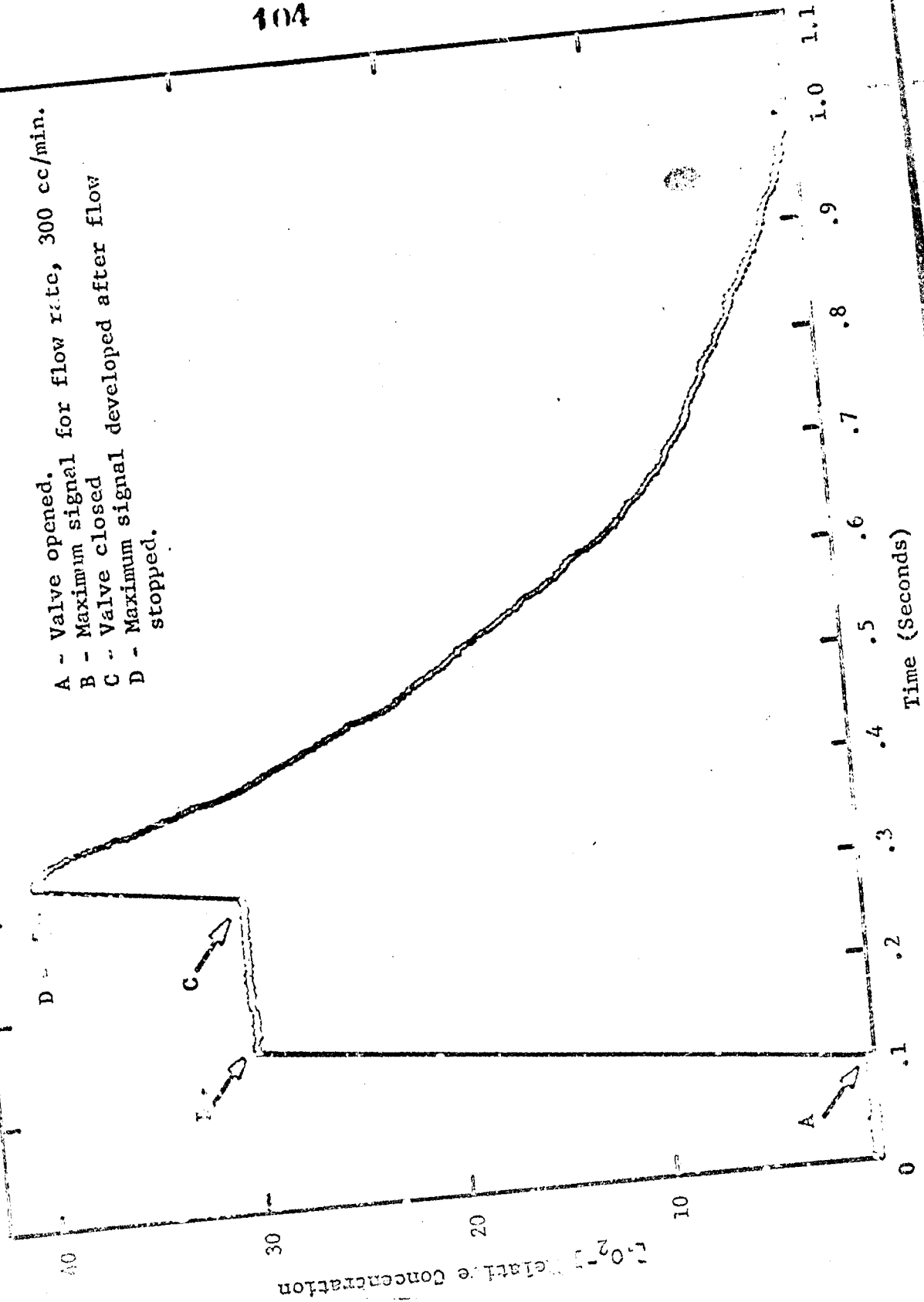
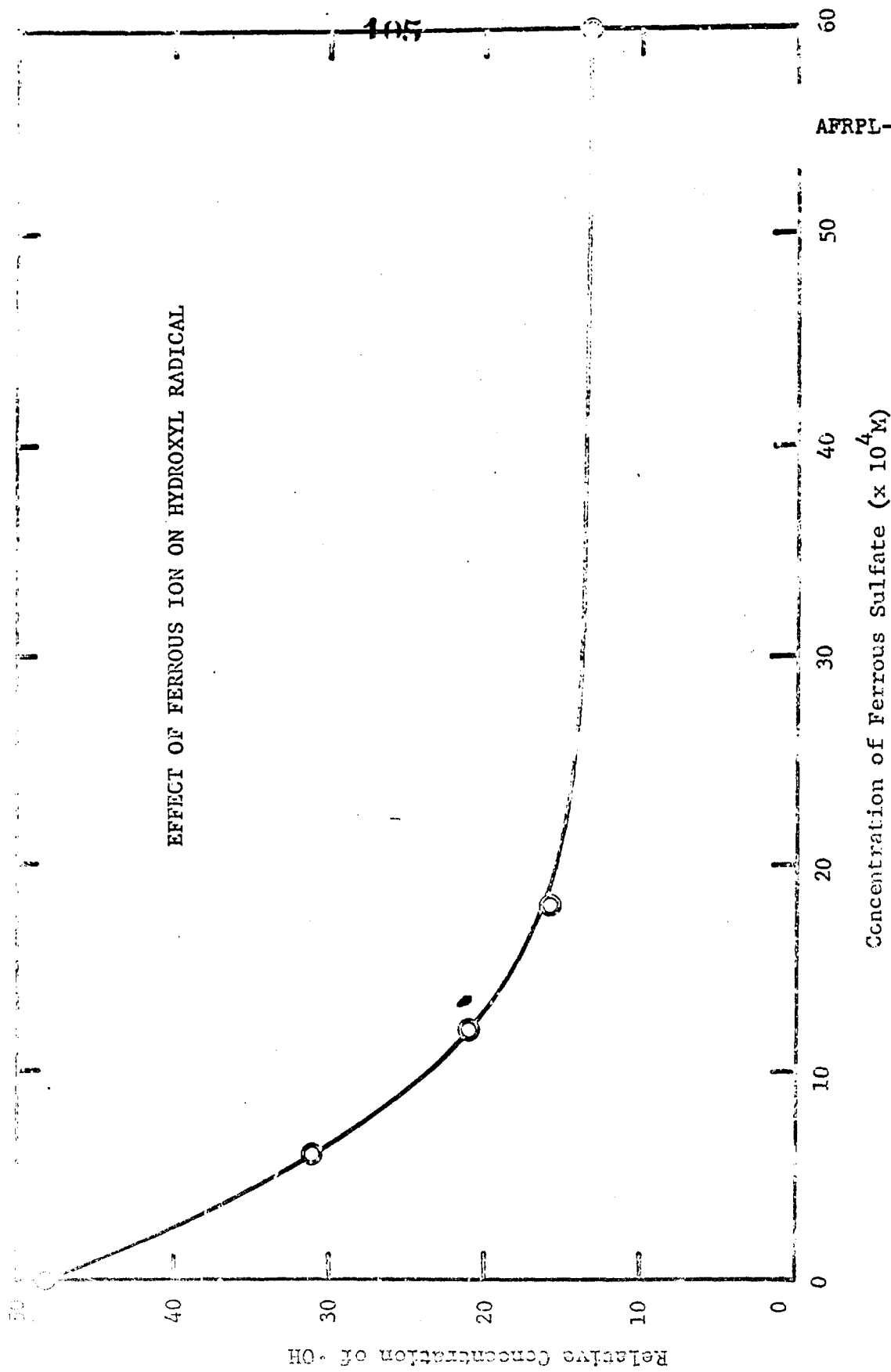
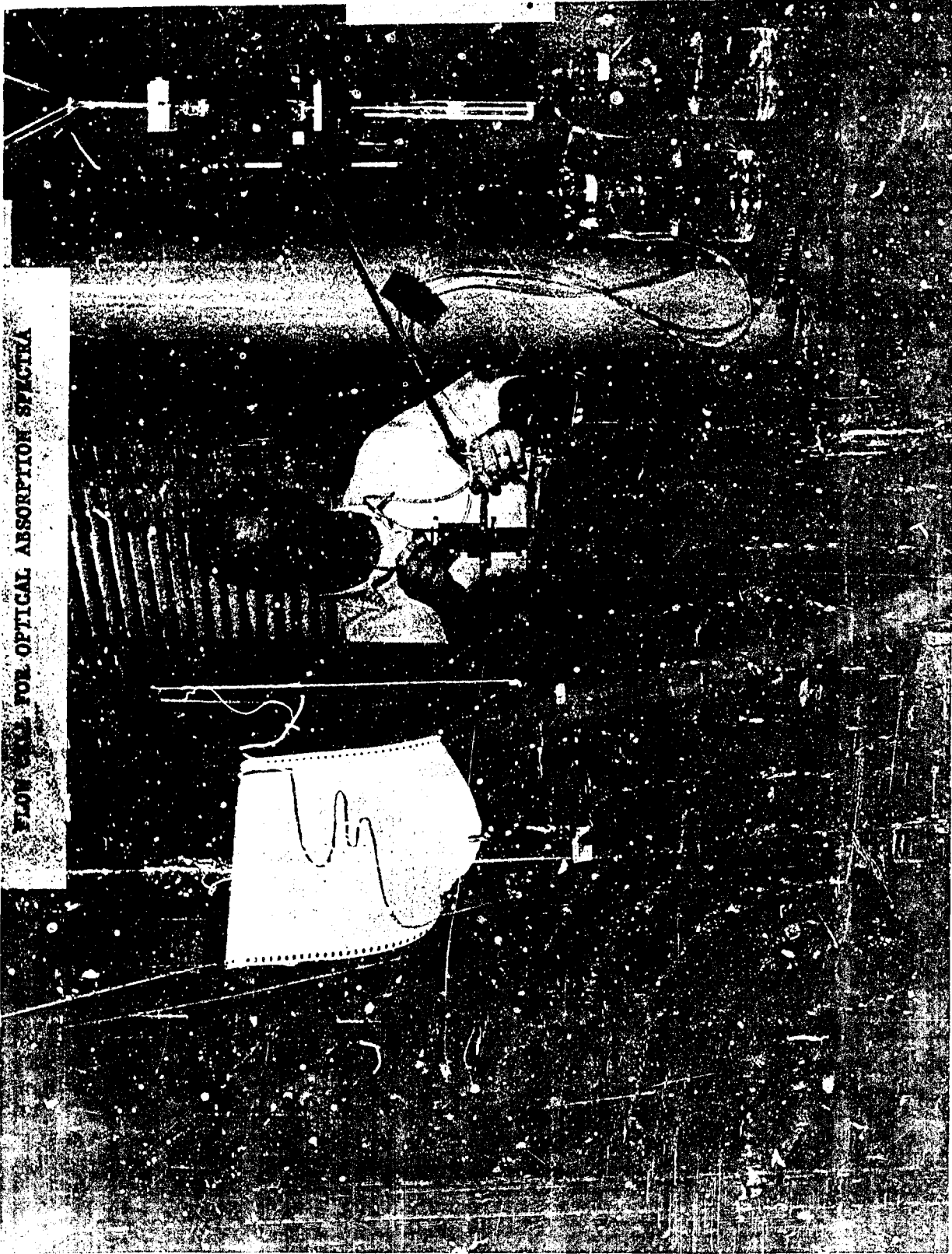


FIGURE 14





FLOW CELL FOR OPTICAL ABSORPTION SPECTRA

FIGURE 16
CONVERSION OF NITRATO-CERATE TO SULFATO-CERATE

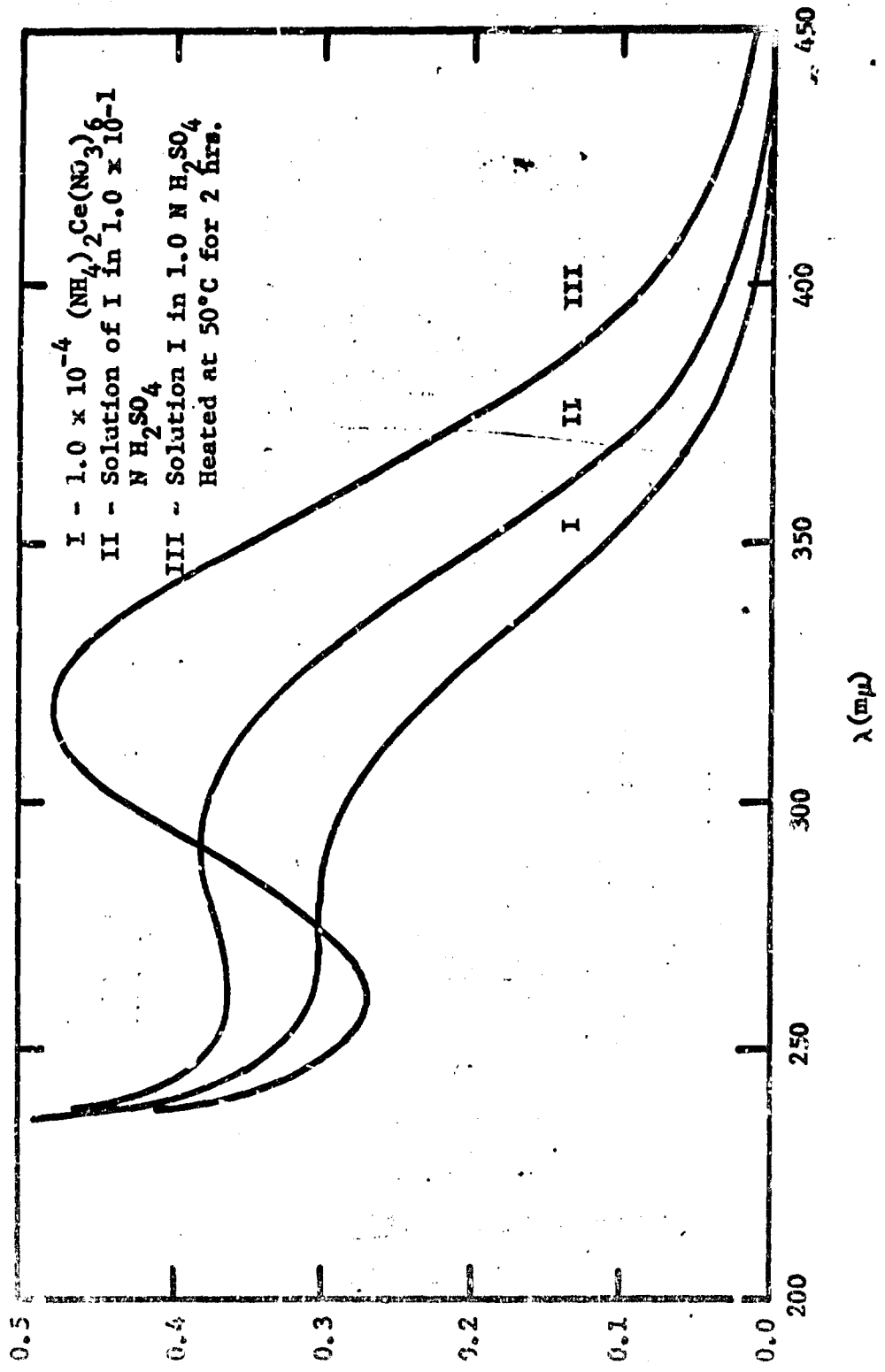


FIGURE 17
RECONSTRUCTED SPECTRUM OF SULFATO-CERATE IN THE PRESENCE OF NITRATE

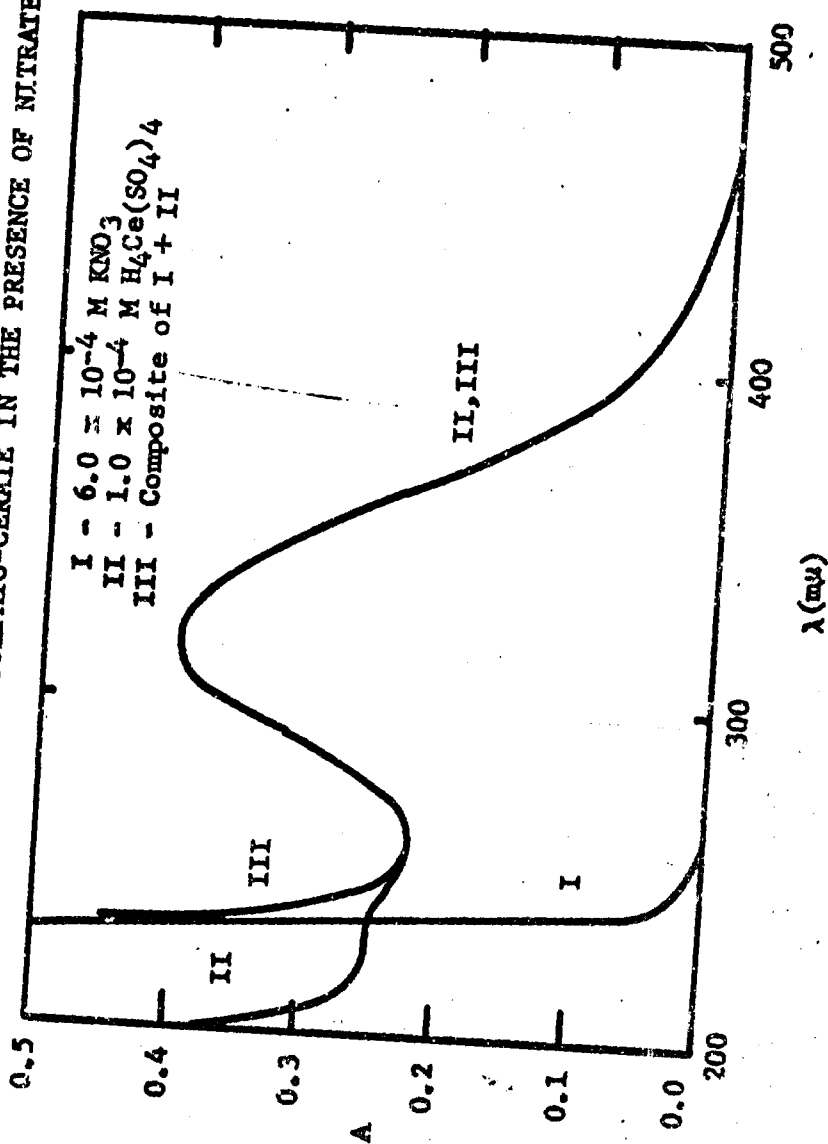
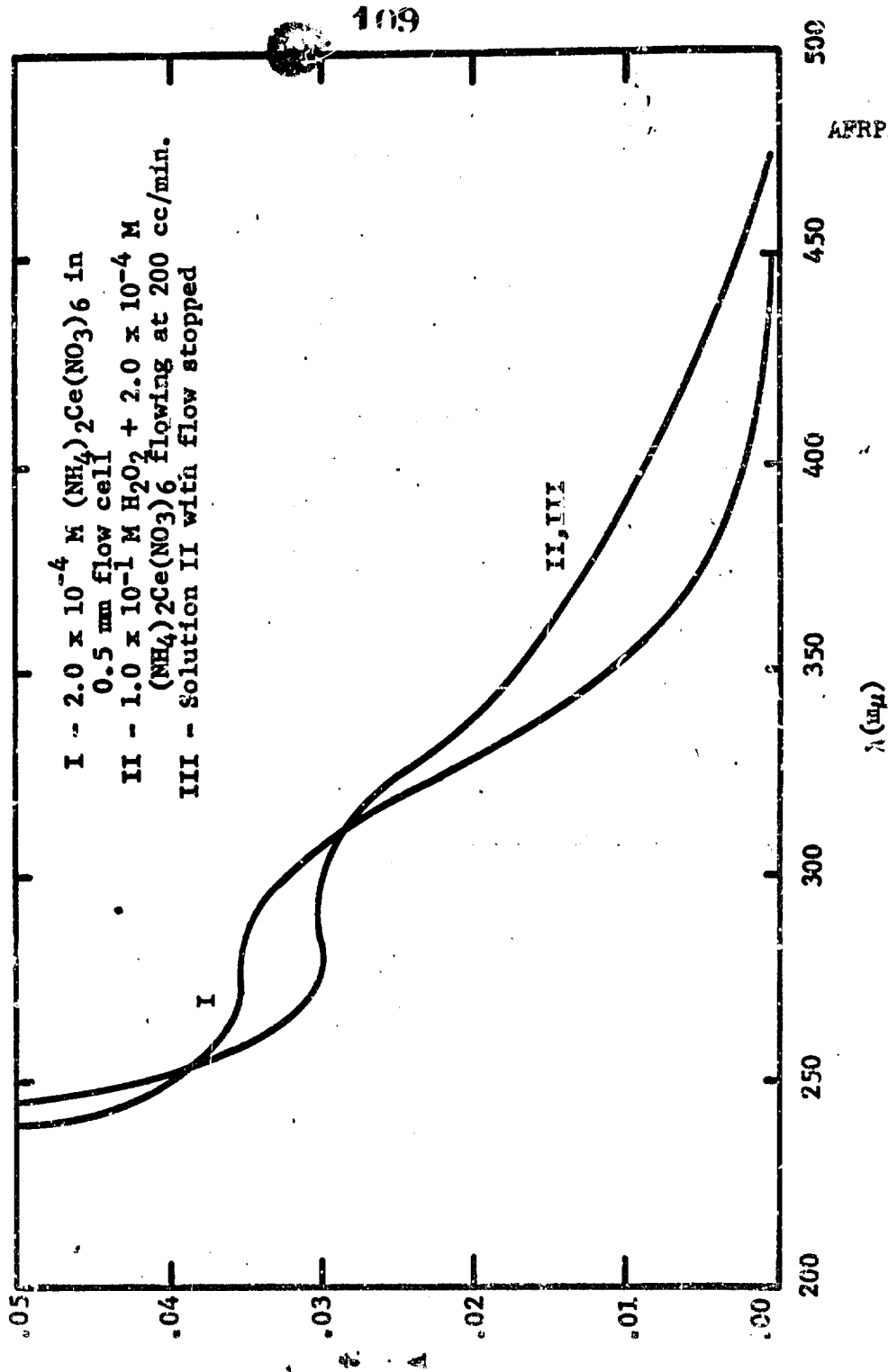


FIGURE 18

OPTICAL FLOW STUDIES ON THE NITRATO-CERATE, HYDROGEN PEROXIDE REACTION



110

FIGURE 19
OPTICAL FLOW STUDIES ON THE SULFATO-CERATE, HYDROGEN PEROXIDE REACTION

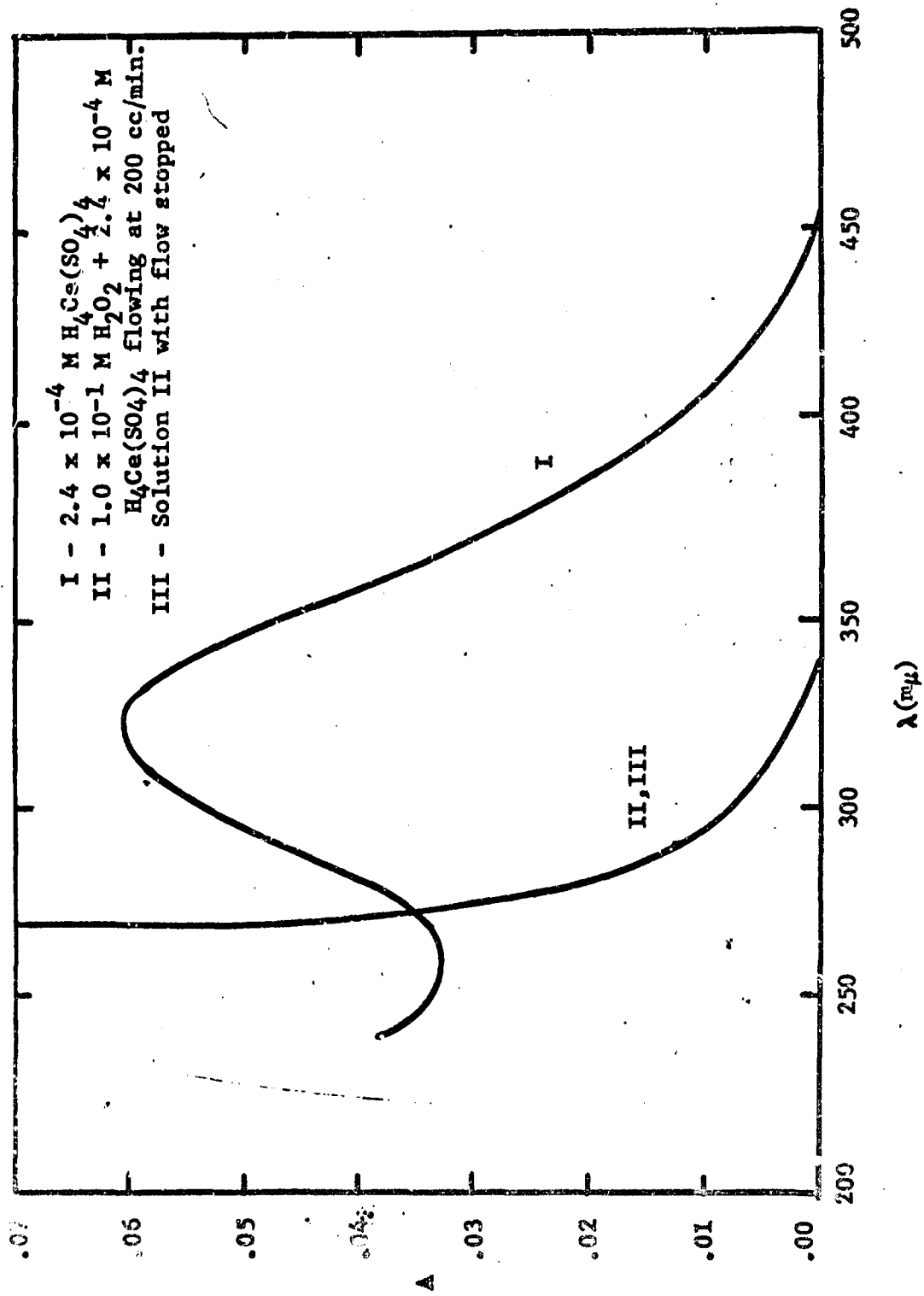


FIGURE 20
PHOTOLYSIS OF HYDROGEN PEROXIDE-TNM SOLUTIONS USING FILTERED 2537 Å IRRADIATION

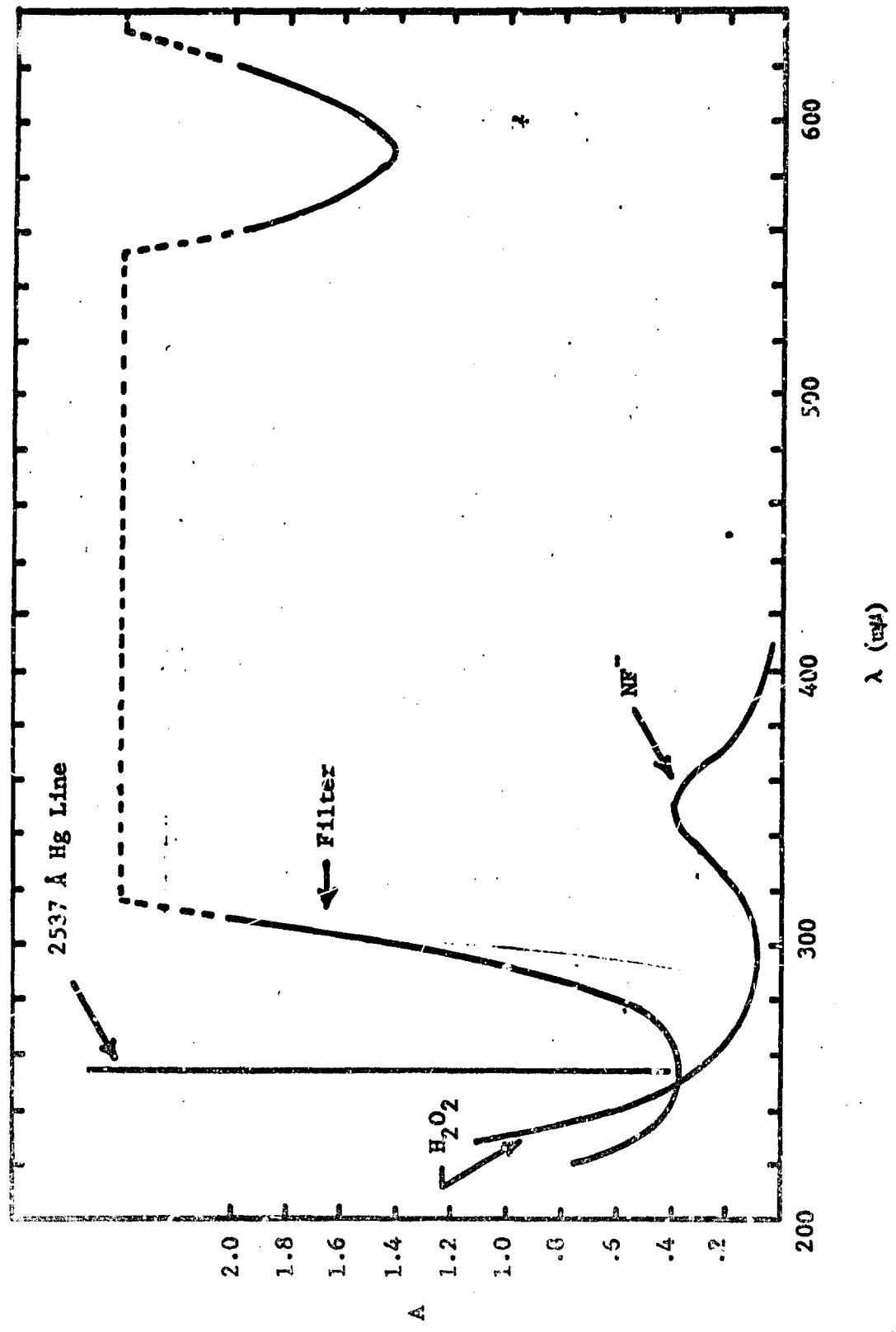
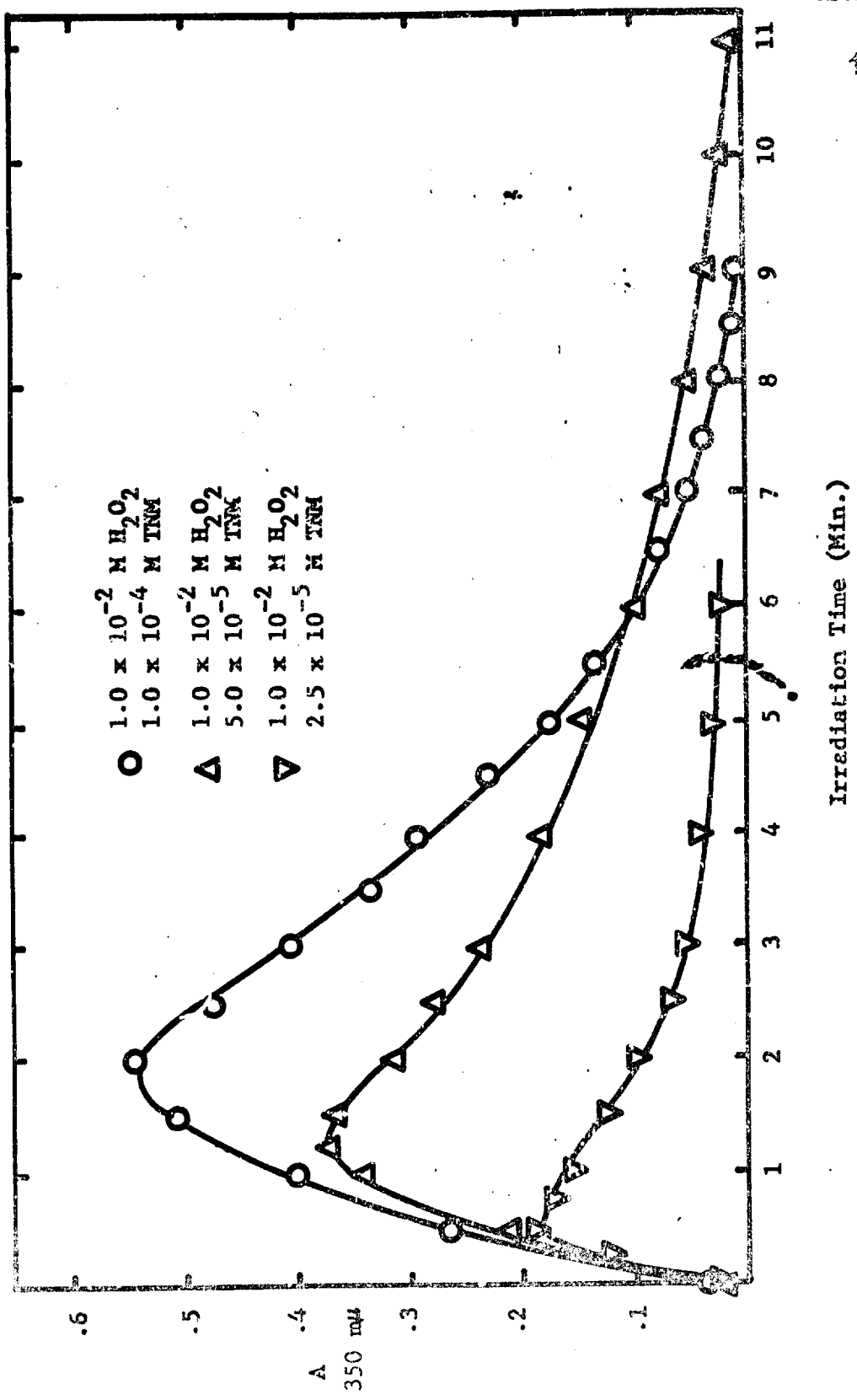


FIGURE 21
GROWTH AND DECAY OF NE^- IN IRRADIATED HYDROGEN PEROXIDE-TM \bar{M} SOLUTIONS



References

1. "Free Radicals in Inorganic Chemistry," Advances in Chemistry Series, No. 36, American Chemical Society, Washington, D. C., 1962, p. 103.
2. W. G. Barb, J. H. Baxendale, P. George and K. R. Hargrave, Trans. Faraday Soc., 47, 462 (1951).
3. H. A. Schwartz, J. Phys. Chem., 66, 255 (1962).
4. S. Nehari and J. Rabani, J. Phys. Chem., 67, 1609 (1963).
5. J. Rabani and M. S. Matheson, J. Am. Chem. Soc., 86, 3175 (1964).
6. M. G. Evans and N. Uri, Trans. Faraday Soc., 45, 224 (1949).
7. G. Czapski and L. M. Dorfman, J. Phys. Chem., 68, 1169 (1964).
8. G. Czapski and B. H. J. Bielski, J. Phys. Chem., 67, 2180 (1963).
9. B. H. J. Bielski and E. Saito, J. Phys. Chem., 66, 2266 (1962).
10. E. Saito and B. H. J. Bielski, J. Am. Chem. Soc., 83, 4467 (1961).
11. G. Czapski and L. M. Dorfman, J. Phys. Chem., 68, 1169 (1964).
12. M. S. Matheson, Private Communication.
13. W. T. Dixon and R. O. C. Norman, J. Chem. Soc., 1963, 3119.
14. L. J. Heidt and V. R. Landi, J. Chem. Phys., 41, 176 (1964).
15. D. A. Csejka, F. Martinez, J. A. Wojtowicz and J. A. Zaslowsky, J. Phys. Chem., 68, 3878 (1964).
16. J. H. Baxendale, Radiation Research, 17, 312 (1962).
17. K. Schmidt, Z. Naturforsch., 16, 206 (1961).
18. M. Burton and K. C. Kurien, J. Phys. Chem., 63, 899 (1959).
19. M. Anbar and J. K. Thomas, J. Phys. Chem., 68, 3829 (1964).
20. G. Ferrandini and A. M. Koulkas, J. Chim. Phys., 1310 (1963).

21. A. Hummel and A. O. Allen, *Radiation Research*, 17, 302 (1962).
22. A. Hummel and A. O. Allen, unpublished; see M. Anbar and P. Neta, *International J. App. Radiation and Isotopes*, 16, 227 (1965).
23. G. E. Adams and J. W. Boag, *Proc. Chem. Soc., London*, 1964, 112.
24. F. S. Dainton and S. A. Sills, *Proc. Chem. Soc., London*, 1962, 223.
25. M. Anbar and D. Meyestein, *Israel AEC Semiannual Report IA-920*, p. 108 (1964).
26. F. S. Dainton and T. J. Hardwick, *Trans. Faraday Soc.*, 53, 333 (1957).
27. J. P. Keene, *Radiation Res.*, 22, 14 (1964).
28. W. G. Rothschild and A. O. Allen, *Radiation Res.*, 8, 101 (1958).
29. H. A. Schwartz, *J. Phys. Chem.*, 66, 255 (1962).
30. D. Bum, F. S. Dainton, G. A. Salmon and T. J. Hardwick, *Trans. Faraday Soc.*, 55, 1760 (1959).
31. J. Rabani and G. Stein, *Trans. Faraday Soc.*, 58, 2150 (1962).
32. J. W. Boyle, S. Weiner and C. J. Hochanadel, *J. Phys. Chem.*, 63, 892 (1959).
33. T. J. Sworski, *Radiation Res.*, 4, 483 (1956).
34. T. J. Sworski, *Radiation Res.*, 6, 645 (1957).
35. G. Czapski, J. Rabani and J. Stein, *Trans. Faraday Soc.*, 58, 2160 (1962).
36. H. A. Schwarz and A. O. Allen, *J. Am. Chem. Soc.*, 77, 1324 (1955).
37. Bulletin No. SD-53, Supplement B, p. 23, Manufacturing Chemists Association, Inc., Chemical Data Sheet on Hydrogen Peroxide, 1961.
38. Bulletin No. 104, Becco Chemical Division of Food Machinery and Chemical Corporation, 1959, p. 7.
39. D. C. Borg, *Nature*, 201, 1087 (1964).

40. W. T. Dixon and R. O. C. Norman, *J. Chem. Soc.*, 1963, 3119.
41. L. H. Piette, G. Bulow and K. Loeffler, Paper presented at the American Chemical Society Meeting, Philadelphia, Pennsylvania, April 5-10, 1964.
42. J. W. Hickman, *Proc. W. Va. Acad. Sci.*, 23, 76 (1951).
43. G. F. Smith, "Cerate Oxidimetry," G. F. Smith Chemical Co., Columbus, Ohio (1942).
44. M. Bobletsky, *J. Chem. Soc.*, 1950, 3615.
45. D. F. Graham, *J. Am. Chem. Soc.*, 52, 3035 (1930).
46. G. E. Eden, A. M. Freke and K. V. Melbourne, *Chem. and Ind.*, 1951, 1104.
47. A. Henglein and J. Jaspert, *Z. physik. Chem.*, 12, 324 (1957).
48. G. Czapski and B. H. J. Bielski, *J. Phys. Chem.*, 67, 2180 (1963).
49. J. Rabani, W. A. Mulac and M. S. Matheson, *J. Phys. Chem.*, 69, 53 (1965).
50. C. G. Hatchard and G. A. Parker, *Proc. Royal Soc. of London*, A235, 518 (1956).
51. D. H. Volman and J. C. Chen, *J. Am. Chem. Soc.*, 81, 4141 (1959).

January 4, 1965

AFRPL-TR-66-13

MINIMUM METAL CONTAINER SURFACE

As a further development of our suggestion dated 12/3/64 it is proposed to explore the possibility of storing small volumes of high strength H_2O_2 as follows:

The storage container should be a jacketed type with automatic temperature control of a sub-zero jacket circulating medium.

The middle portion only, of the H_2O_2 storage volume should be fitted with a group of very small diameter electrical immersion heaters. These would be sheathed in 99.6% pure aluminum.

Precision differential temperature control between the liquified middle portion and the frozen outer portion of the stored H_2O_2 would be required. This would provide constant equilibrium to maintain the desired liquid/frozen condition with minimum heater surface area and heat input.

The feasibility of this idea might be determined in the Research Laboratory using water instead of H_2O_2 at first. In order to do this, the following is suggested:

- a. Purchase several suitable small Aerorod immersion heaters and thermocouples as required.
- b. Install a suitable water container in the "Coldspot" deep freeze cabinet presently used by Dr. Pinkney in Lab. 206.
- c. Fit the above deep freeze unit with a temporary insulated cover with observation window, etc.
- d. Hook up a suitable differential temperature control system (see sketch FBB-1465) using the Precision Temperature Control unit now located in Lab. 105 and presently used by Dr. Roe.

Research should furnish adequate assistance as required. Expenditures for material is estimated at less than \$350. Time involved for the initial tests with water would probably not exceed one or two weeks after completion of the equipment set up.

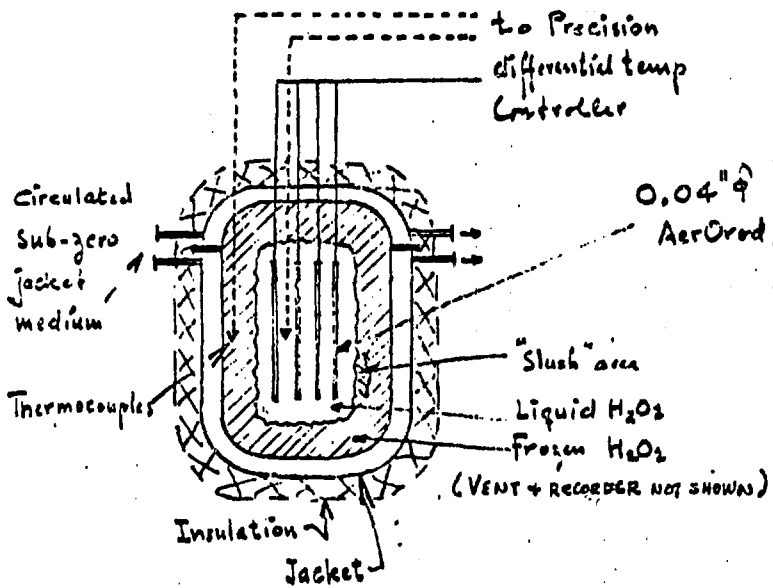
F. B. Hjarnow, Process Engineer
Project Engineering Section

FBB:hm
Attach.



TITLE OF PROJ. OR STUDY LAB STORAGE OF HIGH STRENGTH H₂O₂ PROJ. OR STUDY NO. WR-2161
 SUBJECT A Proposed Storage System and (B) Feasibility WORKS Research - 110000
Demonstration Unit. COMPUTER TRK DATE 1/3 19 65

Originators: Jed B. Stamm 1/4/65
Arthur J. Strohle 1/4/65



0.04" ϕ 99.6+ δ % pure aluminum sheathed AerOrod immersion heaters.

Liquified Volume/Surface Ratio

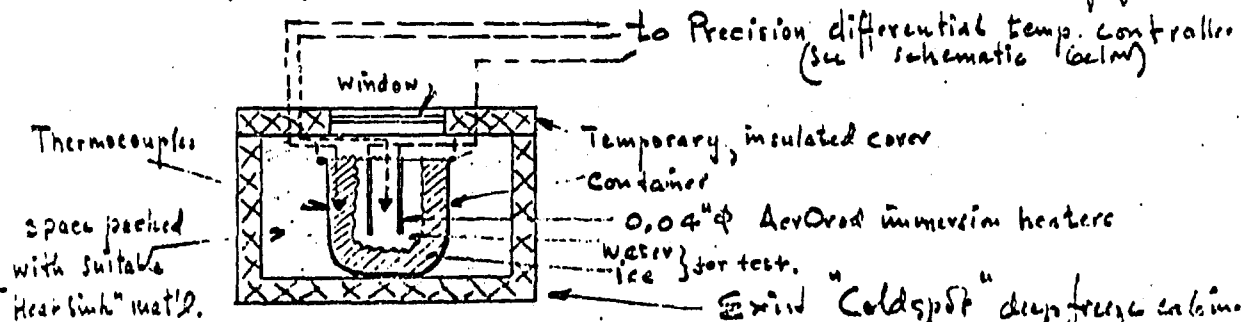
(4) - heaters per sq. in. * = $\frac{5cc}{1cm^2}$
 (2) - heaters per sq. in. * = $\frac{10cc}{1cm^2}$

* = per in.² transverse section of stored vol.

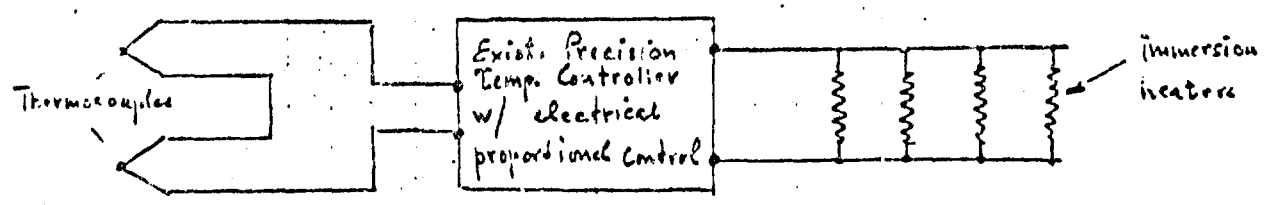
The above Vol/Surface ratios have hitherto only been obtainable in very large capacity storage vessels 50,000 gals. ϕ up.

(A) PROPOSED LAB STORAGE OF 90-100% H₂O₂

(During prolonged storage periods entire H₂O₂ volume may be maintained in frozen condition)



(B) PROPOSED FEASIBILITY DEMONSTRATION UNIT FOR WATER



SCHEMATIC

February 4, 1965

SOLID H₂O₂ CONTAINER SURFACE

P. C. Hoell

The problem of measuring the absolute decomposition rate of liquid H₂O₂ at various temperatures requires that the H₂O₂ be contained in a solid (frozen) shell of the same material in order to avoid catalytic reaction with any foreign substance. Given a means of forming and maintaining such an ice shell, there remains the problem of heating the contained liquid in such a way as to produce a still temperature gradient at the periphery of the container with an essentially uniform bulk temperature.

Calculations and scouting experiments with water, whose dielectric and thermal properties are similar to H₂O₂, show that advantage can be taken of the great difference in dielectric loss between the solid and liquid states in a microwave field to heat the liquid core selectively. For example, the loss factor for water at 1.5°C. is 10⁴ times that of ice at -12°C. at a frequency of 3000 Mc. Moreover, the loss factor is greatest at the lowest liquid temperature (i.e., at the ice-liquid interface) decreasing by a factor of 2 at 25°C. Further advantages of using microwave energy as the heat source are that it is nondirectional and is absorbed equally about the entire interface region, it is of sufficiently low photon energy not to induce decomposition by electronic excitation, and it does not involve direct contact of the liquid with any foreign material. In addition, because the microwave field is rapidly attenuated by the liquid (more than half the absorbed energy is dissipated within 1-cm of the ice-liquid interface), there is relatively

POH/gad

little radial heat transfer from the liquid core and a very small bulk temperature gradient should, therefore, obtain. In an experiment with a microwave "oven," about 200-cc of water, starting at 20°C, was brought to a boil while a block of ice of the same size remained frozen at a few degrees below zero. The use of microwave heating, however, requires that the materials used to enclose the H_2O_2 system and to refrigerate it have low dielectric loss. Such materials include glass, quartz (preferred), "Teflon"TM and polystyrene as structural materials, and liquid diatomic gases (e.g., N_2) and certain "Freons"TM as the refrigerant. The use of simple paraffins is feasible but probably hazardous.

Calculation of Equilibrium Conditions

Because the microwave energy absorption is concentrated about the periphery of the liquid core, it appears that little temperature gradient will exist throughout the bulk of the liquid. Upon this assumption, the model shown in Figure 1 is taken as a fair representation of the actual geometry that would obtain and the equilibrium conditions may be approximated for water by the following computation:

Assuming certain values for the effective vertical surface area of the liquid core, the effective height of the core, and its mean temperature, the rate of heat flow outward through the "liquid heat transfer layer" is given by:

$$Q_w = \left(\frac{k A C_a \Delta T}{1.9 x} \right) \left(\frac{x}{L} \right)^{1/9} \left(\frac{N_{gr} N_{pr}}{N_{pr}} \right)^n$$

where

Q_w = Heat transfer rate, watts

k = Mean thermal conductivity of liquid heat transfer layer, PCU/(hr.)(ft.)(°C)

P. C. Hoell/gad

- x = Thickness of transfer layer, ft. ≈ 0.025 ft.
 A = Area of transfer layer, ft.²
 L = Height of transfer layer, ft.
 N_{gr} = $x^3 \rho^2 g \beta \Delta T / \mu^2$
 L_{pr} = $C_p \mu / k$
 ρ = Mean density of transfer layer, lb./ft.³
 g = Gravitational constant = $4.17 \cdot 10^8$ ft./hr.²
 ΔT = Temperature difference across transfer layer, 1/°C
 β = Mean expansion coefficient of transfer layer, 1/°C
 μ = Mean viscosity of transfer layer, lb./ft. hr.
 C_p = Heat capacity of transfer layer, PCU/(lb.) °C

C_a	n	N_{gr} Range
0.2	1/4	$2 \cdot 10^3$ to $2 \cdot 10^5$
0.071	1/3	$2 \cdot 10^5$ to 10^7

Example (Water)

- Area of core: 0.4 ft.²
 Height of core: 0.5 ft.
 Bulk temperature: 30°C

P. C. Hoell/gad

121

- 4 -

$$\text{Let } k (15^\circ\text{C}) = 0.335 \quad C_p = 1$$

$$\rho (15^\circ\text{C}) = 62.5$$

$$\Delta T = 30^\circ\text{C}$$

$$\beta (15^\circ\text{C}) = 1.41 \cdot 10^{-4}$$

$$\mu (15^\circ\text{C}) = 2.76$$

Then

$$N_{gr} = \frac{(0.025)^3 (62.5)^2 (1.41 \cdot 10^{-4}) (30) (4.17 \cdot 10^8)}{(2.76)^2}$$

$$= 1.4 \cdot 10^4$$

$$C_a = 0.2$$

$$n = 1/4$$

$$C_w = \left[\frac{(0.335)(0.4)(0.2)(30)}{(1.9)(0.025)} \right] \left(\frac{0.025}{0.5} \right)^{1/9} \left[\frac{(1.4 \cdot 10^4)(2.76)}{0.335} \right]^{1/4}$$

$$= \underline{\underline{222 \text{ watts}}}$$

The heat transfer rate through the ice layer is given by:

$$Q_i = \frac{k_i A_i \Delta T_i}{1.9 x_i} \text{ watts}$$

P. C. Woell/gad

where

k_i = Mean thermal conductivity of the ice layer

A_i = Mean area of ice layer

ΔT_i = Temperature difference across ice layer

x_i = Thickness of ice layer

Assuming the external surface temperature of the ice layer to be controlled by suitable refrigeration to (-100°C) , and given the geometry and heat load of the above example (222 watts), then

$$A_i = 1.57 x_i + 0.4$$

$$k_i = 0.69 \quad (-50^\circ\text{C})$$

$$\Delta T = 100^\circ\text{C}$$

$$Q_i = 222 = \frac{(0.69)(100)(1.57 x_i + 0.4)}{(1.9) x_i}$$

$$x_i = 0.088 \text{ ft. or } \underline{\underline{1.05 \text{ inches}}}$$

The temperature profile of such a system should appear somewhat as shown in Figure 2.

P. C. Hoell/gad
Attachment

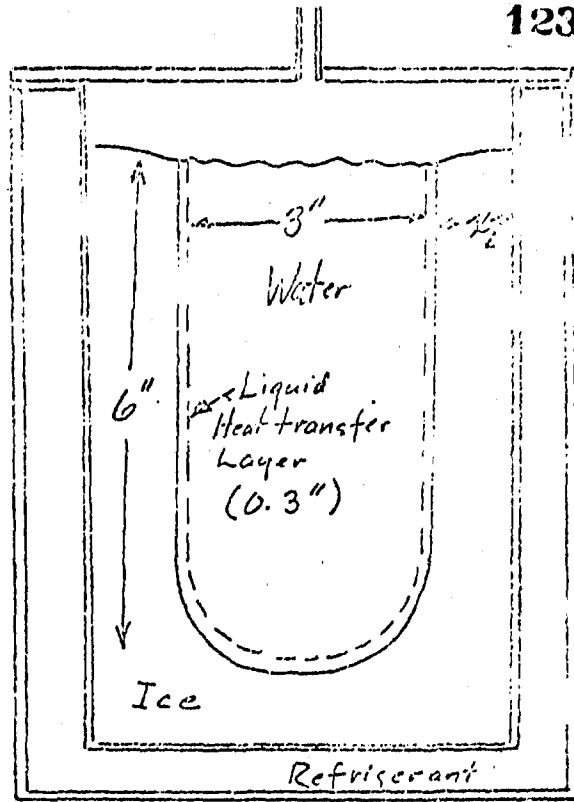


Figure 1
Computation
Model

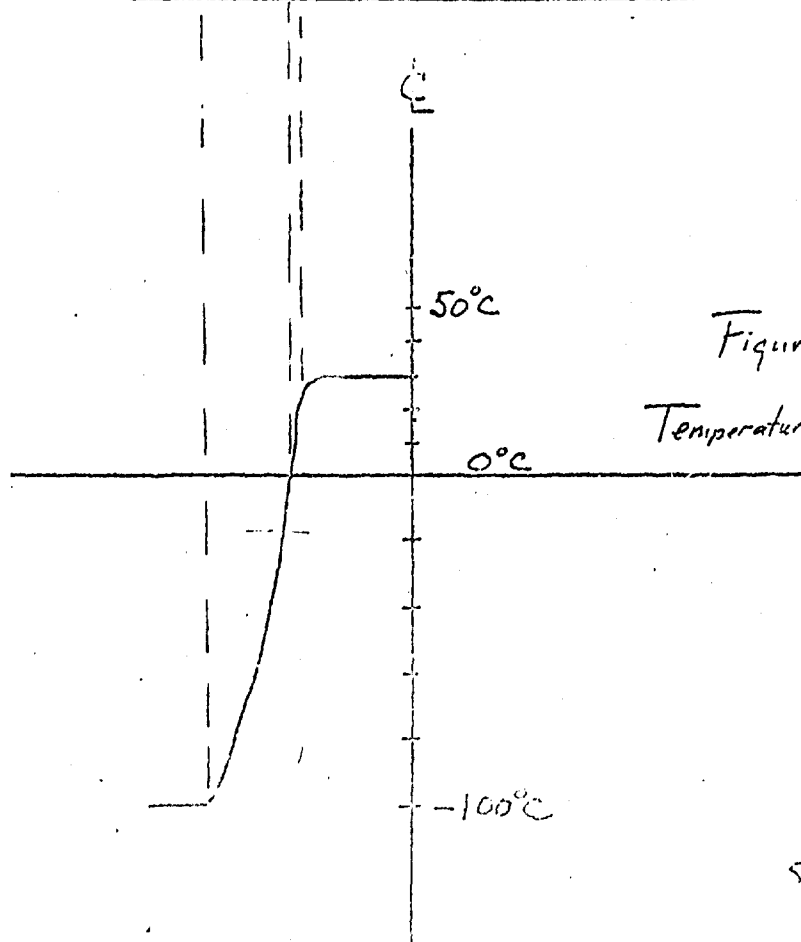


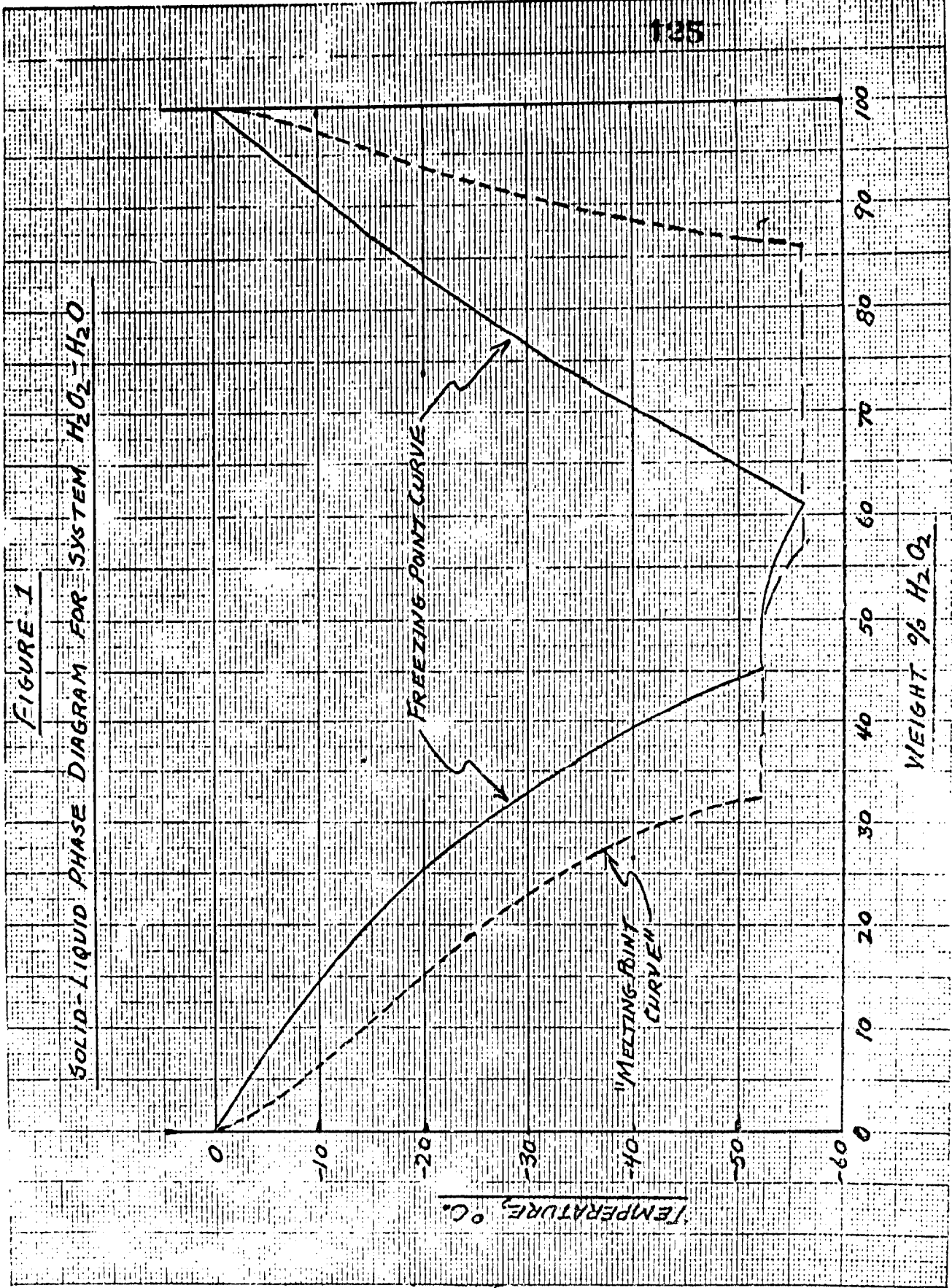
Figure 2
Temperature Profile

Felt
2/11/65

APPENDIX IIIConcentration of 90% H₂O₂ by CrystallizationA. Theory

This discussion will be limited to H₂O₂ concentrations above about 61.2% H₂O₂ and temperatures above about -56.1°C., which are the coordinates of the second eutectic in the system hydrogen peroxide-water (Figure 1).

Solid and liquid phase compositions obtained on partial freezing of H₂O₂ solutions have long been debated. Some investigators, particularly as a result of early work, concluded that the solid phase consisted of a solid solution of H₂O₂-H₂O, and that both solid and liquid phase compositions varied with temperature. Such "solid phase compositions" are indicated by the dotted line in Figure 1. This presumed equilibrium relationship is the basis for the explanatory discussion in the Becco patent (U.S. Patent 2,724,640) on their continuous countercurrent crystallization process for the concentration of H₂O₂ solutions.



The weight of more recent evidence, however, denies the formation of solid solutions and indicates that the solid phase consists of pure H_2O_2 (1). At the same time it is stated in the same reference (1) as a fact that, "except for the most dilute and most concentrated solutions, the solid obtained by the partial freezing of hydrogen peroxide solutions contains both water and hydrogen peroxide, even under conditions encouraging attainment of equilibrium". This is attributed to occlusion within the solid of liquid of the same concentration as the free liquid (mother liquor) surrounding the solid. Attempts to demonstrate analytically that the solid phase itself is 100% H_2O_2 are thus hampered by the difficulty of separating the solid and liquid phases. This is true regardless of the possible occlusion of liquid actually within the solid.

There is no disagreement as to the composition of the liquid phase in equilibrium with a solid phase at a given temperature. Liquid phase compositions are as shown on the "freezing point" curve in Figure 1; i.e., as the temperature of the slurry varies, the mother liquor concentration follows the freezing point curve.

In our approach to concentration by crystallization, it was reasoned that filtration to remove excess mother liquor would of necessity leave the crystals still wet with mother liquor. The average composition of the filter cake would thus depend upon the degree of mother liquor separation achieved. In laboratory trials, when filtration on a fritted glass Büchner funnel, average filter cake compositions were in general somewhat higher than the "solid phase compositions" shown by the dotted line in Figure 1. It was further reasoned that displacement or replacement of the mother liquor remaining on the crystals with a stronger liquid phase by a crystal washing step would result in an effective increase in average H_2O_2 concentration of the filter cake.

It was recognized that such a crystal washing step would be more complex than a simple displacement wash. For the wash solution to be at a higher H_2O_2 concentration than the mother liquor on the crystals, it must necessarily be at a higher temperature. Thus, as the relatively warm wash solution passes through the filter cake it is subjected to cooling by contact with the cold crystals, which tends to induce crystallization from the wash solution. At the same time the warming effect on the crystals tends to induce crystal melting to establish equilibrium at a new temperature. In addition to the heat exchange from the temperature difference, heat will be liberated or absorbed upon crystallization or crystal melting, respectively.

The crystal washing step may then be considered to be a displacement wash modified by the various effects listed above. The extent of the modification will depend upon the speed with which the actual wash is carried out. In any event, upon completion of the physical act of washing, the above temperature exchanges will continue to take place until final equilibrium is reached or until the system is further upset externally by subsequent handling operations.

(1) "Hydrogen Peroxide", ACS Monograph Series, Reinhold, 1955.

The product concentration obtained in a process involving crystallization, filtration and crystal washing will be primarily dependent upon the strength of the wash solution and the efficiency of separation of the solid and liquid phases. Practical attainment of concentrations within the 98-100% H_2O_2 range depend further upon the truth of the theory that the crystals themselves are 100% H_2O_2 and upon the extent to which mother liquor might be occluded within the solid phase in such a way that it is inaccessible to the wash solution.

B. Experimental Procedure

1. Crystallization Process

The general procedure followed in the laboratory investigation of H_2O_2 concentration by crystallization was as follows:

- a. Cool, with stirring, in a beaker immersed in a dry ice - tri bath until crystallization occurs. Continue cooling the crystal slurry with stirring, until the desired temperature is reached.
- b. Discharge the crystal slurry to a fritted glass Büchner funnel on a suction flask.
- c. Apply suction to remove "excess" mother liquor.
- d. Release vacuum (to permit complete coverage of filter cake with wash solution) and add wash solution which has been pre-cooled to about its freezing point.
- e. Reapply suction to draw the wash solution through the filter cake and to remove the wash liquor as completely as possible.
- f. Discharge the washed filter cake product from the filter to a pyrex container covered with aluminum foil. Let the product melt to insure uniformity for analysis.
- g. Analyze product, and intermediate product samples and liquors as desired, for % H_2O_2 .

The following notes and explanatory comments apply to the above general procedure:

- a. A stainless steel spatula was used to stir the crystal slurry. With this exception, only glass equipment was used.
- b. At the lower crystallization temperatures used, the "slurry" has the approximate consistency of wet snow and contained little "excess" mother liquor which was removable on filtration.
- c. The wash solution was in general applied incrementally releasing the vacuum between increments, because of filter capacity limitations and efforts to handle maximum size batches.
- d. Strength determinations were made by standard potassium permanganate titration in the presence of sulfuric acid. Sample size was 8 drops, about 0.4 gram, weighed to four decimal places. $KMnO_4$ strength was approximately 0.5 normal, giving titers of 40-50 ml.

ROUGH DRAFT

APPENDIX IV

128

EFFECTS OF 90 PERCENT
HYDROGEN PEROXIDE UPON ALUMINUM SURFACESI. Introduction

Aluminum of 99.6% purity is the common material of construction for containers which are designed for long-term storage of high-strength H_2O_2 . It has been designated a Class 1 material, highly compatible with high-strength H_2O_2 and causing minimal catalytic decomposition.

The present study has provided an opportunity to determine just how inert aluminum of various purities is when in contact with 90% H_2O_2 . The techniques of light and electron metallography have been used to examine surface changes brought about by exposure to the hydrogen peroxide. (It was not possible to get reliable data comparing the aluminum samples in their abilities to catalyze decomposition of the 90% hydrogen peroxide. This was in all cases minor relative to the decomposition which occurred on the glass surfaces of the test apparatus.)

II. Experimental

Materials used included aluminum in the following forms and purities:

- storage drum for 90% H_2O_2 (99.6% Al)
- single crystal (99.995% Al from Semi-Elements, Inc., Saxonburg, Pa.)
- single crystal (99.5% Al, 0.5% Cr from Semi-Elements, Inc.)
- 2S sheet (99.4% Al)
- 2024 sheet (4.5% Cu, 0.6 Mn, 1.5 Mg, bal. Al)

HARRISON/bwm

- 2 -
ROUGH DRAFT

109

foil supplied by the Aluminum Company of America in these purities - 99.45, 99.88, 99.93 and 99.999%

Specific exposure conditions of samples of these materials are cited in the following Discussion section.

The techniques of examination included those of light microscopy, electron microscopy, electron diffraction, electron probe microanalysis and x-ray diffraction. Where oxide films as such were studied (the primary intention with the Alcoa aluminum foil samples), they were first isolated from the substrate metal by dissolution of the latter in a 3% (vol) solution of bromine in absolute methanol.

III. Results and Discussion

A. 90% H₂O₂ Storage Drum

This drum, received from the Memphis Plant of the Electrochemicals Department of the Du Pont Company, had a long, but otherwise unknown history of service as a container for 90% H₂O₂. Typical surface structures of a section of the drum wall are shown at 250X in Figure 1. The aluminum is irregularly roughened by pitting and "wormtrack" corrosion (1a). Occasional deeply pitted areas were found and were visible to the eye because of the associated tail of corrosion product staining (1b). When polarized light was used instead of the standard green-filtered light, the presence of the surface oxide of varying thickness was discernible (1c).

NAN/dwm

- 3 -
ROUGH DRAFT

130

This oxide was stripped by the bromine-methanol technique and examined both by electron microscopy and x-ray diffraction. The oxide varied greatly in thickness and in continuity. Much of it could not be penetrated by the electron beam. In Figure 2, however, are shown two electron micrographs of stripped oxide. Figure 2a shows an area in which a "thin" oxide has replicated the topography of the underlying aluminum. The intense black areas represent piled-up oxide, opaque to the electron beam.

The dendritic structure of Figure 2b is interpreted as an overgrowth of a second hydrated alumina film over the primary oxide film, probably of a different state of hydration. It might represent the formation of crystalline bayerite (Beta trihydrate) on bohmite (alpha monohydrate), a sequence of oxide-film formation on aluminum (exposed to water at room temperature) described by Hart¹.

Electron probe microanalysis was applied to surface analysis of this storage drum in an attempt to identify chemically the nature of the corrosion-staining associated with pits and the composition of second phase microinclusions. This work was done by N. E. Weston. His report is attached as Exhibit A. It was established that the "tail" of the pit does not contain any unusual concentration of metallic elements (other than aluminum). Phosphorous, tin and sulfur were found associated in the pitted area. Inclusions in the aluminum were rich in silicon. The findings are discussed in the Exhibit.

MAN/dma

- 4 -
ROUGH DRAFT

131

In Table I are x-ray diffraction data (interplanar spacings) of the stripped oxide surface. The patterns are very complex and could not be interpreted beyond the conclusion that they represent a mixture of several hydrated forms of alumina. There may also be lines present due to silicate components.

B. Effects of Metal Purity on Oxide Film Properties

1. 2S (1100) Alloy and 2024 Alloy

Figure 3 indicates differences in the ultrastructure of oxide films stripped from treated and untreated alloys. ["Treated" here refers to an exposure of the aluminum to 90% H₂O₂ for 20 hr at 66 °C. In the "untreated" state the 2S aluminum had been chemically polished for several minutes in a 100°C solution consisting of:

- 700 ml H₃PO₄ (sp.gr. ~ 5)
- 30 ml 70% HNO₃
- 120 ml glacial acetic acid
- 150 ml H₂O

The 2024 Al was left with a mechanically finished surface.]

The oxide stripped from the chemically polished surface of the 2S sample replicated a fine scale roughness developed by the polishing acid solution. Exposure to the 90% H₂O₂ converted this oxide into a heavier one of uniform thickness. High magnification examination, however, revealed this oxide to be a porous matted layer of hydrated oxide films. The film did not give a crystalline diffraction pattern.

The oxide film from the 2024 alloy was initially very thin and structureless except for occasional extracted inclusions.

JAN/bwm

- 5 -
ROUGH DRAFT

132

It also replicated the initial mechanical finish of the surface.

Exposure of the 2024 alloy to 90% H_2O_2 , however, resulted in a much more rapid and non-uniform buildup of surface oxidation product as Figure 3 shows. This would be expected from a higher rate of catalytic decomposition of the H_2O_2 upon the 2024 alloy surface with its 4.5 percent copper content. Thus, any aluminum alloy surface containing catalytically active heavy metal atoms will undergo enhanced oxidation at the site and in the area of the foreign atoms. The extent to which mechanical blanketing of the reactive area by oxide film formation would affect the peroxide decomposition kinetics is not known but could be determined by some careful laboratory experiments in which rate of film thickness buildup is correlated with rate of hydrogen peroxide decomposition upon an aluminum surface of known and controlled heavy metal contamination.

2. Oxide Films from Aluminum Single Crystals

a. 99.995% Al

A chemically polished wafer from a 3/4 in. diam. crystal of this purity was exposed to 90% H_2O_2 for 20 hr at 80°C. There was little apparent change in film thickness. However, as shown in Figure 4 exposure to the H_2O_2 did produce some microroughening in the aluminum surface which was replicated in the isolated surface oxide film. The stripped oxides show cellular markings which are interpreted as the result of structural heterogeneity in the aluminum surface because of the residual cast or dendritic structure of the metal.

- 6 -
ROUGH DRAFT

133

b. 99.5% Al - 0.5% Cr

Oxide films taken from wafers of this single crystal prepared and exposed similarly to the 99.995% Al sample are shown in the electron micrographs of Figure 5. Again there are background cellular markings present which are believed to reflect the dendritic cast structure of the metal. Exposure to the 90% H₂O₂ has left a fine deposit on the surface which may correspond to a chromium-containing residual layer developed by superficial corrosion of the crystal surface. The θ phase, CrAl₇, should be present in equilibrium with the α solid solution aluminum matrix and may be present in this residue.

It is not known to what extent chromium would be expected to catalyze the decomposition of strong hydrogen peroxide. Schumb et al.² state that "as a heterogeneous catalyst chromium is not particularly active," but solution of metallic chromium and preferential solution from stainless steel are stated to occur in concentrated hydrogen peroxide.

3. Surface Changes on Aluminum Foils

Four lots of aluminum foil were employed in this study in an attempt first to determine the effect of purity from 99.45% Al to 99.999% Al on decomposition rate of 90% H₂O₂ at 66°C (arbitrary elevated temperature), and secondly, following test exposure to observe what changes had taken place on the foil surfaces.

This series of tests consisted of sixteen exposures. Each lot of foil was exposed for periods of 16 hr, 70 hr, 135.5 hr and 303 hr in the 66°C 90% H₂O₂. Each foil specimen measured 7.0 ^{cm} ~~sq. in.~~

NAN/bwm

- 7 -
ROUGH DRAFT

134

in surface area and was carefully cleaned and degreased before immersion in 100 ml of 90% H_2O_2 .

Unfortunately, it was not possible to secure valid data on hydrogen peroxide decomposition occurring on these samples because, as stated earlier, the volume of oxygen evolved on the aluminum surfaces was only a small fraction of the total decomposition that occurred in the test flask. However, all foil samples were metallographically examined at the conclusion of all test periods. Oxide films were again isolated (by bromine-methanol dissolution of scissored pieces of the foils) and the films examined by direct transmission in the electron microscope. The remaining figures in this Section have been chosen to illustrate typical results obtained in this part of the investigational program.

a. Comparison of Isolated Oxide Films

It was difficult to find decisive differences between electron micrographs representing the aluminum oxide isolated from the 20 metal samples (including the as-received, control samples). It was evident that all films were much thinner and more uniform than those examined earlier from 2S aluminum exposed at 80°C. The lower temperature, 66°C, and the higher purities undoubtedly controlled the kinetics of surface oxidation and film thickness growth. The oxide films were not appreciably heavier from the samples which had 303 hr of contact with the H_2O_2 than films isolated from the control specimens. There did, however, appear to be a general micropock-marking present in the 303 hr surfaces that was not present initially in the control surfaces. Also small areas of dark nebulosity probably correspond

NAN/bwm

- 8 -
ROUGH DRAFT

135

to sites of superficial corrosion with corrosion product buildup. These features can be seen in the electron micrographs at 84,000X in Figure 6. Even at this magnification the topographical detail is very small. (This may be better appreciated with the realization that 1 inch square on the micrographs is in actuality a square of oxide, 12 millionths of an inch on an edge.)

The considerably higher purity of the 99.999 aluminum did not result in a proportionate improvement in homogeneity of the oxide film formed on exposure to the 90% H_2O_2 . In comparing the 303 hr samples, the 99.93% Al appeared to have the thinnest, most inherently structureless oxide. The 99.999% Al oxide was not unique but similar to those isolated from the 99.45 and 99.88% Al samples. In all cases electron diffraction patterns showed only the broad, diffuse bands typical of an amorphous material.

b. Surface Topography and Corrosion

Metallographic observations were made on all foil samples following their periods of exposure to 90% H_2O_2 . On the basis of this low magnification examination (supplemented, however, with selected surface replicas for electron microscopic study) the 99.45 alloy was judged to have suffered most surface damage in the form of superficial staining, pitting and "wormtrack" corrosion.

Again the 99.93 aluminum foil was found to have changed least from the control sample of the same purity but to have some micropits and one large pit around which a heavy layer of crazed corrosion product had deposited.

- 9 -
ROUGH DRAFT

136

The 99.88 alloy was stained and contained areas of micropitting.

The 99.999 pure aluminum showed many initial surface defects, mechanically induced, which appeared to be areas susceptible to later corrosion attack in the 90% H_2O_2 . The sample also showed after 303 hr of exposure what were interpreted to be crazing cracks in oxide corrosion product precipitated around several sites of localized corrosion.

In all foil samples it was evident that scratches and mechanical damage to the aluminum surface acted as preferential sites for pitting attack.

In Figure 7 are shown the control specimen, the 70 hr and 303 hr specimens of the 99.45 aluminum. Figures 7b, 7d and 7f are carbon replicas (these and others shown in Figures 9 and 10 were produced by direct carbon deposition and stripping in bromine-methanol).

Figure 8 compares photomicrographs of the starting surface and the 303 hr surface of the 99.88 aluminum foil.

Figure 9 includes a photomicrograph of the one area in which crazing cracks were found in the oxidized surface of the 99.93 aluminum foil. A unique pit exhibiting noncubic surfaces was found in replicas of the 135.5 hr sample.

NAN/bwm

- 10 -
ROUGH DRAFT

137

The surfaces of the 99.999 aluminum samples received the most careful scrutiny primarily because of the initial expectation that this metal, because of its purity, might show least surface changes of the four under study. The micrographs illustrating its surface structure show the starting conditions and defects mentioned above (10a, 10b). Blotchy areas of corrosion and pitting were observed in the 135.5 hr sample (10c, 10d).

After 303 hr a few areas of crazing in the corrosion product film were noted (10e) and "wormtrack" pitting of the type appearing in Figure 10f was found.

IV. Summary

Under the test conditions employed in this study it was not established that 99.999 percent aluminum has better resistance to 90% H_2O_2 than aluminum of 99.93 percent purity. Factors which enter into such an evaluation, however, are difficult to control. The degree of segregation of impurities can well determine the incidence of pitting and localized corrosion in different metal lots of the same analyzed level of purity. Mechanical damage in treating and handling and slight differences in chloride ion content and contamination of the exposure or contacting environment may produce surface changes and localized attack microscopically discernible. Over long term contact with high strength H_2O_2 these effects would become much more apparent. (It must be emphasized that with the exception of the 2024 alloy specimen to the eye none of the aluminum test specimens in the present study appeared visibly changed.)

To determine if the surface changes described above are accompanied by or caused by differences in catalytic decomposition activity of the aluminum surfaces, it now appears that the 90% H_2O_2 should contact only the aluminum under test in each case. This would require a special type of cup-type specimen or perhaps a test vessel entirely fabricated out of the aluminum to be evaluated.

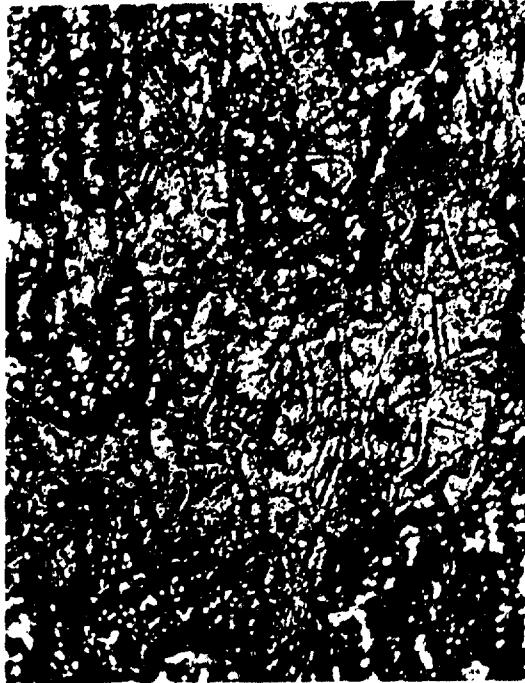
NAN/bwm

TABLE I

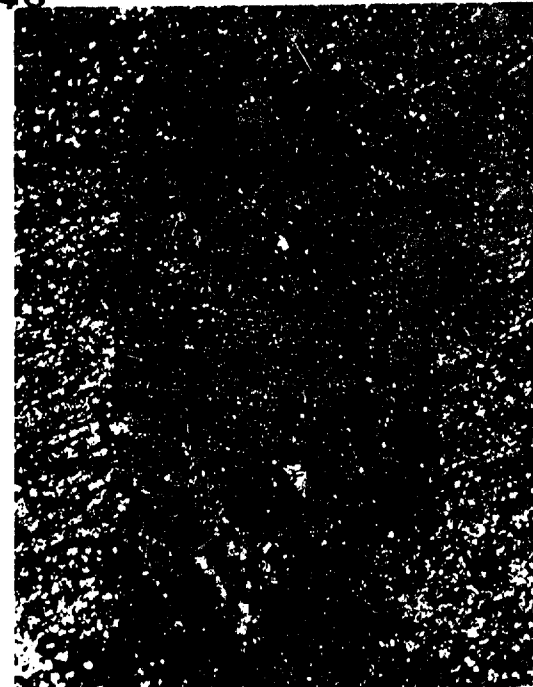
Interplanar Spacings of Oxide from Aluminum Storage Drum

<u>Co(α) Radiation</u>		<u>Cu(α) Radiation</u>	
<u>Intensity</u>	<u>d_0 (Å)</u>	<u>Intensity</u>	<u>d_0 (Å)</u>
MW	8.31	MW	8.46
W	5.52	W	5.48
M	4.55	M	4.58
MST	4.08	ST	4.08
MST	3.92	MST	3.95
MST	3.75	W	3.77
M	3.57	M	3.58
M	3.43	M	3.43
M	3.28	M	3.28
MST	3.17	MST	3.18
W	3.00	W	3.02
W	2.89	W	2.88
W	2.78	W	2.81
W	2.70	W	2.72
MW	2.50	MW	2.51
W	2.40	MW	2.42
W	2.24	W	2.34
W	2.14	MW	2.26
W	2.09	W	2.14
W	2.07	W	2.08
MW	2.03	MW	2.03
W	1.78	W	1.92
W	1.63	MW	1.80
W	1.48	W	1.64
		W	1.49
		W	1.43

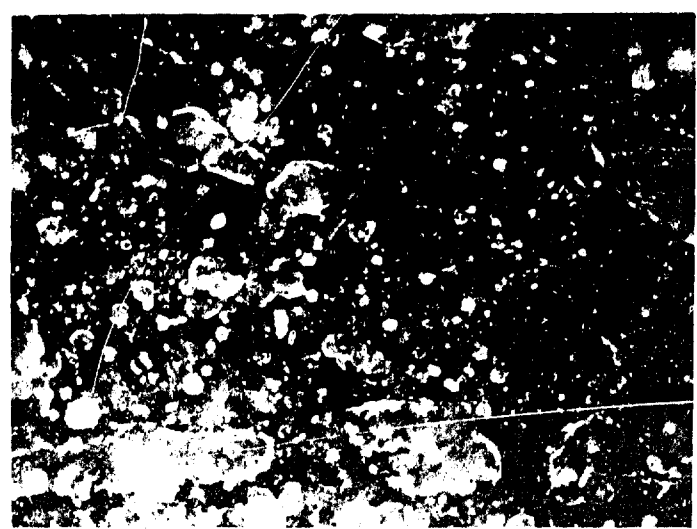
M = medium
 ST = strong
 W = weak



(a) "WORMTRACK" CORROSION

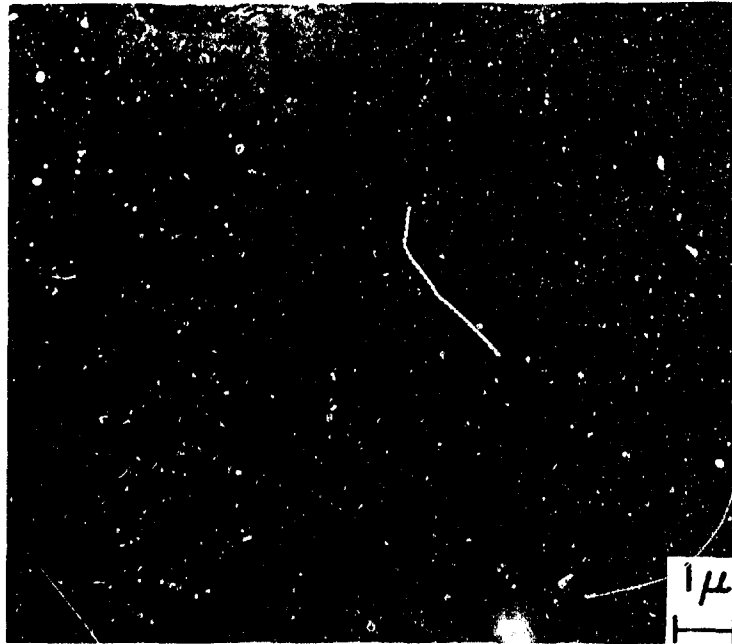


(b) CORROSION PIT AND STAINING

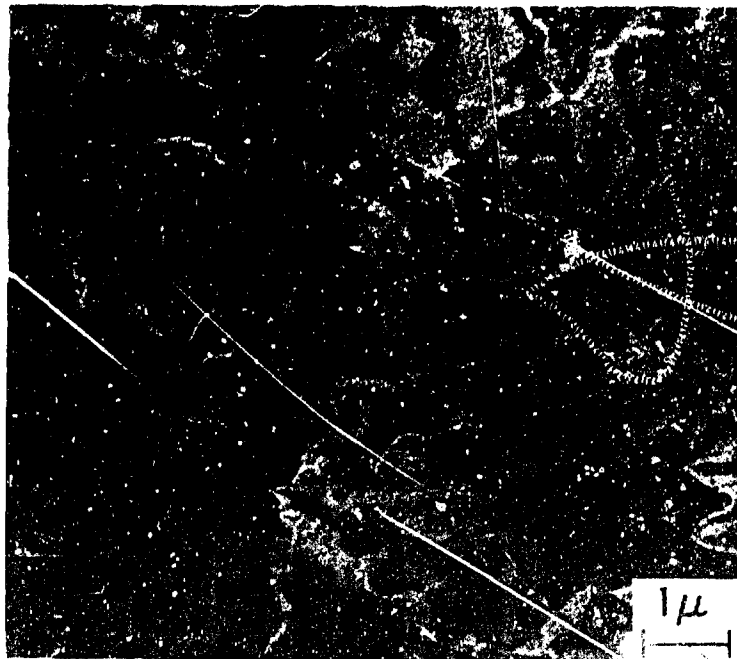


(c) POLARIZED LIGHT SHOWS SURFACE OXIDE

FIG. 1 - ALUMINUM STORAGE DRUM SURFACES (250 X)

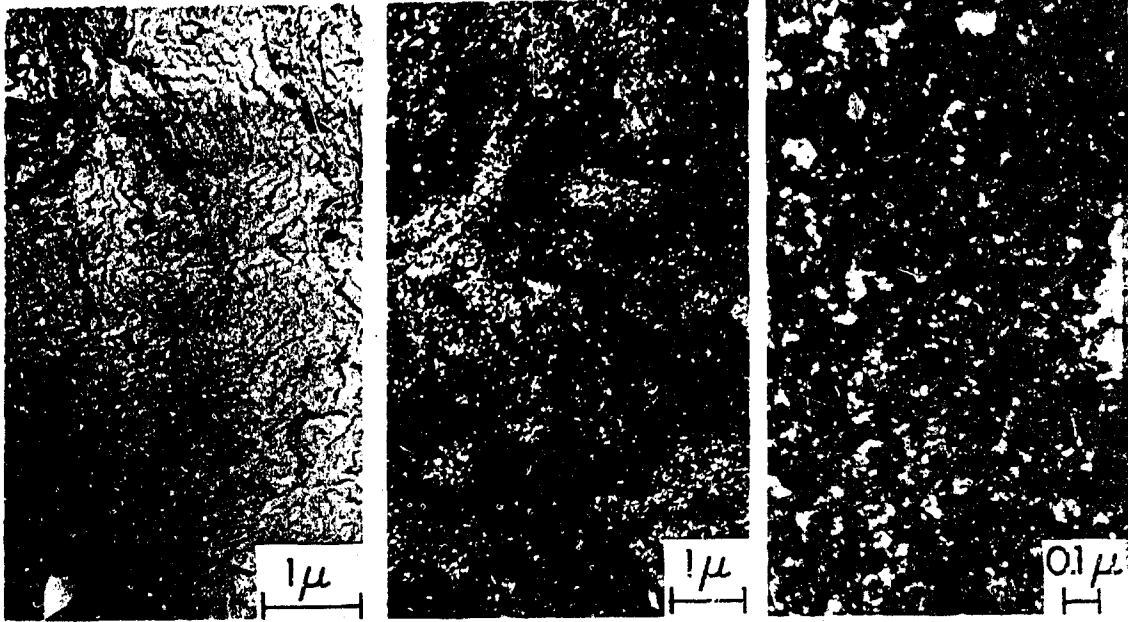


(a) 9,000 x



(b) 14,000 x

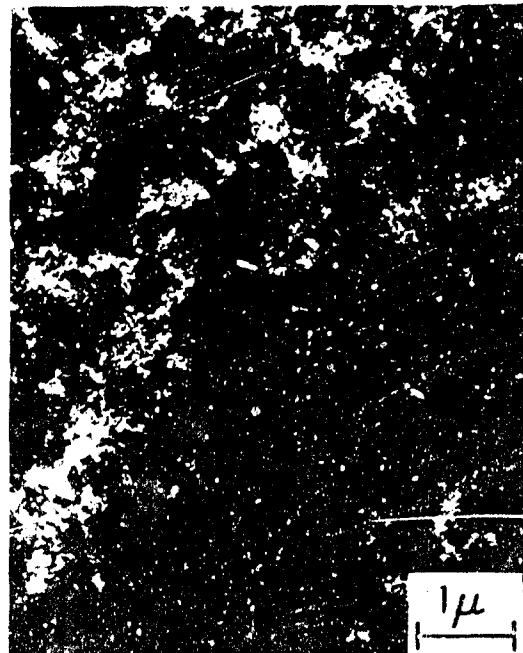
FIG. 2 - OXIDE STRIPPED FROM STORAGE DRUM



(a) - 15,200 x AS-POLISHED CONTROL
(b) - 11,600 x 2S (1100) ALUMINUM
(c) - 52,000 x



(a) - 52,000 x AS-RECEIVED CONTROL

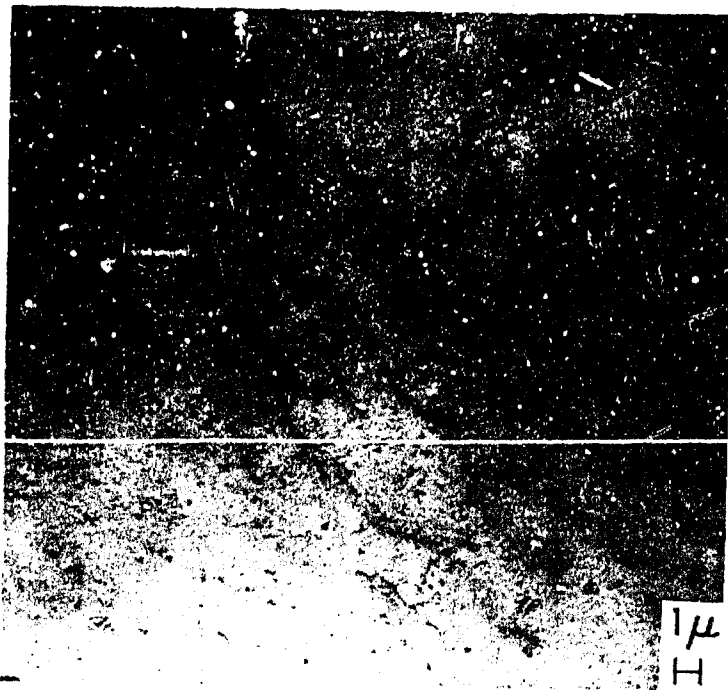


(b) - 15,200 x 2024 ALUMINUM

FIG. 3 - OXIDE FILMS FROM 2S AND 2024 ALUMINUM

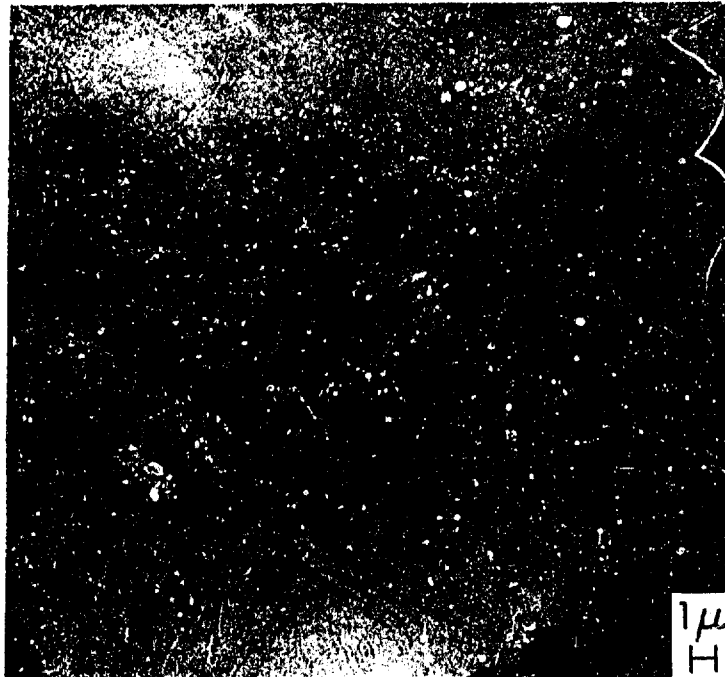


(a) 4,000 x
CONTROL

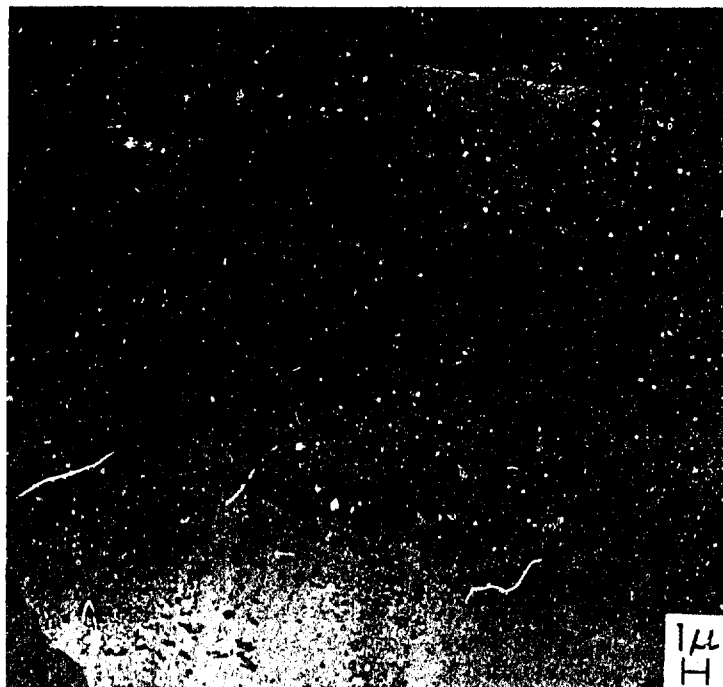


(b) 4,000 x

FIG. 8 - OXIDE FILM FROM 99.995 Al SINGLE CRYSTAL



(a) 4,000 x
CONTROL



(b) 4,000 x

FIG. 5 - OXIDE FILM FROM 99.5 Al-0.5 Cr SINGLE CRYSTAL



(a) CONTROL

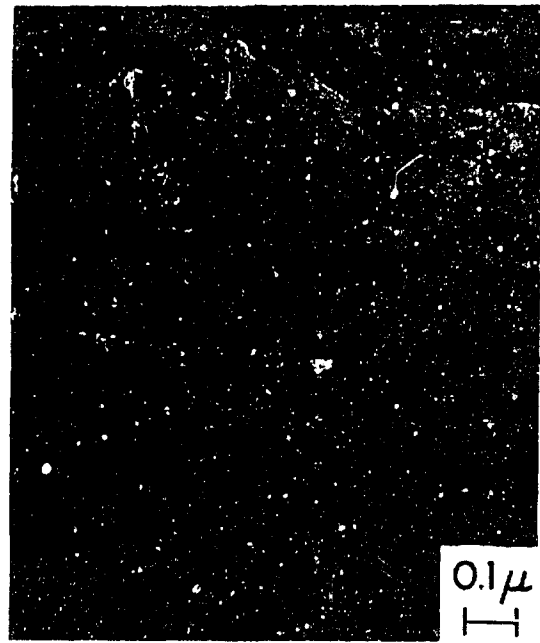


(b) CONTROL



(c) 303 hr. EXPOSURE

99.45 Al



(d) 303 hr. EXPOSURE

99.88 Al

FIG. 6 - OXIDE FILM FROM ALUMINUM FOIL
84,000 x



(e) CONTROL



(f) CONTROL

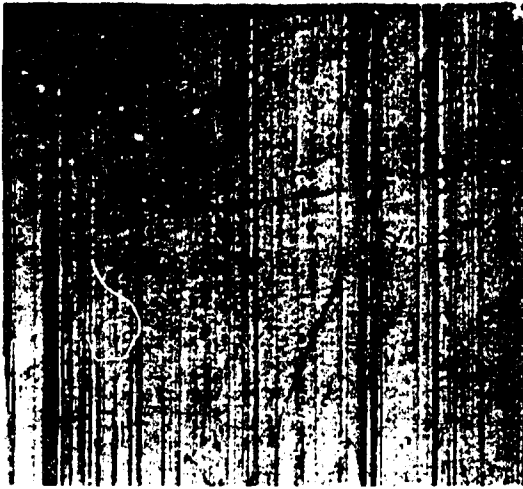


(g) 303 hr. EXPOSURE
99.93 Al

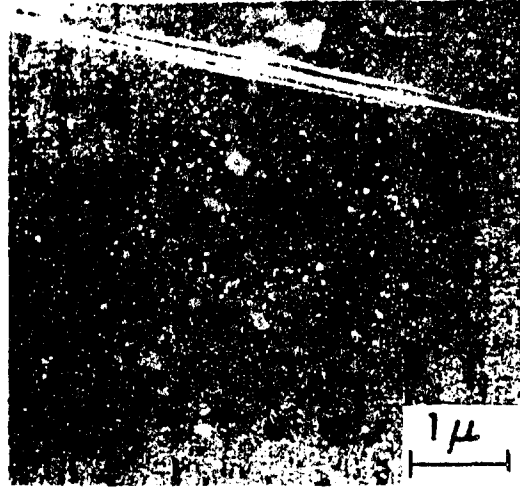


(h) 303 hr. EXPOSURE
99.999 Al

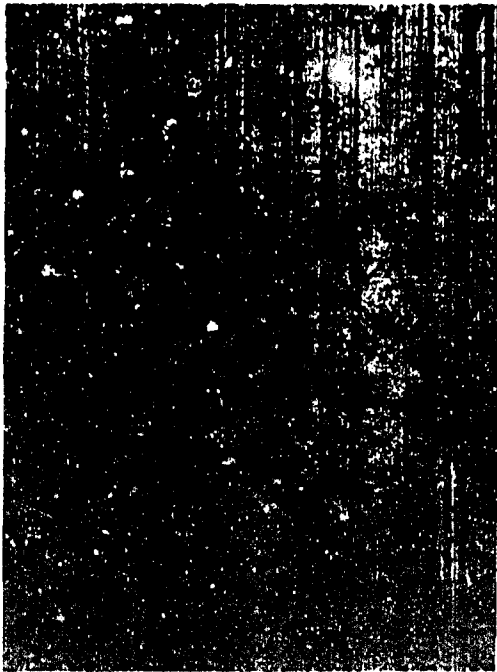
FIG. 6 - OXIDE FILM FROM ALUMINUM FOIL
(cont'd) 84,000 x



(a) 250 x
CONTROL



(b) 15,200 x
CONTROL



(c) 250 x
70 hr. EXPOSURE



(d) 11,600 x
70 hr. EXPOSURE

FIG. 7 - SURFACE STRUCTURE OF 99.45 AL FOIL



(e) 500 x
303 hr. EXPOSURE



(f) 15,200 x
303 hr. EXPOSURE

FIG. 7- SURFACE STRUCTURE OF 99.45 AL FOIL
(con't'd)

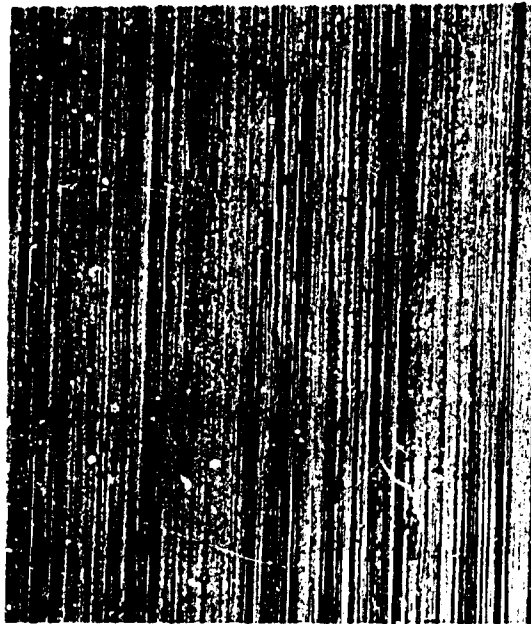


250 x
CONTROL



250 x
303 hr. EXPOSURE

FIG. 8 - SURFACE STRUCTURE OF 99.88 AL FOIL



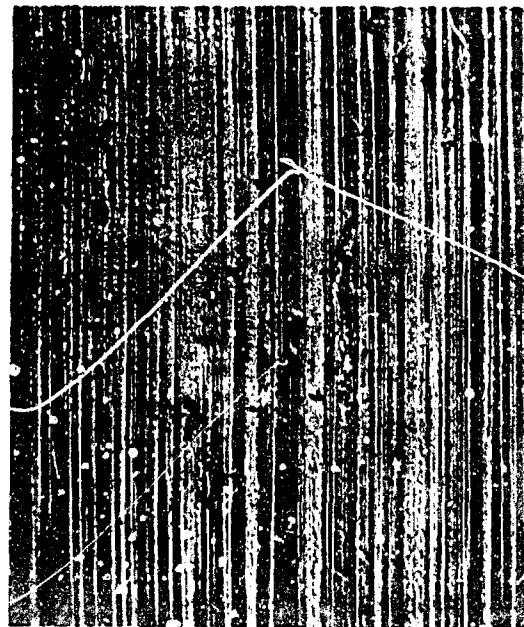
(a) 250 x
CONTROL



(b) 250 x
135.5 hr. EXPOSURE

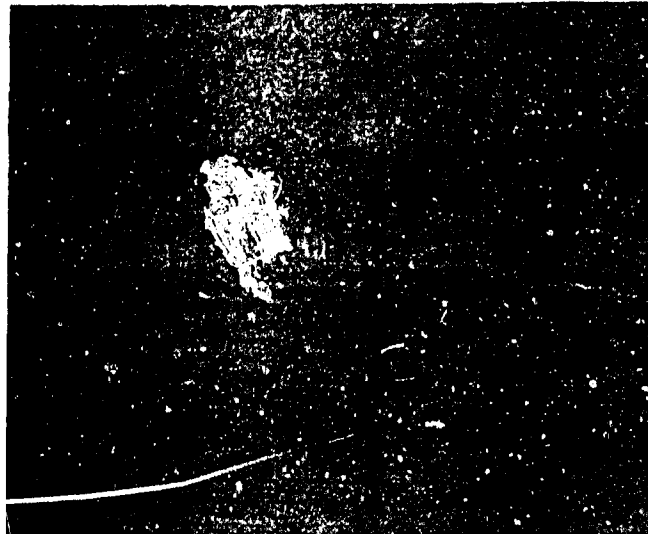


(c) 15,200 x
CORROSION PIT

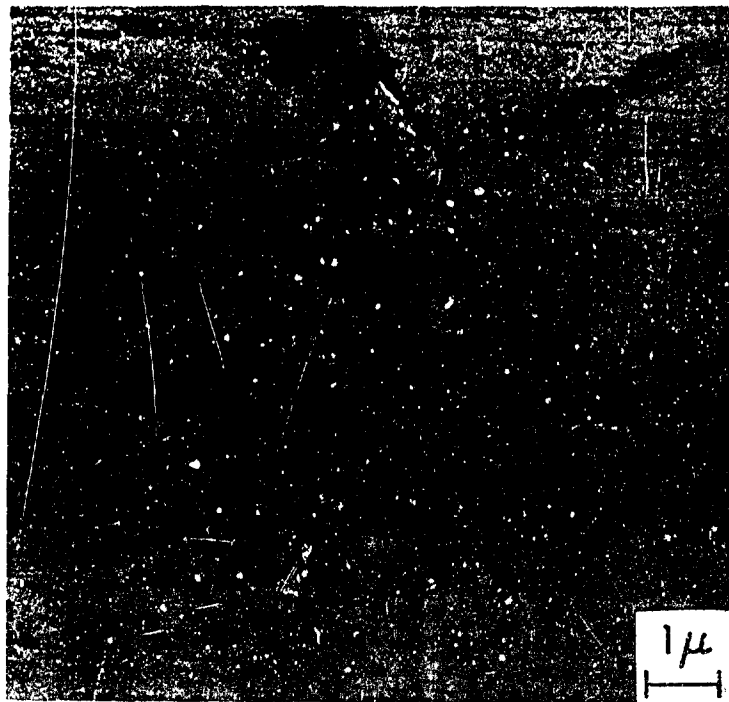


(d) 250 x
303 hr. EXPOSURE

FIG. 9 - SURFACE STRUCTURE OF 99.93 AL FOIL

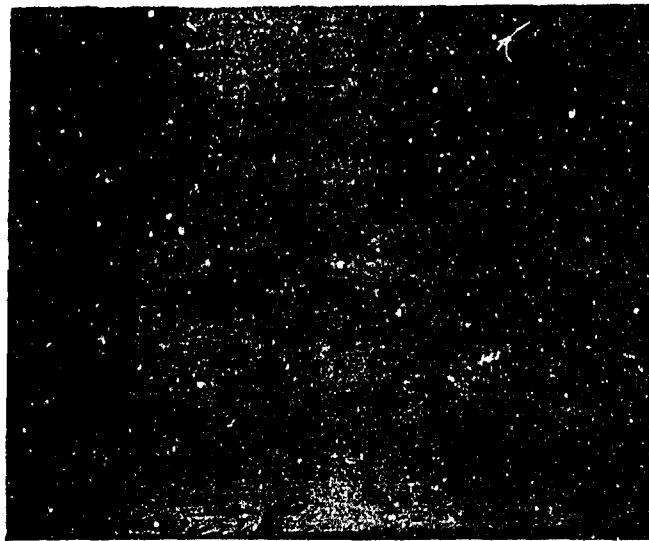


(a) 250 x
CONTROL



(b) 11,600 x
CONTROL

FIG. 10 - SURFACE STRUCTURE OF 99.999 Al FOIL



(c) 250 x
135.5 hr. EXPOSURE



(d) 11,600 x
135.5 hr. EXPOSURE

FIG. 10- SURFACE STRUCTURE OF 99.999 Al FOIL
(cont'd)



(e) 500 x
303 hr. EXPOSURE



(f) 11,600 x
303 hr. EXPOSURE

FIG. 10 - SURFACE STRUCTURE OF 99.999 Al FOIL

REFERENCES

1. R. K. Hart, Trans. Faraday Soc. 53, Part 7, 1020-1027, July 1957.
2. "Hydrogen Peroxide" by W. C. Schumb, C. N. Satterfield and R. I. Wentworth, ACS Monograph Series, Reinhold Publishing Corporation 1955, p. 497.

cc: S. E. Isakoff
W. L. Phillips
R. E. Steigerwald

155

August 18, 1965

AFRPL-TR-66-13

MEMORANDUM

TO: N. A. NIELSEN

FROM: N. E. WESTON (2) *N. E. Weston*

~~512642~~ - ELECTRON PROBE MICROANALYSIS OF CORROSION PITS IN ALUMINUM DRUMS FOR H₂O₂ STORAGE - N. E. Weston

Sample

The sample was taken from the bottom of a 2S aluminum drum used to store 90% H₂O₂. The surface in contact with the H₂O₂ showed occasional large pits. We were asked to examine, with the electron microprobe, the pitted areas for concentrations of elements other than Al. In particular, we were requested to examine the dark stains which tail out from the pits (see, for example, Fig. 1). In addition to examining the "in situ" pits, we also examined a polished section for the presence of second phases. The sample description is recorded in ERD Data Book 3976.

Results"In Situ" Pit

We were able to detect only Si, Sn, P, Fe, S, and Al in the region of a pit shown in Fig. 1. Figures 2 and 3 show that P, Sn, and S are associated together in the pit. The P and Sn compounds are presumably due to reaction of aluminum ions with the stabilizers normally added to H₂O₂. The Fe shows a very fine dispersion and is not apparently uniquely associated with a pit. The Si is associated with small cathodoluminescent (see Fig. 4) inclusions. The pit has a cluster of these inclusions. Although the "tail" is less cathodoluminescent than the surrounding oxide coat on the aluminum, only Al is associated with it. We think that the "tail" is a hydrous aluminum oxide resulting from electrochemical corrosion of aluminum at the pit site.

Polished Section

Optical examination of a polished section of aluminum showed tiny inclusions (see Figs. 5, 7). These inclusions tended to be clustered, but the clusters were microscopically rare. Phenomenologically, the quantity of clusters per unit area is of the same order of magnitude as the number of pits in the previous sample. Electron probe examination of the inclusions shows they are rich in Si (Fig. 6). It is well known that pitting corrosion in aluminum occurs most frequently by electrochemical attack at second phase sites.



(100X)

FIGURE 1

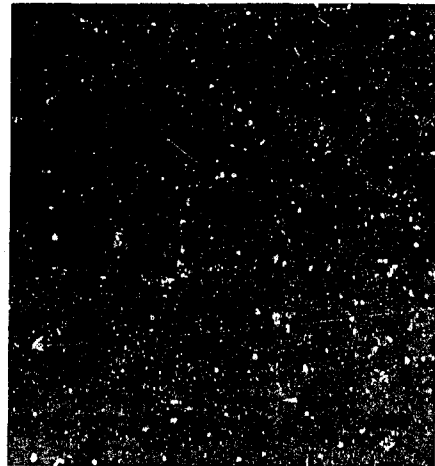
Photomicrograph of Corrosion Pit in Aluminum after Electron Probe Microanalysis (100X)
(Sample surface unpolished)



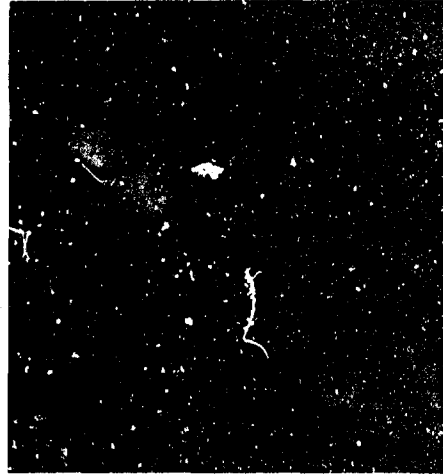
A. Target Current, inv. (200X)



B. FeKα x-rays (200X)



C. Target Current, inv. (405X)



D. FeKα x-rays (405X)

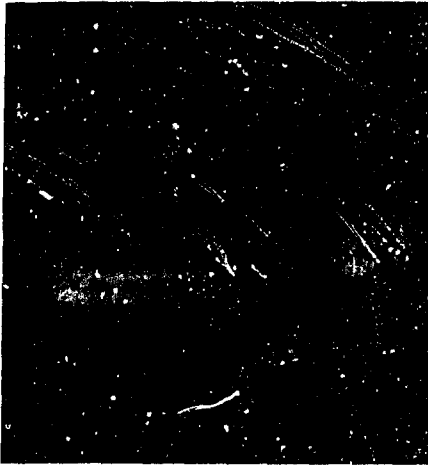
FIGURE 2

Electron Microprobe Area Scans of a Corrosion Pit Area in Aluminum

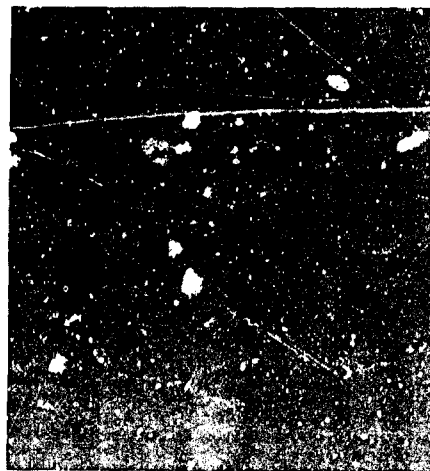
(Refer to Figure 1)



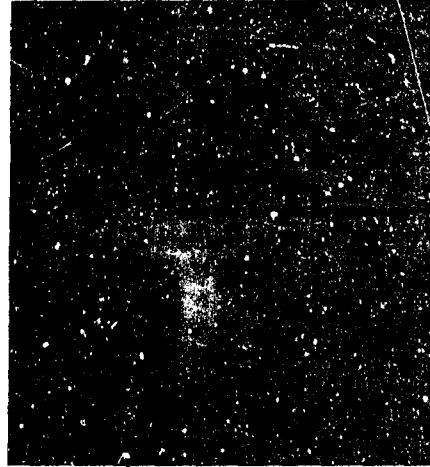
A. FeKα x-rays



B. SnLα x-rays

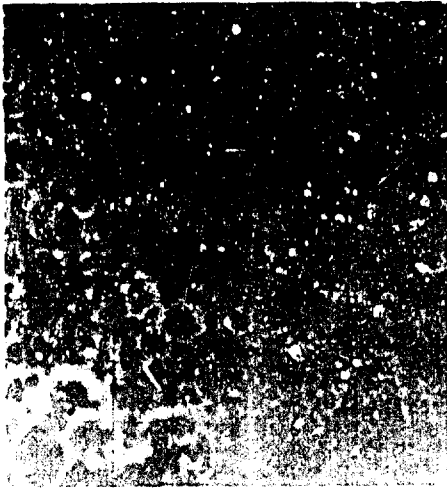


C. SiKα x-rays



D. SKα x-rays

FIGURE 3
Electron Microprobe Area Scans of a Corrosion Pit Area in Aluminum (405X)
(Refer to Figure 1)



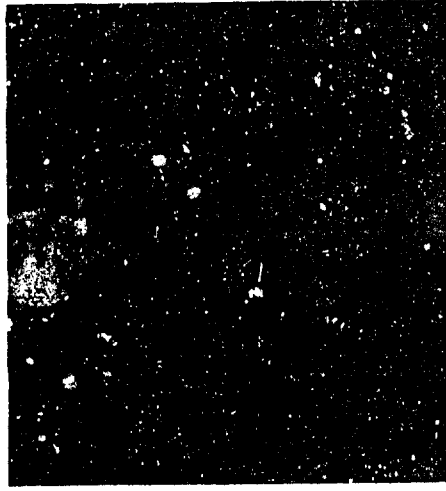
A. Target Current, inv.; Location 2



B. FeKa x-rays; Location 2



C. Cathodoluminescence; Location 2

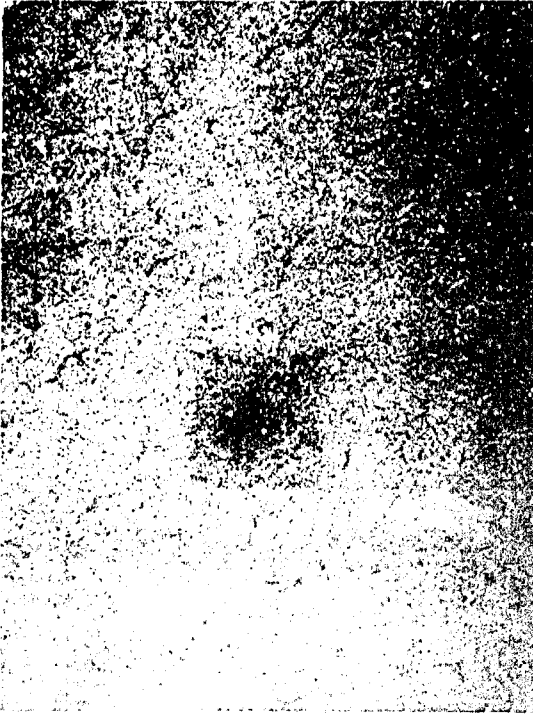


D. Cathodoluminescence; Location 3

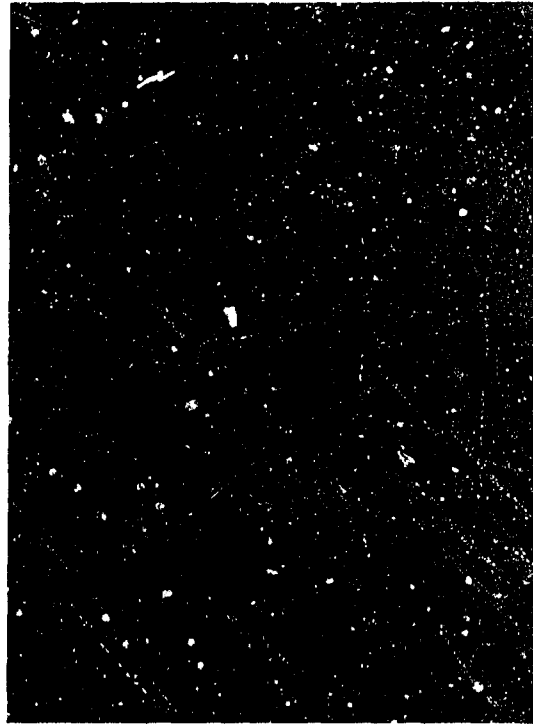
FIGURE 4

Electron Microprobe Area Scans of a Corrosion Pit Area in Aluminum (200X)

(Locations 2 and 3 slightly displaced from Location 1 shown in Figs. 2 and 3)

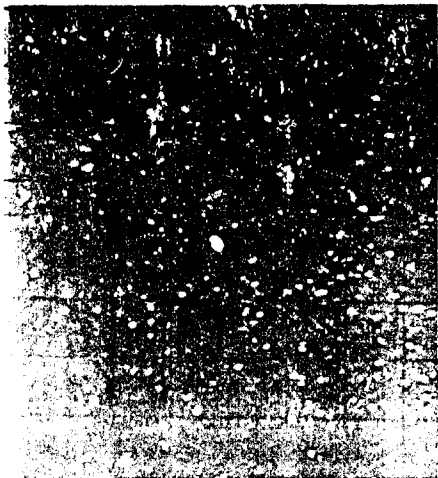


A. 200X



B. 500X

FIGURE 5
Photomicrographs of Polished Section of Aluminum after Electron Microprobe Examination



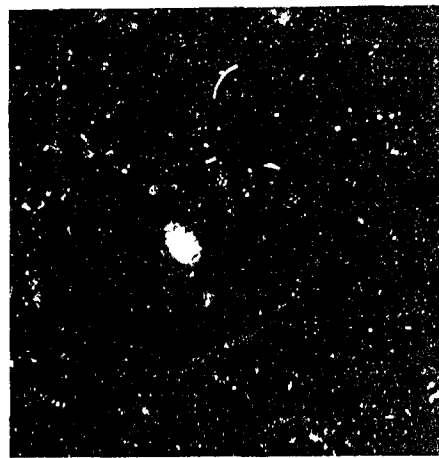
A. Target Current, inv. (200X)



B. Target Current, inv. (810X)



C. FeKa x-rays (810X)



D. SiKa x-rays (810X)

FIGURE 6

Electron Microprobe Area Scans of Polished Section of Aluminum
(Refer to Figure 5)

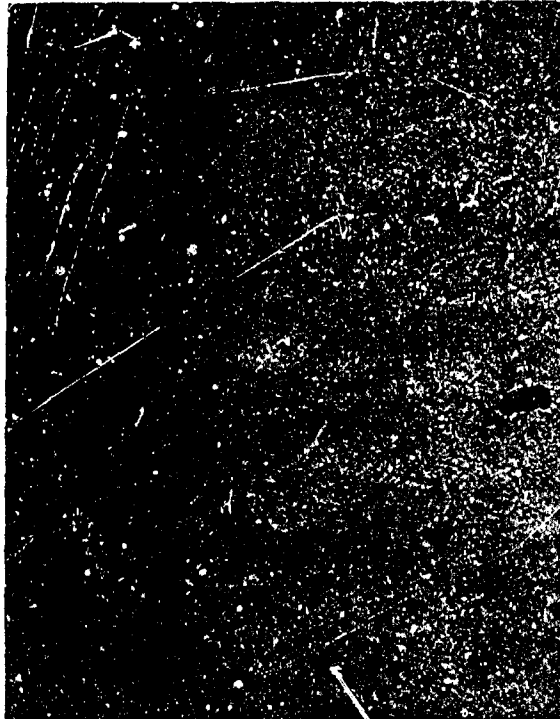


FIGURE 7
Photomicrograph of Polished Section of Aluminum -
Location Showing Numerous Si Rich Inclusions (200X)